IMPACT OF BIOGEOCHEMICAL PROCESSES ON MINERAL WEATHERING AND TRANSFORMATION

A Dissertation
Presented to
The Academic Faculty

by

Emily M. Saad

In Partial Fulfillment
of the Requirements for the Degree
Doctor of Philosophy in the
School of Earth and Atmospheric Sciences

Georgia Institute of Technology
August 2017

IMPACT OF BIOGEOCHEMICAL PROCESSES ON MINERAL WEATHERING AND TRANSFORMATION

Approved by:

Dr. Yuanzhi Tang, Advisor
School of Earth and Atmospheric Sciences
Georgia Institute of Technology

Dr. Ellery Ingall
School of Earth and Atmospheric Sciences
Georgia Institute of Technology

Dr. Martial Taillefert
School of Earth and Atmospheric Sciences
Georgia Institute of Technology

Dr. Owen Duckworth
Department of Crop and Soil Science
North Carolina State University

Dr. Christopher Reinhard
School of Earth and Atmospheric Sciences
Georgia Institute of Technology

Date Approved: July 13, 2017

ACKNOWLEDGEMENTS

I first extend my sincerest appreciation to my advisor, Dr. Yuanzhi Tang, for her patience, guidance and encouragement. I am especially grateful to her for fostering my scientific independence. I express gratitude to my dissertation committee: Dr. Ellery Ingall, without whose support I would not have made it quite so healthily to this point; Dr. Martial Taillefert for providing me with a foundation of enthusiasm for science and for getting me into graduate school twice; Dr. Chris Reinhard for infusing motivating zeal into every conversation; Dr. Owen Duckworth for being such an inspiring resource. My committee also contributed to the improvement of this dissertation.

Thank you to all past and present members of the Tang group, the Taillefert group, and the Ingall group for making the past 4 years interesting. I am appreciative of Meg Grantham for her continued technical expertise and friendship. I am grateful to David Tavakoli for his help with XRD and stories to help make long scans not seem so long. I also thank Yolande Berte, Todd Walters, and Eric Woods for help me take beautiful pictures of my diatoms. Additionally, I thank Dr. Guangxuan Zhu for his FTIR permission.

Finally, I am grateful to John Charbonneau for all of his help in the lab on weekends and late into the night many more nights than he'd have liked. You are my best friend, and I promise that this is the only doctoral program that I will ever put us through.

TABLE OF CONTENTS

LIST OF TABLES

LIST OF FIGURES

LIST OF SYMBOLS AND ABBREVIATIONS

Al	aluminum
BET	Brunauer–Emmett–Teller gas adsorption analysis
$bSiO_2$	biogenic silica
C	carbon
Cr	chromium
$Cr_xFe_{1-x}(OH)_3$	Cr(III)-Fe(III)-(oxy)hydroxide
DFOB	desferrioxamine B
DI	deionized water
DIC	dissolved inorganic carbon
DOC	dissolved organic carbon
DOM	dissolved organic matter
DON	dissolved organic nitrogen
DOP	dissolved organic phophorus
ED	electrodialysis
EDX	energy dispersive x-ray spectroscopy
EELS	electron energy loss spectroscopy
EXAFS	extended x-ray absorption fine structure
Fe	iron
FFT	fast Fourier transform
FT-IR	Fourier transform infrared spectroscopy
Ga	billion years before present
HEPES	4-(2-hydroxyethyl)-1-piperazineethanesulfonic acid
HRTEM	high resolution TEM
ICP-MS	inductively coupled plasma-mass spectrometry
Mn	manganese
NMR	nuclear magnetic resonance
P	phosphorus
PDF	pair distribution function
polyP	polyphosphate
SAED	selected area electron diffraction
SEM	scanning electron microscopy
Si	silicon
T. pseudonana	*Thalassiosira pseudonana*
TEM	transmission electron microscopy
UV/vis	UV/visible spectrophotometry
XANES	x-ray absorption near edge structure
XAS	x-ray absorption spectroscopy
XRD	x-ray diffraction

SUMMARY

The pervasiveness of microbe-mineral interactions in the natural environment requires elucidation of the factors controlling the characteristics of minerals that are subject to biomineralization and/or bioweathering. Determining how microorganisms directly and indirectly affect elemental speciation can offer a more predictive assessment of numerous biogeochemical cycles. Current knowledge gaps include the degree to which microorganisms participate in mineral weathering reactions and associated impacts on the rates and extent of mineral dissolution, chemical exchange with aqueous solutions, as well as the stability, structure, and composition of the new mineral phases that may form. To address these questions, systematic approaches must be taken to constrain the mechanisms involved in microbe-mineral interactions under both controlled laboratory conditions and in the field. Reaction kinetics, product speciation, and parameters that control these factors must be measured to ultimately be included in predictive biogeochemical models.

This dissertation seeks to constrain microbe-mineral interactions from an analytically intensive perspective that includes aqueous phase analyses (e.g. establishing the thermodynamic and kinetic controls of a system) and solid phase analyses (e.g. structural and morphological evolutions) of two model systems, the weathering of chromium (Cr)-containing solids and the reverse weathering of silicon (Si)-containing solids (e.g. biogenic silica), in order to characterize interfacial reactions at the molecular to microscopic scale, and ultimately interpret macroscopic and field scale phenomena.

The choice of the first model system, the weathering of Cr-containing solids, was motivated by missing information regarding Cr(III) transport and fate. Because of its utility

in many industrial processes, Cr has become the second most abundant metal contaminant in the United States. In addition, the Cr isotope system has recently emerged as a potential paleoproxy for tracking redox processes at Earth's surface. The current paradigm for Cr cycling suggests that Cr mobilization is dominantly redox-dependent. Few studies have examined the effect of environmentally relevant organic molecules on the complexation and redox-independent mobilization of Cr(III) from its solid phase host. This study investigated the stability of Cr(III)-containing solids in the presence of common microbial exudates, siderophores and small organic acids (Chapter 2). Microbially-mediated Cr(III) release from the solid phase was promoted via two redox-independent processes, ligand complexation and increased solid solubility. This dissolution process was also accompanied by a range of Cr isotope signatures that were within the range of previously observed Cr isotope signatures in rock records linked to Cr redox cycling (Chapter 3). Thus, ligand-promoted dissolution of Cr-containing solid phases, a redox-independent process, must be considered when using Cr isotope signatures to diagnose redox-dependent processes.

The second model system, the reverse weathering of Si-containing solids, was motivated by gaps in knowledge regarding the global Si cycle. Despite the abundance and necessity of Si in marine environments, aspects of the global Si cycle remain poorly constrained, such as the (de)coupling of biogenic silica from carbon (C) cycle and the fate of biogenic silica produced in surface ocean waters. This study constrained the composition of organic matter produced by siliceous microbes as well as the transformation of biogenic silica under controlled simulated sedimentary conditions. Freshly produced dissolved organic matter derived from diatoms grown under varying nutrient regimes was extracted

and characterized (Chapter 4). Nutrient regime was found to influence the amount and composition of freshly produced dissolved organic matter, which provides insights into the composition and bioavailability of dissolved organic matter under forecasted shifts of nutrient regimes in certain ocean regions. Furthermore, the geochemical and mineralogical factors controlling the extent and rate of biogenic silica transformation into aluminosilicate minerals were examined (Chapters 5 and 6). Bulk aqueous analyses and solid phase characterizations indicate the surface alteration of biogenic silica to Fe-rich aluminosilicate phases under simulated sedimentary conditions.

Overall, the results of this dissertation provide further advances in addressing knowledge gaps regarding microbe-mineral interactions in these two model systems. Reaction kinetics, product characterization, and parameters that control these factors were systematically addressed. Using a suite of complementary approaches, a mechanistic understanding of microbe-mineral interactions can be elucidated.

1. INTRODUCTION

1.1 Microbe-mineral interactions

Biogeochemical processes that control the transport and fate of nutrients and contaminants in the environment are often driven and mediated by the interplay between microbial (e.g. archeal, bacterial, algal, and fungal) activities and mineral (trans)formations (Ehrlich, 1996; Gadd, 2010; Miot et al., 2014). Critical microbe-mineral interactions include biomineralization and bioweathering, both of which can occur through direct and indirect mechanisms and alter the mobility of dissolved species (Gadd, 2010). Biologically-induced (i.e. indirect) mineralization occurs when an organism promotes chemical precipitation of minerals by modifying its surrounding environment, whereas biologically controlled (i.e. direct) biomineralization occurs under metabolically controlled processes (Lowenstam, 1981). Similarly, direct and indirect mechanisms are involved in the bioweathering processes of minerals (Gadd, 2010). Direct bioweathering occurs through mechanical deterioration of minerals (Goudie, 1996). Microbially-mediated (i.e. indirect) bioweathering is believed to be more significant (Gadd, 2010) and occurs through the excretion of protons, organic acids, and other metabolites (Ehrlich, 1998).

Microbe-mineral interactions have demonstrated importance in both environmental and geological settings (Gadd, 2010). Remediation techniques commonly exploit biomineralization as an *in situ* mechanism for removing dissolved species from groundwater (Macaskie, 1991). Similarly, bioweathering has been utilized to solubilize and remove contaminants in soils (Gadd, 2010). Furthermore, biogenic minerals are quantitatively significant in geological deposits and subsurface sediments (Fortin and

Langley, 2005), and bioweathering has been demonstrated to be significant in soil formation (Tazaki, 2006).

The pervasiveness of microbe-mineral interactionshas motivated this investigation of the factors controlling the characteristics of minerals that are subject to biomineralization and/or bioweathering (Templeton and Knowles, 2009). Determining how microorganisms directly and indirectly affect elemental speciation can improve the predictive assessment of numerous biogeochemical cycles. Current knowledge gaps include the degree to which microorganisms participate in mineral weathering reactions, and associated impacts on the rates and extent of mineral dissolution, chemical exchange with aqueous solutions, as well as the stability, structure, and composition of the new mineral phases that may form (Templeton and Knowles, 2009). To address these questions, systematic approaches must be taken to constrain the mechanisms involved in microbe-mineral interactions under both controlled laboratory conditions and in the field. Reaction kinetics, product speciation, and parameters that control these factors need to be measured, in order to ultimately include those parameters in predictive biogeochemical models (Miot et al., 2014). Thus, mechanistic understanding of microbe-mineral interactions requires a combination of complementary approaches to address these questions including both the solution and solid phase perspectives (Templeton and Knowles, 2009).

1.2 Analytical techniques

Measuring the rate and stoichiometry of dissolution and/or (trans)formation offers quantitative predictive power (Stumm, 1992). These constraints are probed by characterizing the concentration and speciation of the aqueous phase. Techniques utilized

in this dissertation to measure concentrations and speciation of aqueous species include quadrupole-inductively coupled plasma-mass spectrometry (Q-ICP-MS) and UV/visible (UV/vis) spectrophotometry. Furthermore, isotopic signatures of dissolved compounds can act as particularly sensitive tracers as they occur generally at low levels of concentration and can be affected by chemical and physical fractionation effects shifting their signatures (Baskaran, 2012). The isotopic composition of dissolved species in this dissertation was measured using multiple collector-inductively coupled plasma-mass spectrometry (MC-ICP-MS). Specific applications of these techniques are detailed in each respective chapter.

Solid phase analyses characterize the initial phase and (trans)formation product(s) of these reactions and are probed by a suite of complementary techniques. X-ray powder diffraction (XRD), which is based on the interference pattern of X-rays scattered by atoms, offers phase characterization (i.e. crystallinity) and identification (Ginder-Vogel and Sparks, 2010). Both laboratory- (i.e. X-rays generated by high voltage applied to anode) and synchrotron- (i.e. X-rays generated by accelerating electrons and changing their direction) based XRD were applied in this dissertation. Synchrotron XRD is advantageous over laboratory XRD for poorly crystalline materials and/or small sample sizes because of increased sensitivity and resolution (Ginder-Vogel and Sparks, 2010). Another synchrotron-based scattering technique, pair distribution function (PDF) of X-ray total scattering, which determines the probability of finding atomic pairs at specific distances, is also advantageous for materials lacking long-range order. X-ray absorption spectroscopy (XAS), which uses excitation and subsequent relaxation of core electrons to generate characteristic X-rays, is an element specific technique capable of providing information on the local geometric and electronic structure of an atom (Penner-Hahn, 2001). Scanning

electron microscopy (SEM), which is based on scattered electrons, offers morphological characterization and, when coupled to energy dispersive x-ray spectroscopy (EDX), can offer elemental composition information (Ginder-Vogel and Sparks, 2010). Transmission electron microscopy (TEM), which probes transmitted electrons, can be coupled to EDX, selected area electron diffraction (SAED), or electron energy loss spectroscopy (EELS) to reveal compositional information on both the interior and surface of the solid phase, as well as to detect the formation of new phases that may be present in trace amounts (Leonard et al., 2002). Nuclear magnetic resonance (NMR) spectroscopy offers molecular structure information of specific elements that have a static magnetic field (Ginder-Vogel and Sparks, 2010). Fourier transform infrared (FT-IR) spectroscopy is a vibrational spectroscopy technique based on the absorption of energy at different frequencies by a sample (Simonescu, 2012). Each technique is employed to answer different questions, which is specifically described in each chapter.

1.3 Chromium system

Beginning with the mass utilization of chromium (Cr) plating during World War II and continuing in pigment and dye manufacturing, steelworks, leather tanning, and wood preservation industries, Cr has become the second most common metal contaminant in the United States (EPA, 2000). Cr contamination results from byproducts of ore processing and leaks during manufacturing, storage, and disposal (Palmer and Wittbrodt, 1991). Additionally, Cr isotopes have recently emerged as a potential proxy for tracking redox processes at Earth's surface (Crowe et al., 2013; Frei et al., 2009; Planavsky et al., 2014). The current paradigm for Cr cycling, which forms the basis of both Cr remediation strategies and the Cr isotope system as a paleobarometer, suggests that Cr mobilization and

isotopic fractionation are predominantly redox dependent (Ellis et al., 2004; Johnson and Bullen, 2004; Schauble et al., 2004). However, few studies have examined redox-independent mobility and isotope fractionation of Cr. This dissertation examines the role of microbial activities (e.g. common microbial exudates) on the redox-independent mobilization and isotope fractionation of Cr(III).

1.3.1 Chromium geochemistry

The most common valence states of chromium in nature are Cr(III) and Cr(VI) (Richard and Bourg, 1991), which exhibit different geochemical properties (Rai et al., 1989). Cr(III) is highly immobile and primarily forms octahedral complexes (Kotas and Stasicka, 2000). In oxic environments, Cr speciation is dominated by the mobile and bioavailable Cr(VI), which exists most commonly as the tetrahedrally coordinated oxyanions, $HCrO_4^-$ and CrO_4^{2-} (Rai et al., 1989). While Cr(III) is an essential micronutrient, Cr(VI) is toxic because it is a strong oxidant that releases free radicals during intracellular reduction to Cr(III). Cr(VI) also coordinates with organic compounds, which may inhibit the function of other metal centered enzymes (Kotas and Stasicka, 2000).

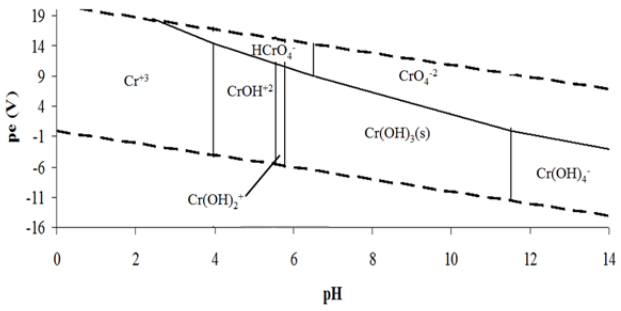

Figure 1.1 Thermodynamic stability diagram for 10^{-6}M Cr (data from Ball and Nordstrom, 1998).

The redox chemistry of Cr in nature is controlled by few natural systems because of the high redox potential of the Cr(VI)/Cr(III) couple. The rate of Cr(III) oxidation by oxygen in nature is slow therefore not a common oxidation pathway; however, manganese oxides are effective and are considered the most significant natural oxidants of Cr(III) to Cr(VI) (Rai et al., 1989). Fe(II) is the most effective reducing agent of Cr(VI) in natural systems, the overall reaction of which is shown in Equation 1, and precipitate as in Equation 2 (Fendorf, 1995).

$$Cr(VI)_{(aq)} + 3Fe(II)_{(aq)} \leftrightharpoons Cr(III)_{(aq)} + 3Fe(III)_{(aq)} \quad (1)$$

$$xCr(III)_{(aq)} + (1 - x)Fe(III)_{(aq)} + 3H_2O \leftrightharpoons (Cr_xFe_{1-x})(OH)_{3(s)} + 3H^+ \quad (2)$$

Organic matter may also reduce Cr(VI) to Cr(III). However, this reduction pathway often leads to soluble Cr(III)-organic complexes, rather than immobile Cr(III) as is the case with Fe (Fendorf, 1995). Chromium fate in the subsurface is ultimately controlled by solubility controlling solid phases. Thus, the Cr(III) product of Cr(VI) reduction must be assessed for their stability in order to constrain chromium fate and transport (Blowes, 2002).

1.3.2 Chromium isotope systematics

Chromium occurs in four stable isotopes, ^{50}Cr, ^{52}Cr, ^{53}Cr, and ^{54}Cr, in the abundances of 4.3, 83.8, 9.5, and 2.4%, respectively (Johnson, 2011). Cr isotopes undergo mass-dependent fractionation, during which chemical processes shift the relative abundances of heavy isotopes relative to lighter isotopes. Most studies utilize the $^{53}Cr/^{52}Cr$

ratio, which provides a mass difference of approximately 2‰ (Johnson, 2011). These shifts are expressed as ratios of abundances as is expressed in Equation 3 (Wasylenki, 2012).

$$\delta^{53}\mathrm{Cr}\ (‰) = \left[\frac{\left(\frac{^{53}\mathrm{Cr}}{^{52}\mathrm{Cr}}\right)_{\mathrm{Sample}}}{\left(\frac{^{53}\mathrm{Cr}}{^{52}\mathrm{Cr}}\right)_{\mathrm{Standard}}} - 1 \right] \times 1000 \qquad (3)$$

Current experimental and theoretical evidence suggest that redox processes result in the most significant Cr isotope fractionation because of significant changes in the local coordination environment (Ellis et al., 2002; Schauble et al., 2004). Furthermore, most likely due to the multi-electron transfer involved in this redox process requiring a long time to reach equilibrium, Cr has only been observed to follow kinetic fractionation during redox transformations, during which the light isotope is preferentially reacted first. Characterization is more tightly constrained on Cr(VI) reduction than on Cr(III) oxidation and suggests that reduction occurs with greater fractionation than oxidation. However, both processes appear to result in ^{53}Cr enriched Cr(VI) (Johnson, 2011).

1.4 Silica system

Silicon (Si), most environmentally relevant as silica (SiO_2), is the second most abundant element in the Earth's crust. In fact, silicate minerals comprise >90% of crustal minerals (Struyf et al., 2010). Si is also an essential element to many marine organisms (Treguer and De La Rocha, 2013). Despite the abundance and necessity of Si, only since the late twentieth century have processes controlling the marine biogeochemistry of silicon been quantified (e.g. (Nelson et al., 1995; Ragueneau et al., 2010)). Several components of the global Si cycle, such as the decoupling of Si from carbon (C) and the ultimate fate of

biogenic silica especially in coastal sediments, remain poorly constrained (Nelson et al., 1995), which results in an apparently unbalanced global biogeochemical Si cycle(Treguer and De La Rocha, 2013). Thus, this dissertation seeks to constrain the composition of organic matter produced by siliceous marine organisms and the early diagenetic transformations of biogenic silica.

1.4.1 Marine silica cycle

The ocean is a major global reservoir of Si with a marine residence time of ~ 10,000 years, compared to a terrestrial residence time of ~775 years (Laruelle et al., 2009). The primary input of Si to the ocean from continental weathering is delivered through rivers (Ragueneau et al., 2010), which transport dissolved silica as silicic acid, H_4SiO_4 (Gerard et al., 2002). Dissolved silica is also delivered to the ocean by submarine groundwater discharge, aeolian inputs, hydrothermal inputs, and dissolution of terrigenous material in marine sediments, albeit to a much less contribution than riverine discharge in most regions (DeMaster, 2002), resulting in a total net input of ~ 9.4 ± 4.7 Tmol Si $year^{-1}$. Removal of Si from the ocean reservoir occurs primarily through the burial of biogenic silica in sediments, and, to a lesser extent, through precipitation of dissolved Si as amorphous silica in hydrothermal vent plumes and transformation of biogenic Si to authigenic aluminosilicates, resulting in a total net output of ~ 9.9 ±7.3 Tmol Si $year^{-1}$ (Treguer and De La Rocha, 2013).

Early diagenetic processes in continental marine sediments may act as a major control on the biogeochemical cycling of Si (Mackenzie and Garrels, 1966). Although coastal regions only contribute to 18% of marine Si fixation (e.g. transformation of

dissolved silica to biogenic silica), coastal sediments are responsible for the burial of 40% of all marine biogenic silica (Laruelle et al., 2009). Increased land use (e.g. changes from forests to farmlands) over the past 400 years created an initially increased load of Si into rivers, and subsequently into the ocean, from the depletion of the soil reservoir (Struyf et al., 2010). Increased land use and the resultant increase in continental weathering in Africa and South America, for example, threaten to further perturbate the marine Si cycle (Treguer and De La Rocha, 2013). Additionally, the anthropogenic increase in river damming results in decreased dissolved Si concentrations in rivers and estuaries by trapping particulate and easily soluble silica as dams retain one third of global sediment discharge (Ittekkot et al., 2006). Damming increases the residence time of water in river reservoirs, which has been shown to increase primary productivity in these reservoirs. This extended residence time promotes the conversion of dissolved Si to biogenic Si, and consequently increases non-bioavailable Si delivery to oceans (Humborg et al., 1997).

1.4.2 Coupled silica-carbon cycles

The marine Si cycle is further influenced by the tight coupling between Si with other nutrients. Diatoms are unicellular, photosynthetic eukaryotes with a siliceous cell wall (Nelson et al., 1995) composed of hydrated amorphous silica, which is mineralogically characterized as biogenic opal-A (Van Cappellen, 2003). Through diatoms, the fate of Si is strongly coupled to the fate of C. Diatoms are the most significant contributor to silica fixation (Treguer and De La Rocha, 2013) as well as major contributors to marine primary production (40%) and organic carbon export from the photic zone (60%) (Dugdale and Wilkerson, 1998).

The density of diatomaceous silica, 2.0 g cm^{-3} (DeMaster), allows for long term sequestration of carbon and increased CO_2 uptake by the surface ocean through diatom sinking and burial. This potential as a carbon sink is even greater than the sink associated with coccolithophore production and sinking because diatom diagenesis does not release CO_2 (Van Cappellen, 2003). Consequently, the Si cycle is strongly coupled to atmospheric CO_2 (Treguer and De La Rocha, 2013). Furthermore, the primary input of Si to the ocean results from chemical weathering of crustal silicate minerals by dissolved CO_2. Hence, even the source of dissolved Si to oceans plays a role in carbon sequestration (Gerard et al., 2002), serving as a negative feedback for atmospheric CO_2 (Berner et al., 1983).

1.4.3 Silica solubility in the marine environment

The external cell wall of diatoms is coated with an organic material that prevents diatom dissolution in ocean water, which is undersaturated with respect to silica (DeMaster 2003). After diatom death, the degradation of this organic casing significantly controls the dissolution rate of the diatom frustule. Organic casing degradation occurs by either zooplankton grazing or, more significantly, by marine bacterial degradation through hydrolytic attack of the organic material (Bidle and Azam, 1999). Organic membrane deterioration is considered to complete within a few days of cell death (Grill and Richards, 1964). Once the silica frustule is exposed to undersaturated seawater, dissolution rate is increased to five times of that with the organic casing intact (Bidle and Azam, 1999).

Several factors, both compositional and environmental, influence biogenic silica solubility. The substitution of aluminum (Al) for Si in the frustule during biosynthesis significantly affects frustule solubility in the water column (Gehlen et al., 2002), decreasing

the solubility of the frustule from ~ 1 to ~ 0.6 mM at an Al/Si ratio of 0.6×10^{-3} to 7×10^{-3} (VanBennekom et al., 1991). Al content in the cell corresponds to the Al/Si ratio in ambient sea water, which results in lower solubility of diatoms in coastal waters where Al concentrations are higher. However, this compositional ratio has also been demonstrated to be species dependent (Gehlen et al., 2002).

Approximately half of the biogenic silica produced in the photic zone dissolves without being exported to the seabed (Treguer and De La Rocha, 2013). Of this dissolved silica, 97% is recycled and sequestered by diatoms (Struyf et al., 2010). Of this recycled dissolved Si, 60% is recycled within the first 100 m of the water column (Nelson et al., 1995). An incomplete recycling suggests that the remaining 3% of dissolved silica is required to be supplemented by other inputs in order to maintain diatom production at a steady state (Treguer and De La Rocha, 2013), reaffirming the impacts of altering river delivery of silica to the ocean.

In fact, about 10% of the biogenic silica produced in the photic zone actually reaches the seabed, and 3% of that fraction is buried (Treguer and De La Rocha, 2013). The balance between dissolution and burial controls marine silica concentrations (Gehlen et al., 2002). Burial of biogenic silica acts as the primary sink in the marine reservoir for the influx of dissolved and biogenic silica from rivers. However, the silica concentrations in pore waters are lower than thermodynamically predicted based on amorphous silica equilibrium (Van Cappellen, 2003).

Silicic acid concentrations increase with sediment depth until reaching an asymptote with no further dissolution (Hurd, 1973). Decreased reactivity at a certain depth

most likely reflects mineralogical alterations that reduce surface defect density. In fact, kinetic data demonstrates that amorphous silica dissolution is controlled by localized dissolution on surface defects, for example in the pores of the frustules (VanCappellen and Qiu, 1997b). Sediment pore water concentrations of Si reach an asymptotic value around 200-800 μM, which is much less than the saturation concentration (~ 1 mM) driven by amorphous silica dissolution (Hurd, 1973). This asymptotic behavior cannot be explained by solubility differences or sequential dissolution of more reactive silica aging to less reactive silica (VanCappellen and Qiu, 1997a). These profiles are best explained by early diagenetic processes (Van Cappellen et al., 2002). Consequently, other mineral phases from reprecipitation of silica may then be significant in marine sediments (Schink et al., 1975).

In fact, the strongest control on pore water silica profiles is the ratio of biogenic silica to detrital material (Van Cappellen, 2003), which releases dissolved Al. Dissolved Al prevents pore waters from reaching saturation with biogenic silica through simultaneous reprecipitation of dissolved Al with dissolved silica. This interaction increases the preservation of biogenic silica in sediments by reducing silica solubility (Van Cappellen et al., 2002). When soluble Al^{3+} concentrations reach some threshold, precipitation of distinct aluminosilicate phases is observed. The formation of mineral phases distinct from biogenic silica accounts for the concentration of silicic acid in pore waters below the reduced saturation concentration of Al incorporation into the silica (Johnson and Grimm, 2001). Thus, the silicic acid profile is best explained by the precipitation of authigenic aluminosilicate minerals (Dixit et al., 2001).

1.4.4 Reverse weathering

The higher the ratio of detrital material to biogenic silica in marine sediments, the more extreme the departure of pore water silicic acid from thermodynamic saturation with biogenic silica. This correlation is most likely due to authigenic clay mineral formation (Van Cappellen et al., 2002). Authigenic clay mineral formation in marine sediments is referred to as reverse weathering because this process produces CO_2 with mineral formation instead of consuming CO_2 as in the weathering of primary minerals on land (Mackenzie and Kump, 1995).

Reverse weathering was initially proposed as a way to rectify the imbalance between the sources and sinks of some major marine elements. The mass balance between the sources and sinks of Mg^{2+}, K^+, HCO_3^-, and H_4SiO_4 indicate additional and traditionally unconstrained sinks. Specifically, nearly all river inflow of Mg^{2+}, K^+, and H_4SiO_4 is not accounted for in the formation of major authigenic minerals in marine sediments, such as halite, calcite, anhydrite, pyrite, and opal. Furthermore, only 25% of the HCO_3^- input from rivers is accounted for in the balance between weathering and marine $CaCO_3$ precipitation (Mackenzie and Garrels, 1966). The proposed neglected sink was the reverse weathering reaction,

$$\text{biogenic silica} + \text{detrital Al} + \text{Fe oxides} + \text{cations} + HCO_3^- \rightarrow \text{authigenic clays} + CO_2 \quad (4)$$

during which biogenic Si and detrital Al react to form cation rich authigenic clay minerals and release CO_2 (Mackenzie and Garrels, 1966). In fact, thermodynamic calculations demonstrate that Mg- and K-rich clay minerals are thermodynamically stable at the pH of sea-water. These results imply that upon entering seawater, ion-poor clay minerals (such as kaolinite) could undergo alteration by consuming cations, specifically K^+ and Mg^{2+}, to

form more cation rich mineral phases (Helgeson and Mackenzi.Ft, 1970). Upon delivery to oceans, clay minerals undergo transformation reactions, for example cation exchange reactions, that most often occur in estuaries and the coastal ocean due to the difference in cation concentrations between river and marine water (Libes, 2009).

The proposed transformation of biogenic silica through the reverse weathering pathway may resolve the imbalance in the mass balance of Mg^{2+}, K^{+}, and HCO_3^{-} and also explain the pore water profiles of H_4SiO_4. In order to completely account for the missing sinks, authigenic clays would need to constitute approximately 7% of total sedimentary mass (Murray, 1993).While most clay minerals in marine sediments are of detrital origin (Drever, 1971), in the Amazon River delta alone, authigenic clay formation is responsible for up to 10% of the missing sinks (Michalopoulos and Aller, 1995). Furthermore, the original mass balance does not account for hydrothermal reactions in regions of seafloor spreading (Mackenzie and Garrels, 1966), so reverse weathering may need to account for even less of the missing sinks than originally proposed

1.5 Research scope and objectives

The work presented in this dissertation seeks to constrain components of biogeochemical cycles from an analytically intensive perspective that includes aqueous phase analyses (e.g. establishing the thermodynamic and kinetic controls of a system) and solid phase analyses (e.g. structural and morphological evolutions) of two model systems, the weathering of Cr-containing solids and the reverse weathering of Si-containing solids (e.g. biogenic silica), in order to characterize interfacial reactions at the molecular to microscopic scale, and ultimately interpret macroscopic and field scale phenomena.

Chapters 2 and 3 address the Cr system and detail experiments that seek to examine and constrain the microbially-mediated weathering of Cr(III)-containing solids. Specifically, the kinetics and transformation products during the bioweathering of Cr(III)-Fe(III)-(oxy)hydroxides by ubiquitous microbial exudates (siderophores and small organic acids) are examined in Chapter 2. Chapter 3 presents a survey of the effects of common environmental ligands on the dissolution and isotope fractionation of Cr(III)-(oxy)hydroxide. Chapters 4-6 address the Si system and detail experiments that seek to 1) provide insight into the composition of freshly produced dissolved organic matter supplied to marine systems by diatoms, and 2) constrain the kinetics, controls, and (trans)formation products of diatom-derived biogenic silica during early diagenetic processes under controlled laboratory conditions. Chapter 4 demonstrates the nutrient-dependence on the composition of diatom-derived dissolved organic matter. Chapter 5 offers a quantitative comparison and assessment of organic matter removal methods on biogenic silica in order to assess their efficacy for use in reactivity studies. Finally, Chapter 6 investigates the mechanism and kinetics of the transformation of biogenic silica during early diagenesis and provides detailed structural characterization of the reaction product(s).

2. SIDEROPHORE AND ORGANIC ACID PROMOTED DISSOLUTION AND TRANSFORMATION OF CR(III)-FE(III)-(OXY)HYDROXIDES

2.1 Abstract

The role of microbial activities on the transformation of chromium (Cr) remediation products has generally been overlooked. This study investigated the stability of Cr(III)-Fe(III)-(oxy)hydroxides, common Cr(VI) remediation products, with a range of compositions in the presence of common microbial exudates, siderophores and small organic acids. In the presence of a representative siderophore, desferrioxamine B (DFOB), iron (Fe) was released at higher rates and to greater extents relative to Cr from all solid phases. The presence of oxalate alone caused the release of Cr, but not of Fe, from all solid phases. In the presence of both DFOB and oxalate, oxalate acted synergistically with DFOB to increase the Fe, but not the Cr, release rate. Upon reaction with DFOB or DFOB + oxalate, the remaining solids became enriched in Cr relative to Fe. Such incongruent dissolution led to solid phases with different compositions and increased solubility relative to the initial solid phases. Thus, the presence of microbial exudates can promote the release of Cr(III) from remediation products via both ligand complexation and increased solid solubility. Understanding the potential reaction kinetics and pathways of Cr(VI)

Saad EM, Sun JY, Chen S, Borkiewicz OJ, Zhu MQ, Duckworth O, Tang YZ. Siderophore and organic acid promoted dissolution and transformation of Cr(III)-Fe(III)-oxyhydroxides. *Environmental Science & Technology*. 2017, 51 (6), 3223–3232.

remediation products in the presence of microbial activities is necessary to assess their long-term stability.

2.2 Introduction

Chromium (Cr) is a significant contaminant in the United States (EPA, 2000) and around the globe. The most common valence states of Cr in soils and natural waters are Cr(III) and Cr(VI) (Richard and Bourg, 1991). Under oxic conditions, Cr speciation is dominated by the highly soluble and mobile Cr(VI) species, chromate (CrO_4^{2-}) and bichromate ($HCrO_4^{2-}$) (Rai et al., 1989). Due to its higher bioavailability and strong oxidizing capability, Cr(VI) exhibits a toxicity threat that is 100 times greater than that of Cr(III) (Norseth, 1981). Contrastingly, under circumneutral pH conditions, Cr(III) is traditionally considered insoluble and stable (Rai et al., 1989). A wide range of reactants are capable of reducing Cr(VI) to Cr(III), including biotic (e.g. dissimilatory metal reducing microbes) (Francis et al., 2000; Fredrickson et al., 2000; Lovley and Phillips, 1994; Tebo and Obraztsova, 1998) and abiotic (e.g. sulfide, Fe(0), Fe(II), and organic compounds) (Deng and Stone, 1996; Eary and Rai, 1988; Pettine et al., 1998; Pettine et al., 1994; Wittbrodt and Palmer, 1995) pathways. The common reduction products are either pure Cr(III)-(oxy)hydroxides or a mixed Cr(III)-Fe(III)-(oxy)hydroxide solid solution series in the presence of iron (Fe) and due to the structural similarities between Cr(III) and Fe(III) (Eary and Rai, 1988; Sass and Rai, 1987; Tang et al., 2010). These (oxy)hydroxides are sparingly soluble (Sass and Rai, 1987) and are typically considered as the ultimate sink of Cr in subsurface environments (Richard and Bourg, 1991).

Cr(III) can be oxidized by ubiquitous manganese (Mn) oxides to Cr(VI), which leads to contamination (Bartlett and James, 1979). Studies have shown that the oxidation kinetics of Cr(III) by Mn oxides are affected by Cr speciation (e.g. soluble Cr(III) or Cr(III)-organic complex vs solid $Cr(OH)_3$) (Bartlett and James, 1979; Carbonaro and Stone, 2015; Fendorf, 1995; James and Bartlett, 1983; Namgung et al., 2014; Yang et al., 2014). Thus, understanding the potential solubilization mechanisms of Cr(III)-containing solids under environmental conditions and their subsequent oxidation efficiency by Mn oxides is critical for constraining the fate of Cr in the subsurface (Papassiopi et al., 2014) and evaluating the long-term efficiency of biotic/abiotic Cr(VI) remediation techniques.

Siderophores and small organic acids are both ubiquitous organic molecules produced by a wide range of microorganisms (e.g. bacteria and fungi) and plants (Ahmed and Holmstrom, 2014; Gadd, 2000) and are often co-exuded (Cheah et al., 2003; Reichard et al., 2007). Siderophores are organic chelating agents with a high affinity for Fe(III) and can facilitate Fe solubilization and bioavailability from low solubility Fe(III)-containing mineral phases (e.g. hematite) (Neilands, 1995). Siderophores have also been shown to have strong affinities for other trivalent metal cations, such as Cr(III), Mn(III), and Co(III), due to their structural (i.e. coordination) similarity to Fe(III) (Budzikiewicz et al., 2002; Duckworth et al., 2009; Parker et al., 2004). A wide range of common organic acids (e.g. oxalic, citric, fulvic, and humic acids) have been demonstrated to complex with Cr(III) (Gustafsson et al., 2014; James and Bartlett, 1983; Srivastava et al., 1999; Walsh and Ohalloran, 1996). In fact, measurements on natural waters, including sites with anthropogenic contaminations, revealed concentrations of dissolved Cr(III) above the solubility of $Cr(OH)_3$ in the absence of organic chelating agents, which was suggested to

be due to the complexation of Cr(III) with organic molecules (Ahern et al., 1985; Icopini and Long, 2002; Kaczynski and Kieber, 1994; Nakayama et al., 1981). Both siderophores (e.g. desferrioxamine B, rhizoferrin, protochelin) (Duckworth et al., 2014) and organic acids (e.g. citric acid, ethylenediaminetetraacetic acid, nitrilotriacetic acid) (Carbonaro et al., 2008) were recently shown to be capable of solubilizing Cr(III) from the pure Cr(III)-(oxy)hydroxide solid phase under environmentally relevant conditions. However, to our knowledge no studies have examined the solubilization of the mixed Cr(III)-Fe(III)-(oxy)hydroxide solid solution series by these common organic molecules, as well as the transformation of the solid phases upon reaction. Interestingly, the co-existence of siderophores and small organic acids can have positive, neutral, or negative effects on trivalent metal oxide dissolution rate, depending on the metal oxide type, siderophore type, and solution conditions (Duckworth et al., 2014; Reichard et al., 2007; Saal and Duckworth, 2010). Such information is missing for the mixed Cr(III)-Fe(III)-(oxy)hydroxide phases.

In this study, we investigated the dissolution of the Cr(III)-Fe(III)-(oxy)hydroxide solid solution series in the presence of a representative siderophore, desferrioxamine B (DFOB), and the common biogenic organic acid, oxalate. The compositional and structural evolutions of the solid phases were also monitored using a suite of complementary spectroscopic and microscopic techniques. Results from this study provide important insights on the long-term stability of Cr remediation products in the presence of microbial activities.

2.3 Experimental Methods

2.3.1 Synthesis of Cr(III)-Fe(III)-(oxy)hydroxides

Representative samples from the Cr(III)-Fe(III)-(oxy)hydroxide solid solution series, hereafter referred to as $Cr_xFe_{1-x}(OH)_3$, were synthesized following previous procedures with x = 0, 0.2, 0.5, 0.8, and 1 (Tang et al., 2010). These samples are referred to as Fe10, Cr2Fe8, Cr5Fe5, Cr8Fe2, and Cr10, respectively (Table A.1). Briefly, $Fe(NO_3)_3 \cdot 9H_2O$ and $Cr(NO_3)_3 \cdot 9H_2O$ (both ACS grade) were dissolved in deionized water (18 MΩ cm) to obtain a total metal concentration of 0.1 M with desired Cr(III):Fe(III) molar ratios. The solutions were slowly titrated to pH 7 with 1 M NaOH. Precipitates formed from the suspension were aged for 24 h followed by dialysis to remove remaining electrolytes. The resulting wet pastes were recovered, freeze dried, and finely ground. Portions of the powders were dissolved in nitric acid for analysis of Cr and Fe compositions by inductively coupled plasma-mass spectroscopy (ICP-MS). Specific surface area of each dried solid was determined by Brunauer–Emmett–Teller (BET) gas adsorption analysis using an Autosorb-1-MP surface pore analyzer (Quantachrome Corp.) (Table A.1).

2.3.2 Ligand solubilization experiments

Stabilities of the synthesized $Cr_xFe_{1-x}(OH)_3$ solids were investigated in the presence or absence of a representative siderophore, DFOB, and/or a representative small organic acid, oxalate. The solids (0.2 g/L) were suspended in a 0.1 M NaCl electrolyte solution with 10 mM 4-(2-hydroxyethyl)-1-piperazineethanesulfonic acid (HEPES, high purity grade) buffer at pH 7 and sonicated for 15 min. This buffer has been previously shown to not influence the rates of siderophore promoted dissolution of metal hydroxides (Bi et al., 2010; Cheah et al., 2003; Duckworth et al., 2014). After addition of the solid, the suspensions were sonicated for 15 min to disperse particles. For the treatments containing

oxalate, oxalic acid (ACS grade) was added to the suspension to achieve a final concentration of 0.1 or 1 mM. For the treatments containing DFOB, a mesylate salt of DFOB (Sigma-Aldrich) was added to the suspensions for a final DFOB concentration of 0.1 mM. For the treatments containing both DFOB and oxalate, oxalic acid was added 1 min prior to DFOB addition in order to account for the potential effect of oxalate on metal hydroxide dissolution during the initial duration of exposure to oxalate (Reichard et al., 2007). Each treatment was conducted in duplicate in batch reactors in the dark by using amber bottles or by wrapping the reaction bottles in aluminum foil. Reaction bottles were constantly agitated at room temperature on an orbital shaker.

Aliquots of each sample were collected throughout a time series, syringe filtered (0.2 μm, cellulose acetate, VWR), and analyzed for total dissolved Cr and Fe concentrations by ICP-MS. The formation and concentration of Fe(III)-DFOB complex was monitored at 430 nm by UV/visible (UV/vis) spectroscopy (Cary 60, Agilent) (Albrecht-Gary and Crumbliss, 1998). Cr(VI) concentration in the filtrates was analyzed using the diphenylcarbazide assay by UV/vis at 540 nm (Bartlett and James, 1979) and was below the detection limit for all treatments. Thus, the total dissolved Cr concentration in the filtrate was considered to be Cr(III). The pH value of each suspension stayed at 7.0 ± 0.1 throughout the entire experiment for all treatments. No microbial growth was observed for the duration of the experiment. Release rates were determined by fitting a regression line through the dissolution profile over the same time frame (21 days) for each condition and normalizing to BET surface area of each solid. Additionally, mass normalized dissolution rates are also presented as the BET measured specific surface area of non-crystalline solid phases may be limited by the size of the gas molecule used (Brunauer et al., 1938) and underestimated due to increased aggregation (Anschutz and Penn, 2005; Villalobos and Antelo, 2011) and surface decomposition during degassing (Davis and Leckie, 1978). Uncertainty estimates represent the variance of the rate determined from

regression analysis and error from duplicates. At the end of the experiment, the reacted solids were freeze dried and characterized using X-ray absorption spectroscopy (XAS), pair distribution function (PDF) analysis of X-ray total scattering, and high resolution transmission electron microscopy (HRTEM).

2.3.3 Synchrotron X-ray scattering analysis of solid phases

High-energy X-ray total scattering data of both pristine and reacted $Cr_xFe_{1-x}(OH)_3$ samples were collected at beamline 11-ID-B (~58.6 keV, λ = 0.2117 Å) of the Advanced Photon Source (APS), Argonne National Laboratory, IL. Conversion of data from 2D to 1D was performed using the program Fit2D (Hammersley, 1998; Hammersley et al., 1996). The experimental total scattering structure function S(Q), reduced experimental structure function f(Q), and PDF, or G(r), were obtained using PDFgetX2 (Qiu et al., 2004). Compositions used for the normalization of the experimental structure functions are included in Table A.1. Since there are currently no detailed structure models for the compositional series, we adopted a self-consistent method assuming the general formula of $(Cr,Fe)_2O_3 \cdot nH_2O$ for all samples. Information obtained regarding the Fe:Cr ratio of the unreacted solids (from ICP-MS analysis) was incorporated in the compositions used for PDF normalization. Total hydration information from thermal gravimetric analysis (TGA) of the weight loss for the unreacted samples (Tang et al., 2010) was used for estimating the hydration states of all other samples and was incorporated in the normalization. This normalization approach resulted in consistent reduced structure functions for all samples, and the PDFs were calculated from the Fourier transforms of these data truncated at 29 $Å^{-1}$. The size of the coherent scattering domain for each sample was estimated from the attenuation of the PDF as a function of r (Å).

2.3.4 Synchrotron X-ray absorption spectroscopy (XAS) of solid phases

Cr and Fe K-edge XAS data were collected for all pristine and reacted samples at beamlines 5-BM-D and 12-BM-B at APS, and beamline 4-1 at Stanford Synchrotron Radiation Lightsource (SSRL), CA. Freeze dried, finely ground sample powders were evenly brushed on Kapton tapes and excess powders were blown off. Several layers of the sample-loaded tapes were stacked to achieve desired thickness. Depending on Cr or Fe concentrations, X-ray absorption near edge structure (XANES) data were collected either in transmission or fluorescence mode (using a Lytle or Vortex detector depending on beamline setup). Energy calibration used Cr or Fe metal foils. A monochromator detuning of 50% were used for both Cr and Fe K-edges to minimize higher-order harmonics. Data processing was performed with the data analysis programs SIXPack50 and Ifeffitm (Ravel and Newville, 2005).

2.3.5 High resolution transmission electron microscopy (HRTEM)

HRTEM images of both pristine and DFOB-reacted $Cr_xFe_{1-x}(OH)_3$ samples (reaction time of 32 days) were taken on a JEOL 2010F TEM. A small amount of each sample was dispersed in ethanol and ultrasonicated for ~1 min. Then, a drop of the suspension was placed onto a 200-mesh Cu grid with a holey-carbon support film and air dried. To avoid beam damage, image focus was obtained on the carbon film adjacent to the particles of interest, and then the beam was moved onto the sample particle. Due to the small crystal sizes (5 nm and less), the electron diffraction is very weak. Therefore, we used fast Fourier transform (FFT) to appraise the diffraction and crystallinity of each sample.

2.4 Results and Discussion

2.4.1 DFOB and/or oxalate mediated solid dissolution

In the absence of DFOB and oxalate (i.e. control experiments), dissolved Fe and Cr remained less than 0.5 µM for all $Cr_xFe_{1-x}(OH)_3$ solids throughout the experiments (30–35 days) (Figure 2.1A). The presence of DFOB and/or oxalate promoted the dissolution of Cr and/or Fe to different extents, as discussed below.

The presence of 0.1 mM DFOB promoted the release of both Fe and Cr from all solid phases as compared to the control experiments, with Fe released at both a higher rate and extent than Cr (Figure 2.1B). For all experiments, Fe concentrations gradually increased until reaching plateaus after ~20 days. At the end of experiments, sample Fe10 released the most Fe into solution (~60 µM), followed by Cr5Fe5 (~30 µM), Cr8Fe2 (~10 µM), and Cr2Fe8 (~5 µM) (Figure 2.1B). All Fe was released as the Fe(III)-$HDFOB^+$ complex (Figure A.1) as expected at pH 7.52 Cr release was slightly promoted in the presence of DFOB as compared to control experiments, with dissolution plateaus reached after ~25 days for all solids except for Cr10, which continued to release Cr through the end of the experiment. At the end of experiments (32 days), Cr10 released the most Cr into solution (~1.5 µM), followed by Cr5Fe5, Cr2Fe8, and Cr8Fe2 (all ~1 µM). No Cr(VI) was detected in all experiments. Thus, the total dissolved Cr was considered Cr(III). We were not able to differentiate Cr(III)-DFOB complex from dissolved Cr(III) because there were no observable spectra for the Cr(III)-DFOB complex by UV/vis spectroscopy (200–800 nm). The absence of spectral features is due to the low molar absorptivity coefficient of the Cr(III)-DFOB complex (λ_{max} < 70 L mol^{-1} cm^{-1}) (Leong and Raymond, 1975) and small concentrations present in this study, as has been previously described (Duckworth et al., 2014). However, by comparing Cr(III) release in the control experiments (Figure 2.1A) and DFOB experiments (Figure 2.1B), the additional release of Cr(III) in the DFOB experiments can be attributed to the complexation between Cr(III) and DFOB, as DFOB has been previously shown to promote the dissolution of $Cr(OH)_3$ through complexation (Duckworth et al., 2014). The higher dissolution rate and extent for Fe relative to Cr from

the solid phases in the presence of DFOB is consistent with the greater stability constant for the Fe(III)-HDFOB^{+} complex ($10^{32.2}$) (Martell and Smith, 2003) relative to that of the Cr(III)-HDFOB+ complex ($10^{30.6}$) (Duckworth et al., 2014). In fact, siderophore-promoted dissolution rates have been shown to correlate with the stability constant of the corresponding aqueous metal-siderophore complex (Akafia et al., 2014). The preferential mobilization of Fe from the solid phases resulted in the enrichment of Cr in the remaining solid phases, which is discussed later. The dissolution rate of the Fe10 endmember (previously described as 2-line ferrihydrite) (Tang et al., 2010) is consistent with previously reported surface area normalized and mass normalized rates of DFOB-promoted dissolution of ferrihydrite (Neubauer et al., 2002) and surface area normalized rates of DFOB-promoted dissolution of goethite (Kraemer et al., 1999; Neubauer et al., 2002; Wolff-Boenisch and Traina, 2007), on the order of 10^{-13} mol $m^{-2}s^{-1}$ and 101 μmol $g^{-1}day^{-1}$, at circumneutral pH and similar experimental conditions (Tables A.2 and A.3). When rates are normalized to surface area, the dissolution of goethite is directly comparable to that of ferrihydrite (Neubauer et al., 2002). The surface area normalized dissolution rate of the Cr10 endmember is an order of magnitude less than the rate reported by Duckworth et al. (Duckworth et al., 2014). This difference in rate may be the result of small differences in experimental conditions and properties of the initial $Cr(OH)_3$ solids.

The effect of oxalate alone on the release of Cr from all solids was dependent on oxalate concentration. The presence of 0.1 mM oxalate did not have a significant impact on Cr release rate and extent (Figure A.2A), whereas 1 mM oxalate (Figure 2.1C) not only enhanced the extent of Cr release (up to ~1-2 μM Cr), but also resulted in continuous increase at 30 days. As a hard acid, Cr(III) forms strong complexes with hard bases, including carboxylate ligands such as oxalate (Pearson, 1963). Oxalate has been shown to adsorb to Cr(III) hydroxide via inner sphere coordination (Degenhardt and McQuillan, 1999), which is the initial step for ligand promoted surface detachment and dissolution

(Loring et al., 2007). Citrate has also been shown to dissolve amorphous $Cr(OH)_3$ at pH ~7 (Carbonaro et al., 2008). Contrastingly, no Fe was released throughout the experimental course in the presence of oxalate alone (Figure 2.1C and A.2A), which is consistent with previous studies that showed negligible dissolution of Fe oxides in the presence of oxalate in the circumneutral pH range (Akafia et al., 2014; Eick et al., 1999; Kraemer, 2004; Loring et al., 2008).

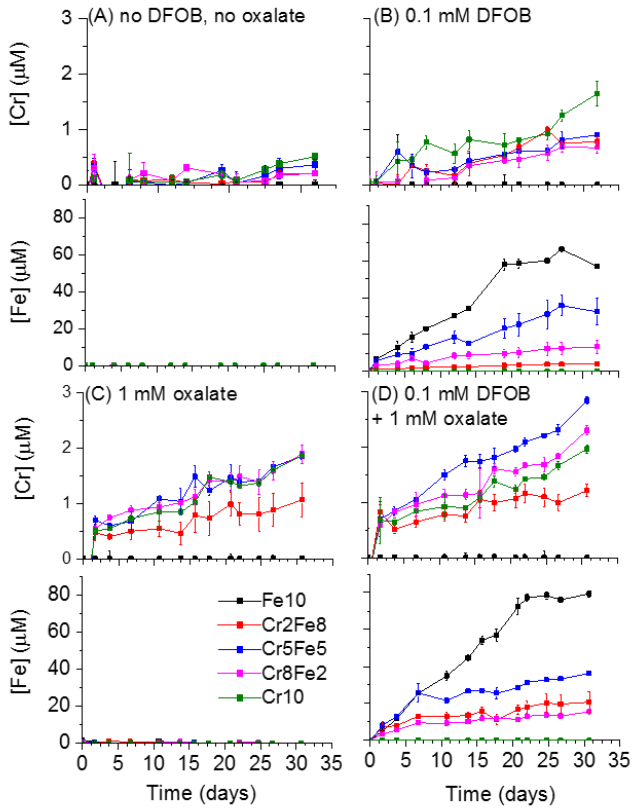

Figure 2.1 Concentrations of dissolved Cr and Fe from the $Cr_xFe_{1-x}(OH)_3$ phases in the presence of (A) no DFOB, no oxalate (control), (B) 0.1 mM DFOB, (C) 1 mM oxalate, and (D) 0.1 mM DFOB + 1 mM oxalate. Experiments were conducted at pH 7 in 0.1 M NaCl with 0.2 g L^{-1} of each solid.

In the presence of both DFOB (0.1 mM) and oxalate, the addition of 1 mM oxalate increased the release rate of Fe from each solid phase in a synergistic manner (i.e. the rate of dissolution in the presence of both oxalate and DFOB is greater than the sum of each rate) (Figure 2.2, Tables A.2 and A.3). This synergistic effect of oxalate on DFOB-promoted dissolution has been previously reported for Fe oxides and was attributed to the formation of a kinetically labile Fe-oxalate species at the solid surface followed by rapid ligand exchange with DFOB in solution (Reichard et al., 2007). While this effect was apparent for Fe release from these mixed solids, it was not observed for Cr release rate (Figure 2.2, Tables A.2 and A.3), similar to previous observations for Mn and Co oxides (Akafia et al., 2014). The greater impact of oxalate on DFOB-promoted release of Fe relative to Cr most likely reflects the much lower ligand exchange rate for Cr(III) relative to Fe(III) (Richens, 1997), which may limit the synergistic effects of ligand combinations on dissolution rates.

Interestingly, in the presence of 0.1 mM DFOB and 0.1 mM oxalate, the effect of oxalate addition on DFOB-promoted release of Cr and Fe can be either synergistic, inhibitive, or exhibit no effect on the metal release rates (see A.1). A previous study on the dissolution of Al-substituted goethite phases in the presence of DFOB and oxalate found a similar dependence of Fe release rate on oxalate concentration and solid Al content (Cervini-Silva and Sposito, 2002). Although the reason for such observations is unclear, the combined effect of DFOB and oxalate seems to be affected by oxalate concentration (or DFOB/oxalate ratio) and solid phase composition/structure. It is possible that the exchange between the surface formed labile metal-oxalate surface complex and metal-DFOB complex is affected by the ligand exchange rate of each metal ion, and the water exchange rate for Cr(III) is known to be much slower than Fe(III) (Richens, 1997). Higher concentrations of oxalate might facilitate the formation of surface metal-oxalate labile complex and provide more opportunities for metal exchange with DFOB. Furthermore,

different concentration ratios of organic acid and siderophore may affect the competition for surface sites, as has been proposed to explain the inhibition of citrate on DFOB-promoted dissolution of Fe oxides (Bondietti et al., 1993; Reichard et al., 2007).

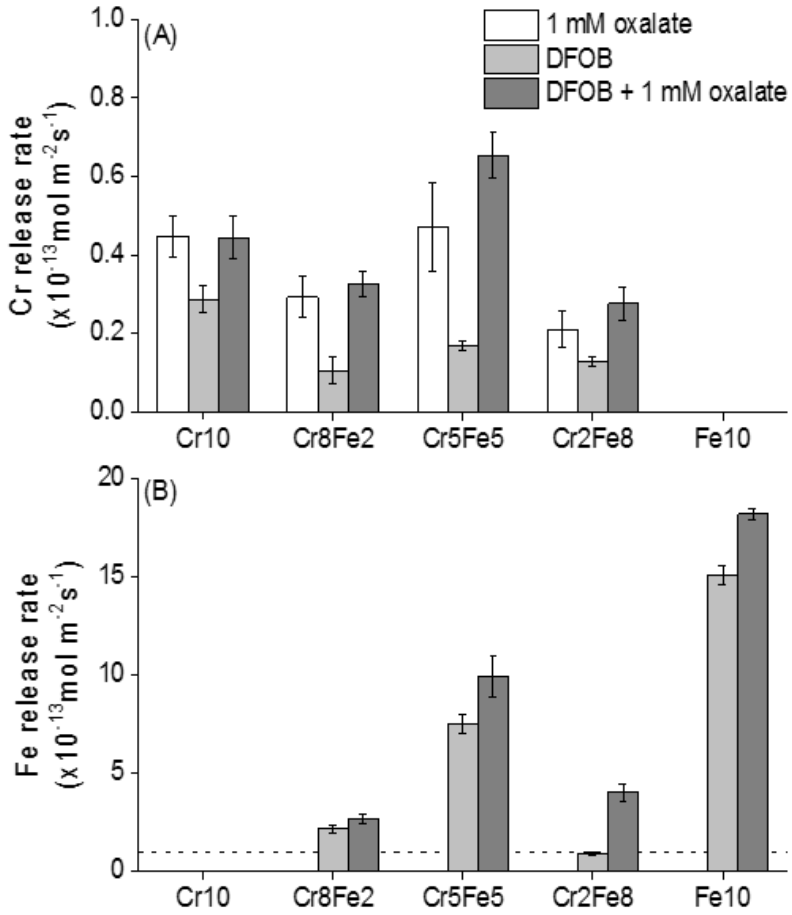

Figure 2.2 Release rates (mol m^{-2} s^{-1}) of (A) Cr and (B) Fe of each solid phase in the presence of 1 mM oxalate (white), 0.1 mM DFOB (light gray), or 0.1 mM DFOB + 1 mM oxalate (dark gray). Release rates were normalized to surface area of each starting solid and were determined by fitting a regression line through the dissolution profile over the same time frame (~21 days). Error bars represent variance of the rate determined from regression analysis and error associated with duplicates. The dashed line in (B) is at a release rate of 1 mol $m^{-2}s^{-1}$, which is the maximum value of the y-axis in (A).

The impact of the $Cr_xFe_{1-x}(OH)_3$ solid composition on the DFOB + oxalate combined effect is likely related to the structural and/or surface properties of these solids. A consistent trend observed throughout our treatments is that both the dissolution rate and extent of Fe and Cr from Cr5Fe5 are greater than those of the other intermediate composition phases, Cr2Fe8 and Cr8Fe2 (Figure 2.1B-D, Table A.2). Under all conditions, the rate of Fe release ($\mu M\ day^{-1}\ g^{-1}$) is consistent when normalized to Fe content (Table A.3) for all solids, except for Cr2Fe8, suggesting that perhaps this solid phase behaves inconsistently. Our previous study demonstrated that this nano-sized $Cr_xFe_{1-x}(OH)_3$ solid solution series does not follow the structural characteristics of traditional solid solutions of bulk crystalline materials (Tang et al., 2010). The Fe10 end member (i.e. 2-line ferrihydrite) is a nano-crystalline phase (Michel et al., 2007a; Tang et al., 2010), and the Cr10 end member is truly amorphous (Tang et al., 2010). Under HTREM, the loss of lattice fringes and discontinuation of nano-crystallinity seemed to occur between Cr5Fe5 and Cr7Fe3 (Tang et al., 2010). Therefore, it is possible that such structural/crystallinity change (i.e. different arrangements of surface atoms) and compositional change (e.g. hydration state) can expose different amount and type of Fe and/or Cr sites on the surface for complexation with oxalate and/or DFOB.

2.4.2 Composition evolution of solid phases

The preferential mobilization of Fe from all solid phases in the presence of DFOB alone or DFOB + oxalate led to the evolution of the solid phases to be more enriched in Cr relative to the initial solid phases (i.e. all solids exhibited an increased Cr/(Cr+Fe) molar ratio after reaction) (Figure 2.3). The most drastic changes were observed in Cr5Fe5 (30% change in solid Cr/(Cr+Fe) ratio relative to initial composition), followed by Cr8Fe2 (11%) and Cr2Fe8 (7%), all in the presence of DFOB + 1 mM oxalate. Similar to the effects of the microbially produced organic compounds in this study (i.e. siderophores and organic acids), direct microbial activity (e.g. anaerobic respiration of dissimilatory iron reducing

bacteria) has also been shown to lead to the evolution of the $Cr_xFe_{1-x}(OH)_3$ phases toward Cr enrichment through the respiration and reduction of Fe(III) within the mixed solid phases (Hansel et al., 2003). Although the presence of oxalate alone preferentially removed Cr relative to Fe, the composition change of the solid Cr/(Cr+Fe) relative to the initial composition based on this Cr depletion was negligible in all solid phases (< 3%).

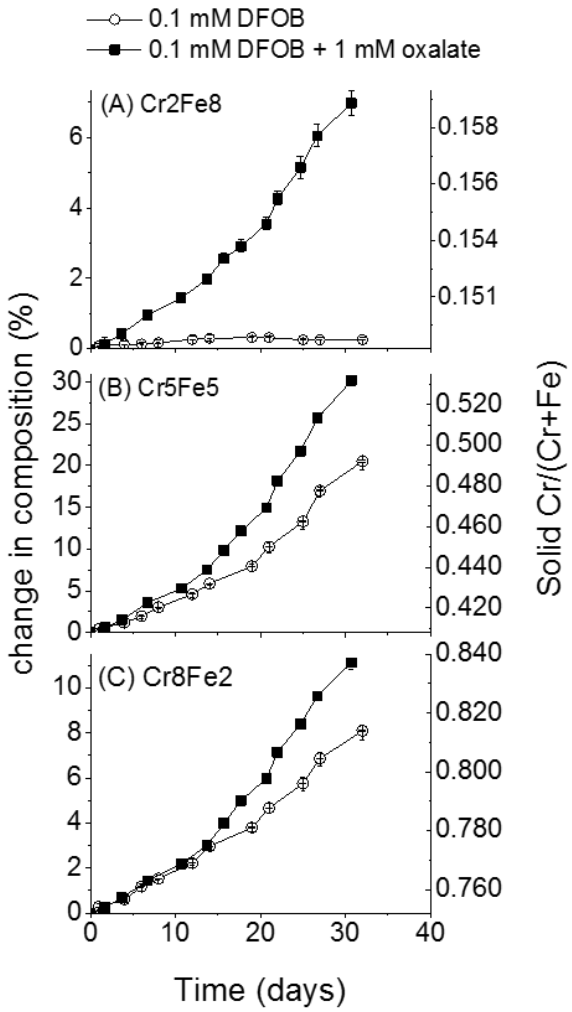

Figure 2.3 Composition evolution of the of $Cr_xFe_{1-x}(OH)_3$ phases as a function of time in the presence of 0.1 mM DFOB alone or 0.1 mM DFOB + 1 mM oxalate. Change in composition (%) is presented as percent change in solid Cr/(Cr+Fe) molar ratio over time.

2.4.3 Structural evolution of solid phases

The compositional enrichment of Cr in the solid phases was expected to alter the structure of the reacted solid phases relative to the initial solid phases. As previously mentioned, the mixed $Cr_xFe_{1-x}(OH)_3$ phases comprise a non-traditional solid solution series with gradual structural and compositional changes, albeit the two end members have different structures, crystallinity, and chemical compositions (Sass and Rai, 1987; Tang et al., 2010). The Cr end member exhibits only short-range order with a particle size of ~ 10 Å and has a greater hydration state than the Fe end member (2-line ferrihydrite), which exhibits intermediate range order with a coherent domain size of ~27 Å (Tang et al., 2010). In this study, complementary PDF, XAS, and HTREM characterizations were conducted on both the pristine (i.e. initial) and reacted solids to determine (1) whether the reacted solids still have similar structural features as the original solid solution, and if so, (2) where they fall within the solid solution series.

PDF analysis can be used to evaluate coherent domain size and atomic pair correlations of the reacted solids compared to the initial solids. The PDFs of all pristine and reacted solid phases under control (no DFOB, no oxalate) or 0.1 mM DFOB conditions are shown in Figure A.3. For pristine samples, from Cr10 to Fe10 the PDF spectra show a gradual increase of the coherent domain size with increasing Fe content (Figure A.3A). The atomic pair correlations of the reacted solids are overall similar to the original solid phases (Figure A.3B). The prominent feature at ~2 Å is indicative of the metal-oxygen pair correlation, as both Cr and Fe have similar ionic radii in the +3 valence state. With increasing Cr content, there is a shift of the features at 3 Å (edge-sharing metal-metal octahedra) and 3.4 Å (corner-sharing metal-metal octahedra), indicating gradual structural changes. The coherent domain sizes of reacted samples are slightly larger than those of the pristine samples, possibly due to an aging effect (Figure A.3A). Interestingly, the solids

reacted with DFOB exhibit smaller coherent domain sizes than the respective control experiments, likely due to the partial dissolution promoted by DFOB complexation.

Because PDF is not an element sensitive technique and Cr and Fe have similar scattering properties, Cr and Fe K-edge XAS analyses were conducted to confirm that the increased structure order revealed by PDF was not indicative of the formation of different phase(s) other than the solid solution series. Both Cr and Fe XAS spectra of the ligand-reacted samples showed spectral features similar to those observed within the solid solution series (Figures 2.4, A.4, and A.5). As previously observed with the solid solution series (Tang et al., 2010), gradual structural transformations were also observed for the reacted samples, as indicated by the vertical lines in Figure 2.4 and A.4. No Cr(VI) was observed in any of the samples, as evidenced by the absence of an intense pre-edge peak at ~5989 eV (Brown et al., 1988). The weak pre-edge feature at ~5992 eV is typical of Cr(III)-containing compounds (Peterson et al., 1996) and further confirms that no redox reactions have occurred during the experiments. The Cr XANES spectra of the reacted solids also differ significantly from the reported spectra of most likely products (e.g. Cr-substituted goethite; CrOOH)(Frommer et al., 2010) if a transformation of the local structure had occurred. Moreover, if these crystalline phases indeed formed in our system, they would have showed long range order in the PDF data of the reacted samples, which was not observed. Thus, the reacted solids had slight increases in crystallinity and structure order (as revealed by PDF) without changes in local coordination environment, similar to ferrihydrite phases with different structure order (e.g. 2-line ferrihydrite vs 6-line ferrihydrite) (Kukkadapu et al., 2003; Michel et al., 2007b).

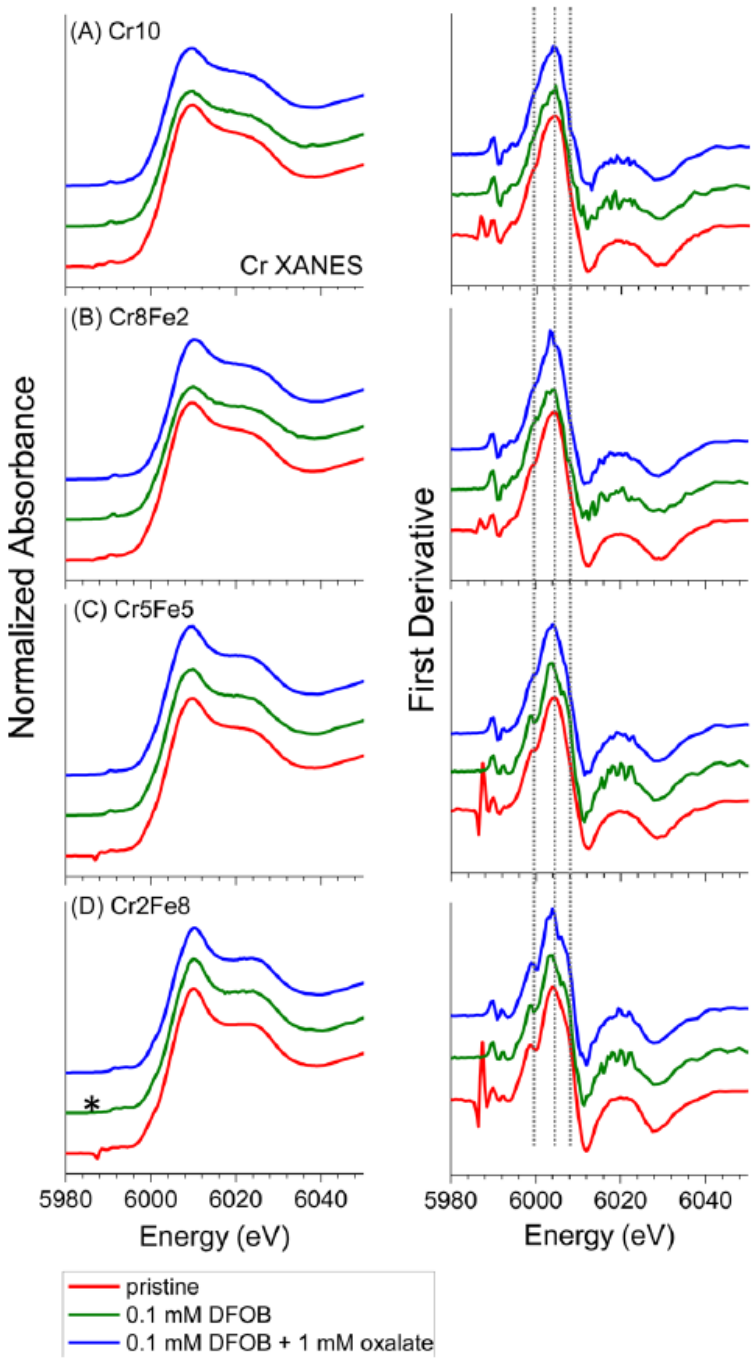

Figure 2.4 Cr K-edge XANES spectra (left) and corresponding first derivatives (right) of (A) Cr10, (B) Cr8Fe2, (C) Cr5Fe5, and (D) Cr2Fe8 under pristine, control, 0.1 mM DFOB alone, and 0.1 mM DFOB + 1 mM oxalate conditions. Vertical lines indicate regions where gradual transformations are observed. The sharp feature at ~5985 eV present in the pristine samples (indicated by the asterisk) is a monochromator glitch.

Representative HRTEM images and FFT analysis further support the change in crystallinity of the solid phases upon reaction (Figure 2.5). All samples show heavy aggregation, however, in this current study it is not possible to constrain whether the level of aggregation was present in the reaction suspensions or whether more aggregation was induced due to the sample preparation procedure for HRTEM. In general, there is a loss of structural order from Fe10 to Cr10, and the samples reacted with DFOB are less crystalline than the control samples. HRTEM images show that Fe10 and Cr2Fe8 both have clear lattice fringes and the grain sizes are ~5 nm in both the control and reacted samples. With increasing Cr content (e.g. samples Cr5Fe5, Cr8Fe2, and Cr10), the lattice fringes are only vaguely seen, and amorphous structures dominate the samples. Bright spots can be seen in the FFT patterns of samples Fe10, Cr2Fe8, and Cr5Fe5, reflecting the existence of nanocrystalline structure. However, in samples Cr8Fe2 and Cr10, bright spots are not obvious and only broad diffuse rings are observed. The diffuse rings also broaden from Cr8Fe2 to Cr10, which is consistent with the disappearance of lattice fringes and decrease of structural order.

Taken together, solid phase analyses reveal that the reacted solids belong to the same solid solution series, with each reacted solid having higher Cr content and a structure representative of Cr enrichment. However, because of the relatively small compositional changes (< 10% of the overall solid Cr/(Cr+Fe) mole ratio, Figure 2.3), the changes are subtle in XAS and HRTEM analyses.

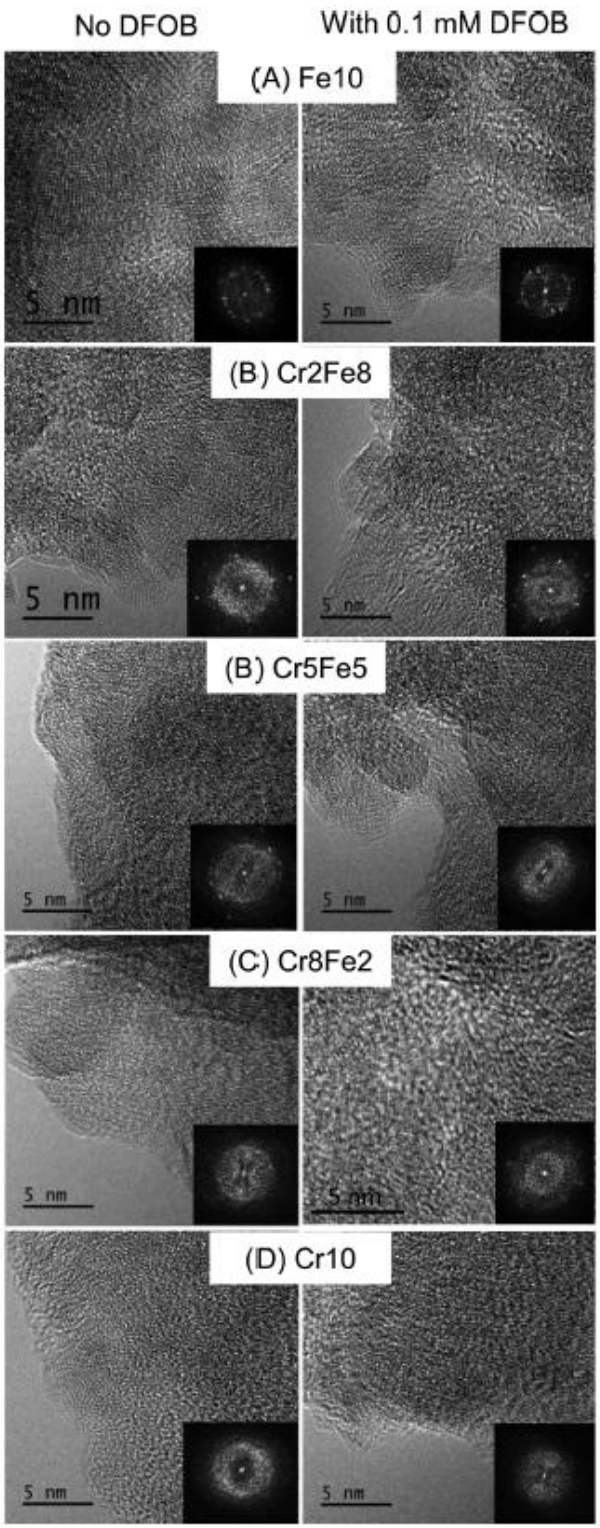

Figure 2. 5 HRTEM images and corresponding FFT patterns of reacted (32 days) solid phases under control (left panels) or 0.1 mM DFOB (right panels) conditions. Scale bars are 5 nm.

2.4.4 Incongruent dissolution of the solid phases

Based on the observed structural changes, dissolution requires some mechanism to induce changes in the local coordination environment of Cr and Fe. The dissolution mechanism itself is not straightforward because these mixed solids represent a non-traditional solid solution where the structures of the end members are not the same, and there is a gradual change in the structure along the compositional series (Tang et al., 2010). For solid phases containing both Cr and Fe (i.e. Cr2Fe8, Cr5Fe5, Cr8Fe2), regardless of ligand type and concentration, the release (both rate and extent) of Cr and Fe are not proportional to their molar ratio in the solid [i.e. x/(1-x)]. Therefore, the overall dissolution is incongruent and produces a secondary solid phase with compositions different from the unreacted solid. In the presence of DFOB alone or DFOB + oxalate, the produced secondary solid phase is more enriched in Cr. In the presence of oxalate alone, the preferential release of Cr (but not Fe) from these solids results in the slight enrichment of Fe. Incongruent dissolution of traditional solid solution series is typically discussed in the context of geological weathering. For example, previous studies showed that in the presence of oxalate, Al and Ca were preferentially removed (relative to Si) from feldspars (Chou and Wollast, 1984; Holdren and Speyer, 1985), resulting in a leached layer depleted in Al and Ca on the mineral surface (Shotyk and Nesbitt, 1992). A leached layer is defined as a chemically altered zone at the solid-solution interface, which exhibits a different elemental composition than the bulk solid composition (Brantley, 2008; Casey et al., 1993). The most likely mechanism leading to the observed structural changes in our system can occur from the structural reconstruction of this leached layer to minimize the surface energy configuration as has been observed in silicate minerals (Casey et al., 1993). In the case of a leached layer, the preferential dissolution of Fe would result in a Cr enriched leached layer, which may spontaneously reconstruct to form a structure that would be identical to the solid phase initially precipitated with the corresponding Cr/Fe ratio.

Because of the nanoscale size of the $Cr_xFe_{1-x}(OH)_3$ primary particles (i.e. 1–2 nm as identified by PDF) and associated large surface:bulk ratio, the reorganization of the surface is more evident as the overall transformations observed in the XAS and HRTEM analyses.

2.5 Environmental Implications

Understanding the potential reaction kinetics and pathways of Cr(VI) remediation products in the presence of microbial activities and/or metabolites has significant implications for assessing their long term stability under natural conditions. In this study, we investigated the single and combined effects of a siderophore, DFOB, and an organic acid, oxalate, on the stability of the Cr(III)-Fe(III)-(oxy)hydroxide solid solution series. Siderophores and organic acids are both common microbial exudates in the natural environments. Our study reveals that Cr(VI) remediation products may be remobilized in the subsurface by these common microbially-secreted ligands via (1) the direct ligand-promoted solubilization of Cr(III) from the Cr(III)-Fe(III)-(oxy)hydroxide solid phases, as well as (2) increased solubility of the secondary solid phases resulted from incongruent dissolution of the starting solid phases, as discussed below.

(1) Ligand promoted solubilization. The presence of DFOB and/or oxalate led to enhanced release of Cr(III) from the solid phases as a ligand complexed species (Figure 2.1). Thus, Cr mobility is expected to be promoted in the presence of environmentally relevant organic compounds. Oxalic acid is abundant in soils with concentrations on the order of 10-5 to 10^{-3} M range (Fox and Comerford, 1990). DFOB is a trihydroxamate siderophore produced by bacteria and fungi under low Fe availability conditions to solubilize Fe(III) from its low solubility (oxyhydr)oxide forms (Neubauer et al., 2002; Powell et al., 1980). Although the average concentration ranges of siderophores in soil and sediment environments are typically low and difficult to detect (e.g. hydroxamate siderophores in soils typically range from 10^{-8} to 10^{-7} M) (Powell et al., 1980), the concentration of siderophores can be highly

concentrated locally to facilitate the dissolution and mobilization of Fe from the Cr(III)-Fe(III)-(oxy)hydroxide and consequently mobilize Cr(III) at the same time (Winkelmann, 2002).

(2) Increased solubility of the secondary solid phases produced by incongruent dissolution of the starting solid phases. As previously discussed, the incongruent dissolution of the initial solids produces secondary solid phases with different composition and structure within the CrxFe1-x(OH)3 solid solution series. In the presence of DFOB alone or DFOB + oxalate, the secondary solid phases have higher mole fraction of Cr (x) and are predicted to be more soluble than the starting solids (Figure 2.6, Table A.4) based on the data from Sass and Rai (Sass and Rai, 1987) and equation derived in Rai et al. (Rai et al., 1986):

$$\log K_{Cr_xFe_{1-x}(OH)_3} = 4.23 - 0.172(1-x)^2 - 1.392(1-x)^3 + \log x \quad \text{where } x = 0 \text{ to } 1 \qquad (5)$$

This equation describes the solubility product (Ksp) of each solid phase within the solid solution series as a function of the mole fraction of Cr (and Fe). Based on this equation, the calculated solubility product of the secondary solid phases increased by ~0.1 to 9% in the presence of DFOB (Table A.4). Such increased solubility can lead to increased opportunity for the oxidation of Cr(III) to the toxic Cr(VI). Ligand-promoted dissolution leading to increased solubility of the remaining solid phase has previously been observed in hausmannite ($Mn(II)Mn(III)_2O_4$) (Pena et al., 2007). During DFOB-promoted dissolution of hausmannite, the depletion of Mn(III) from the solid phase led to structural instability that induced dissolution of the remaining solids and release of Mn(II).

The above-mentioned processes both produce soluble Cr(III) species (i.e. dissolved or ligand-complexed) that may be more susceptible to reoxidation to Cr(VI) than the solid phase species, leading to subsequent recontamination. Mn oxides are the most dominant environmentally relevant oxidants for Cr(III) (Amacher and Baker, 1982; Bartlett and

James, 1979; Eary and Rai, 1988). Several studies have examined the oxidation of dissolved Cr(III) by Mn oxides (Fendorf and Zasoski, 1992; Kim et al., 2002; Landrot et al., 2012; Tang et al., 2014). Studies have also shown that the oxidation of Cr(III) bounded by organic ligands, while kinetically slower than inorganic aqueous Cr(III), is a viable mechanism for Cr(III) oxidation to Cr(VI) (Luo and Chatterjee, 2010; Yang et al., 2014).

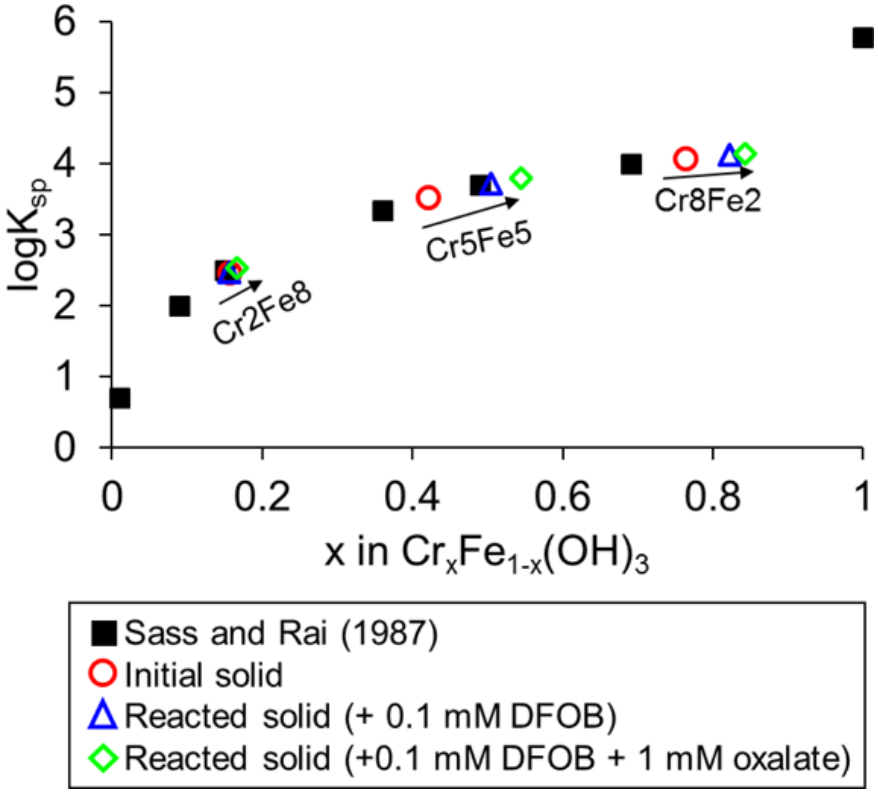

Figure 2.6 Predicted Ksp changes in the reacted $Cr_xFe_{1-x}(OH)_3$ solids in the presence of DFOB alone or DFOB + oxalate as compared to the initial solids, using calculated Ksp values and relationship from Sass and Rai (1987) and given by the equation $\log K_{CrxFe1-x(OH)3} = 4.23 - 0.172(1-x)^2 - -1.392(1-x)^3 + \log x$ for $0 < x < 0.9$.

Under complex environmental conditions, besides the above mentioned processes (e.g. dissolution of Cr-containing solids, production of dissolved Cr(III) and/or Cr(III)-ligand complex, oxidation of dissolved Cr(III) ion or Cr(III)-ligand complex by Mn oxides), other biogeochemical processes and factors should also be taken into consideration to better constrain the ultimate fate of Cr and its remediation byproducts. Organic ligands might interact with Mn oxides and influence their oxidation efficiency. For example, at circumneutral pH, DFOB has been shown to dissolve Mn oxides, either through reductive dissolution (leading to the degradation of DFOB and production of aqueous Mn(II)) or ligand complexation (leading to Mn(III)-DFOB complex formation) (Duckworth and Sposito, 2007). The presence of oxalate can promote and enhance the reductive dissolution pathway (Saal and Duckworth, 2010). The DFOB-promoted dissolution rates of Mn oxides under experimental conditions similar to this study are 10^{-9} mol m^{-2} s^{-1} (Akafia et al., 2014). Therefore, the interaction between organic ligands and Mn oxides may be a kinetically competitive process to the ligand-promoted dissolution of $Cr_xFe_{1-x}(OH)_3$ solids and subsequently reduce the opportunity for Cr mobilization.

Although our study was only conducted at the environmentally relevant pH value of 7, previously described trends can help provide implications for other pH values. For example, at lower pH values, proton-promoted dissolution of the solid phases becomes more dominant (Duckworth et al., 2014). However, this process is expected to have a similar effect as siderophores on the dissolution kinetics of the solid phases with different compositions, because proton-promoted dissolution rates correlate to the water exchange rates of the cation (Pokrovsky and Schott, 2002). Therefore, Fe is expected to preferentially release from the solid phases relative to Cr at lower pH values. At higher pH values, ligand promoted dissolution is the dominant dissolution mechanism and, in general, the rate may increase with increasing pH values (Duckworth et al., 2014). Furthermore, the organic acid and siderophore choice made in this study can help provide insights for other ligands. For

example, DFOB as a trihydroxamate siderophore may have a weaker effect than catecholate siderophores and, thus, is expected to result in lower dissolution rates than catecholate siderophores (Akafia et al., 2014; Duckworth et al., 2014). Additionally, the synergistic effect of oxalate may be higher than that of other organic acids (Reichard et al., 2007). Overall, in mixed metal solid phases, the water exchange rate and metal coordination environment are important factors in predicting the stability and transformation products of solids in the presence of microbial activities.

3. REDOX-INDEPENDENT CHROMIUM ISOTOPE FRACTIONATION INDUCED BY LIGAND-PROMOTED DISSOLUTION

3.1 Abstract

The chromium (Cr) isotope system has emerged as potential proxy for tracing Earth's atmospheric evolution based on the framework that Cr mobilization and isotope fractionation are strictly redox-dependent. Studies have demonstrated that redox-independent pathways, such as ligand solubilization, can also mobilize Cr. However, there are no quantitative constraints on the isotope fractionations that may occur during this process. This study surveyed the effect of common environmental ligands on the dissolution and isotope fractionation of Cr(III)-(oxy)hydroxide. For a variety of organic acids and siderophores, δ^{53}Cr values of dissolved Cr(III) were -0.27 to 1.23‰, within the range of previously observed Cr isotope signatures in rock records linked to Cr redox cycling. Thus, ligand-promoted dissolution of Cr-containing solids, a redox-independent process, must be taken into account when using sedimentary Cr isotope signatures to diagnose atmospheric oxygen levels. This work is a first step towards establishing a robust framework for using Cr isotopes to track the chemical evolution Earth's atmosphere.

Saad EM, Wang X, Planavsky NJ, Reinhard CT, Tang Y. Redox-independent chromium isotope fractionation induced by ligand-promoted dissolution, *Nature Communications*, in revision.

3.2 Introduction

The chromium (Cr) isotope system has recently been exploited as a highly discriminating tracer of redox processes in Earth's surface environments, and is under development as a novel paleobarometer for atmospheric oxygen levels (Cole et al., 2016; Crowe et al., 2013; Frei et al., 2009; Planavsky et al., 2014). Many of these applications are grounded in the notion that Cr isotope fractionations are linked predominantly to changes in Cr oxidation state. Consistent with this view, theoretical and experimental studies up to this point have also suggested very little Cr fractionation during redox-independent processes (Ellis et al., 2004; Schauble et al., 2004). Cr isotopes have also been extensively employed in environmental geochemistry as a quantitative proxy of Cr transport and remediation efficiency (Berna et al., 2010; Ellis et al., 2002; Raddatz et al., 2011; Wanner et al., 2012). However, in order to quantitatively apply this isotope system as a tracer for Earth surface processes, it is critical to more precisely quantify a wider range of factors controlling the global Cr isotope budget (Gueguen et al., 2016).

The current Cr isotope paradigm suggests that significant isotope fractionations are only associated with redox transformations between Cr(III) and Cr(VI), the two most common oxidation states of Cr in natural environments (Ellis et al., 2004; Johnson and Bullen, 2004; Schauble et al., 2004). Cr(III) is typically insoluble and is the most common form of Cr in rocks and minerals at Earth's surface, and is typically present in igneous and sedimentary reservoirs as oxides, oxyhydroxides, or silicates (Cotton and Wilkinson, 1972). Cr(VI) is typically soluble and is the mobile form of Cr in natural environments. Oxidation of Cr(III) is assumed to be required for the production of soluble and mobile Cr species (Bartlett and James, 1988). In fact, conventional understanding of the Cr isotope

paleoproxy is based on the process of oxidative weathering of Cr(III) by manganese (Mn) oxides, the formation of which requires free oxygen. Soluble Cr(VI) is released during this weathering process and is transported to the oceans, where it is subsequently reduced to Cr(III) under reducing environments and deposited in marine sediments (Frei et al., 2009; Schoenberg et al., 2008). Thus, authigenic marine sediments capture an integrated isotopic signature reflective of the redox processes involved in mobilization, downstream reduction, and ultimate Cr(III) burial in sediments (Frei et al., 2009).

The redox transformation between Cr(III) and Cr(VI) causes a significant change in the local coordination environment of Cr. Cr(III) typically occurs in octahedral coordination, whereas Cr(VI) primarily occurs as tetrahedrally coordinated oxyanion species, chromate ($HCrO_4^-$ and CrO_4^{2-}) or dichromate ($Cr_2O_7^{2-}$) (Schauble et al., 2004). The large change in Cr coordination environment during redox transformations leads to significant isotopic fractionation, similar to other redox-sensitive elements (Johnson and Bullen, 2004). Unweathered igneous rocks exhibit a narrow range of $\delta^{53}Cr$ values of -0.124 ± 0.101‰ (defined as $\delta^{53}Cr = [(^{53}Cr/^{52}Cr)_{sample}/(^{53}Cr/^{52}Cr)_{standard} - 1] \times 1000$) (Schoenberg et al., 2008). Cr(III) oxidation to Cr(VI) has been shown to result in significant isotopic fractionations, both negative and positive ($^{53}\varepsilon$Cr(VI)-Cr(III) ~ -2.5 to +1.1‰), depending on the reaction conditions, while reduction of Cr(VI) to Cr(III) has consistently been shown to leave the remaining Cr(VI) isotopically heavy ($^{53}\varepsilon$Cr(III)-Cr(VI) ~ -7.6 to -0.4‰) ((Qin and Wang, 2017) and references therein). The equilibrium isotope fractionation between Cr(III) and Cr(VI), defined as $\Delta^{53}Cr(VI)\text{-}(III) = \delta^{53}Cr(VI) - \delta^{53}Cr(III)$, is theoretically determined to be 6–7‰ at 25 °C (Ottonello and Zuccolini, 2005; Schauble et al., 2004), which agrees with the experimentally determined value of 5.8 ± 0.5‰ (Wang et al., 2015a).

Because the isotopic exchange and subsequent ability to achieve isotopic equilibrium between Cr(III) and Cr(VI) requires the transfer of three electrons with a significant coordination reconfiguration, the isotopic exchange rate of these species is extremely slow (Altman and King, 1961; Wang et al., 2015a). Under settings where dissolved Cr(VI) and Cr(III)-containing solids are in contact for long periods, equilibrium fractionation may become a relevant process. However, the significance of such process under environmentally relevant settings can vary and is dependent on factors, such as the relatives masses of Cr(VI) and exposed Cr(III) (Wang et al., 2015a). Therefore, Cr isotope systematics during Earth's surface processes are generally assumed to be most likely dominated by kinetic fractionations. Regardless, current experimental and empirical work suggest that both kinetic and equilibrium processes lead to Cr(VI) that is isotopically heavy(Schauble et al., 2004; Wang et al., 2015a).

Measurements on natural waters have revealed elevated concentrations of dissolved Cr(III) that are higher than the solubility of $Cr(OH)_3$ and likely complexed with organic molecules (Ahern et al., 1985; Icopini and Long, 2002; Kaczynski and Kieber, 1994; Nakayama et al., 1981; Yusof et al., 2007); however, there are no constraints on the isotope fractionation associated with this process. Similarly, the speciation of Cr in hydrothermal fluids is also thought to be organically complexed Cr(III) (Sander and Koschinsky, 2000; Sander and Koschinsky, 2011). In addition, two classes of organic ligands, siderophores (e.g. desferrioxamine B, rhizoferrin, protochelin) (Duckworth et al., 2014) and organic acids (e.g. citric acid, ethylenediaminetetraacetic acid, nitrilotriacetic acid) (Carbonaro et al., 2008), were recently shown to be capable of solubilizing Cr(III) from the Cr(III)-(oxy)hydroxide solid phase under environmentally relevant conditions. Both siderophores

and organic acids are ubiquitous organic molecules in natural environments produced by a wide range of microorganisms (e.g. archea (Offre et al., 2013), bacteria (Banik and Dey, 1982), and fungi (Gadd, 2007)) and are often co-exuded (Fan et al., 1997). Organic acids are known to contribute to the mobilization of metals in soils (Pohlman and McColl, 1986), and a wide range of organic acids (e.g. oxalic, citric, fulvic, and humic acids) have been demonstrated to complex with Cr(III) (Gustafsson et al., 2014; James and Bartlett, 1983; Srivastava et al., 1999; Walsh and Ohalloran, 1996). Organic acids were also likely present throughout Earth's history through abiotic or biotic synthesis pathways ((Boenigk et al., 2015; Dalai et al., 2016) and references therein) and may have played an important role in weathering for long periods of Earth's history (Neaman et al., 2005). Siderophores are organic chelating agents with a high affinity for Fe(III) that can enhance Fe solubilization and bioavailability from low solubility Fe(III)-containing mineral phases (Neilands, 1995). Siderophores have also been shown to have strong affinities for other trivalent metal cations such as Cr(III), Mn(III), and Co(III) due to their structural similarity (e.g. size, coordination environment) to Fe(III) (e.g. (Budzikiewicz et al., 2002; Duckworth et al., 2009; Parker et al., 2004).

Despite the potential importance of Cr(III)-ligand complexes in the Earth surface Cr cycle, Cr isotope fractionation during Cr(III)-ligand complexation has not been experimentally measured, although the potential for this fractionation has been previously suggested by theoretical studies (Ottonello and Zuccolini, 2005; Wang et al., 2015a). Furthermore, different ligands most likely involve different binding and dissolution mechanisms with Cr(III), and therefore, may potentially induce distinct isotope fractionations. Studies have shown that the chain length and carboxyl group arrangements

of organic acids determine their complexation geometry on Fe(III)-containing mineral surfaces and ultimately the dissolution efficiency (Duckworth and Martin, 2001). The specific binding moiety of a siderophore determines the stability of its metal complexes (Albrecht-Gary and Crumbliss, 1998) and ultimately their reactivity (Duckworth et al., 2014), which may also generate distinct isotope signatures.

The goal of this study is to survey the extent of Cr isotope fractionation that occurs during ligand complexation and dissolution of Cr(III). Given the potential for analytically significant fractionations, these redox-independent processes may complicate attempts to use Cr isotopes to track Cr oxidation for the estimation of paleo-O2 levels and Cr reduction during environmental remediation (Figure 3.1). Specifically, we systematically characterized the dissolution of a Cr(III)-containing solid by a wide range of organic ligands, and attendant isotope effects were quantified with an eye toward better understanding the potential role of Cr(III)-ligand complexes on global Cr isotope mass balance.

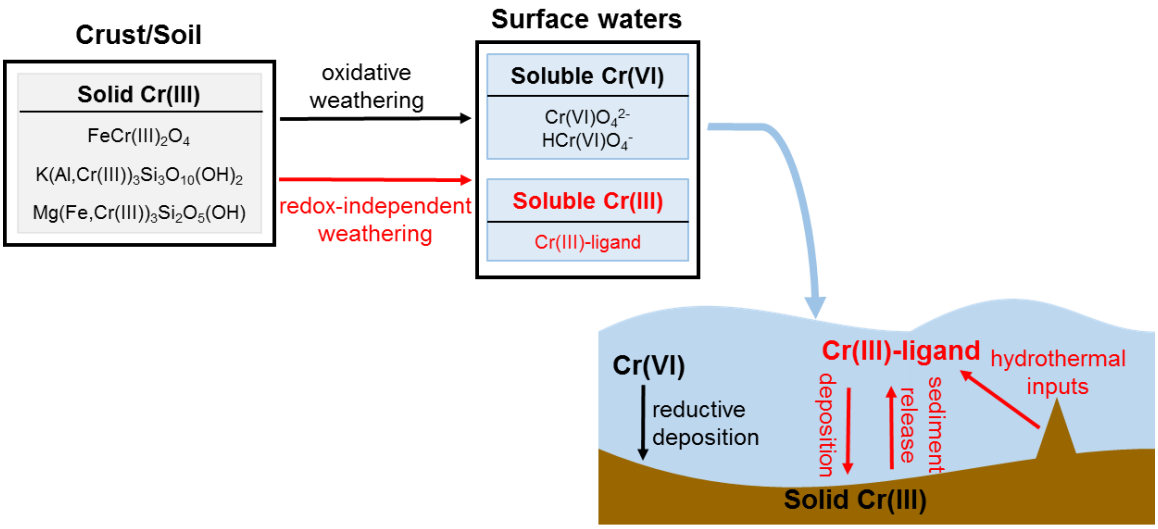

Figure 3.1 Schematic of Cr cycle as a paleobarometer for atmospheric oxygen level. Red text and arrows indicate pathways contributing to isotope fractionation that are currently unconstrained.

3.3 Methods

Amorphous Cr(III)-(oxy)hydroxide (hereafter referred to as $Cr(OH)_3$) was selected as a representative compound for solid phase Cr in natural environments as it is a common Cr(III)-solid phase, and an endmember in the Cr(III)-Fe(III)-(oxy)hydroxide solid solution series(Tang et al., 2010). A variety of organic ligands were employed in order to develop a survey of their impacts on Cr dissolution and isotope fractionation. Siderophores and organic acids were studied as they are two common classes of metal-complexing organic ligands in the natural environment as previously discussed. Siderophores are divided into three primary types depending on the characteristic metal binding functional group, including α-hydroxycarboxylic acid (hydroxycarboxylate type), catechol (catecholate type), and hydroxamic acid (hydroxamate type) (Ahmed and Holmstrom, 2014). The most common bacterial siderophores are catecholates and the most common fungal siderophores are hydroxamates (Winkelmann, 2007), though the other types, including a mixed type, are

also produced ((Ahmed and Holmstrom, 2014) and references therein). We chose the following types of siderophores with different functional groups and microbial origins (bacterial vs. fungal): desferrioxamine B (DFOB; hydroxamate type), enterobactin (catecholate type), and pyoverdine (mixed type). A range of organic acids with different chain lengths and metal binding tendencies were also studied, including oxalate, acetate, succinate, and citrate (Tables 3.1 and 3.2). Critically, Cr speciation was monitored throughout the experiment to ensure that the effects of redox-independent processes were specifically isolated.

Table 3.1 Structures and categories of the siderophores used in this study (see Methods Section for details).

Type	Species	Functional group	Structure
Hydroxamate	Desferrioxamine B	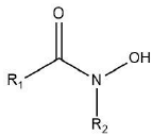	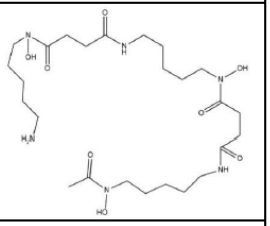
Catecholate	Enterobactin	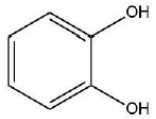	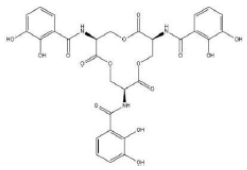
Mixed (hydroxamate-catecholate)	Pyoverdine	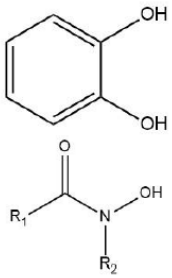	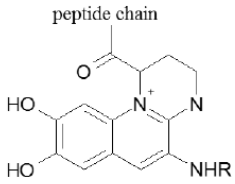 peptide chain: cOHOrn-Ser-Glu-Ala-Thr-Ser-OHAsp-εLys-Asp R = Succinic acid or succinamid, Glu or Kgl

Table 3.2 Structures of the organic acids used in this study

Species	Structure
Acetate	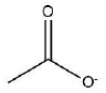
Oxalate	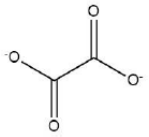
Succinate	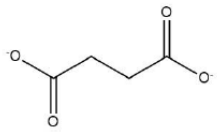
Citrate	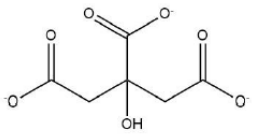

3.3.1 Synthesis of Cr(III)-(oxy)hydroxide

$Cr(OH)_3$ was synthesized following a previous procedure (Tang et al., 2010). Briefly, $Cr(NO_3)_3 \cdot 9H_2O$ (ACS grade) was dissolved in deionized water (18 MΩ cm) to obtain a total Cr concentration of 0.1 M. The solution was slowly titrated to pH 7 with 1 M NaOH. Precipitates formed from the suspension were aged for 24 h followed by dialysis to remove remaining electrolytes. The resulting wet pastes were recovered through centrifugation, freeze dried, and finely ground. Portions of the powders were dissolved in nitric acid for Cr concentration analysis by inductively coupled plasma-mass spectroscopy (ICP-MS) on an Agilent 7500a at the Georgia Institute of Technology. The specific surface area was determined to be 95 m^2 g^{-1} by Brunauer–Emmett–Teller (BET) gas adsorption analysis using an Autosorb-1-MP surface pore analyzer (Quantachrome Corp.) (Saad et al., 2017).

3.3.2 Ligand solubilization experiments

Rates and extents of $Cr(OH)_3$ solubilization were investigated in the presence of a single type of siderophore or organic acid, or a combination of siderophore and organic acid. The representative siderophores included DFOB (mesylate salt, Sigma-Aldrich), enterobactin (*Escherichia coli*, Sigma-Aldrich), and pyoverdine (*Pseudomonas putida* ATCC 12633, EMC Microcollections, Germany). The representative organic acids included acetate, oxalate, succinate, and citrate (all ACS grade from Sigma-Aldrich).

For each ligand solubilization experiment, the $Cr(OH)_3$ solids (0.2 g/L) were suspended in a 0.1 M NaCl electrolyte solution with 10 mM 4-(2-hydroxyethyl)-1-piperazineethanesulfonic acid (HEPES, high purity grade) buffer at pH 7 and sonicated for 15 min to disperse the particles. HEPES buffer has previously been shown to not influence the rates of siderophore-promoted dissolution of metal hydroxides (Bi et al., 2010; Cheah et al., 2003; Duckworth et al., 2014; Saad et al., 2017). For the treatments containing an organic acid, the organic acid was added to the suspension to achieve a final concentration of 1 mM. For the treatments containing a siderophore, the siderophore was added to the suspensions for a final concentration of 0.1 mM. For the treatments containing both a siderophore and an organic acid, the organic acid was added 1 min prior to the siderophore addition in order to account for its potential effect on metal hydroxide dissolution during the initial exposure (Reichard et al., 2007). Treatments containing organic acids were conducted in triplicate, and treatments containing siderophores were conducted in duplicate. Each treatment was conducted in batch reactors in the dark using amber bottles. Reaction bottles were constantly agitated at room temperature on an orbital shaker.

Filtered aliquots (0.2 μm, cellulose acetete) of each sample were collected throughout a time series and analyzed for total dissolved Cr on an Agilent 7500a ICP-MS at the Georgia Institute of Technology ICP-MS. Cr(VI) concentrations in the filtrates were analyzed using the diphenylcarbazide assay (Bartlett and James, 1979) on a UV/vis spectrophotometer (Cary 60, Agilent) and were below the detection limit (0.2 μM) for all treatments. Thus, the total dissolved Cr concentration in the filtrate was considered to be Cr(III). The pH value of the suspension stayed at 7.0 ± 0.1 throughout the entire experiment for all treatments. No microbial growth was observed for the duration of the experiment. Cr release rates were determined by fitting a regression line through the linear portion of the dissolution profile for each condition and normalizing to BET surface area.

3.3.3 Cr isotope analysis

At various time points along the dissolution profile, an entire sample bottle was sacrificed for Cr isotope analysis, thus reflecting the cumulative isotope signature at that time point. The ^{50}Cr-^{54}Cr double spike method was used to correct for fractionation during sample purification and isotope measurement (Ellis et al., 2002; Schoenberg et al., 2008). The double spike solution with known ^{50}Cr/^{54}Cr ratio (~1) was added as early as possible in the sample preparation process and was added in the same valence(s) as the Cr in the sample (i.e. Cr(III)). Proper amount of spike was added to the samples to ensure an optimum spike/sample ratio of $^{54}Cr_{spike}/^{52}Cr_{sample}$ ~ 0.5. Cr was purified from matrix ions using a cation exchange resin method modified from Bonnand et al. (2011). Briefly, the sample-spike mixtures were gently evaporated to dryness and refluxed with 6 N HCl to allow full isotopic equilibrium between spike and sample. Samples were then dissolved in 0.5 N HCl and loaded onto Bio-Rad AG50W-X8 (100-200 mesh) cation exchange resin.

Cr was eluted from the resin after loading and collected for isotope analysis. Purified Cr samples were dissolved in 0.7 N HNO_3 and measured for Cr isotopic compositions on a NeptunePlus multicollector ICP-MS at Yale University. Ti, V, and Fe interferences were monitored and corrections were made. The unprocessed standard SRM 979 with similar concentrations was analyzed before and after every sample to monitor instrument drift. Sample values were normalized to the average values of the bracketing standards. Based on standards and duplicate preparation and analysis of various types of real samples, our analytical precision was about ±0.08‰ (95% confidence level) using 200–1000 ng Cr. The starting $Cr(OH)_3$ solid was dissolved by 0.7 N HNO3 and analyzed for Cr isotopic composition as described above. The total procedural blank ranged from 0.2 to 1 ng, which is negligible to the sample Cr amount; therefore, blank correction was not performed.

3.4 Results

In the absence of organic ligands, dissolved Cr remained less than 0.5 μM throughout the experiment with detectable release only occurring after 14 days (Figure 3.2a). The presence of organic ligands promoted the dissolution of Cr to variable extent (Figure 3.2). In the presence of organic acids alone, citrate released the greatest amount of Cr into solution reaching a plateau at 3.5 μM, followed by oxalate, which reached 2.4 μM by the end of the experiment (Figure 3.2a). Succinate and acetate promoted Cr release to a similar extent as the control (i.e. no organic ligands), reaching 0.5 and 0.4 μM, respectively, but with detectable Cr throughout the experiment. The presence of organic acids in addition to DFOB resulted in similar trends in dissolution extent as the organic acid-only treatments (Figure 3.2b). Citrate, followed by oxalate, induced the greatest Cr release extent, reaching 4.1 and 2.7 μM, respectively, and with continuous increase at the end of the experiment.

The addition of succinate and acetate with DFOB both resulted in ~0.8 μM Cr release extent at the end of the experiment, less than in the presence of DFOB alone (1.5 μM Cr release). The extent of Cr release was also dependent on siderophore type (Figure 3.2c). Enterobactin resulted in the greatest dissolution extent of Cr (20 μM), followed by pyoverdine (15 μM), and DFOB (1.5 μM). None of the siderophore only treatments reached a concentration plateau by the end of the experiment.

Both siderophores and organic acids increased the initial Cr release rates (surface area normalized) relative to the absence of a ligand, for which an initial dissolution rate could not be calculated by linear regression (R^2 = 0.2) (Figure 3.3). In the presence of organic acids, initial Cr release rates were highest for citrate (1.6 ± 0.1 × 10-13 mol m^{-2} s^{-1}), followed by oxalate (6.5± 0.6 × 10^{-14} mol m^{-2} s^{-1}), and succinate and acetate (both ~ 2 × 10^{-14} mol m^{-2} s^{-1}) (Figure 3.3a). The addition of DFOB to the organic acid treatments did not significantly affect the dissolution rate relative to the presence of organic acids alone. In the presence of siderophores alone, initial Cr release rates were highest for enterobactin (7.7 ± 0.4 × 10^{-13} mol m^{-2} s^{-1}), followed by pyoverdine (5.7 ± 0.9 × 10^{-13} mol m^{-2} s^{-1}), and finally DFOB (4.8 ± 0.1 × 10^{-14} mol m^{-2} s^{-1}) (Figure 3.3b). In general, organic acids released less Cr into solution than siderophores. The exception is citrate, which resulted in a dissolution rate around 3 times greater than that of DFOB.

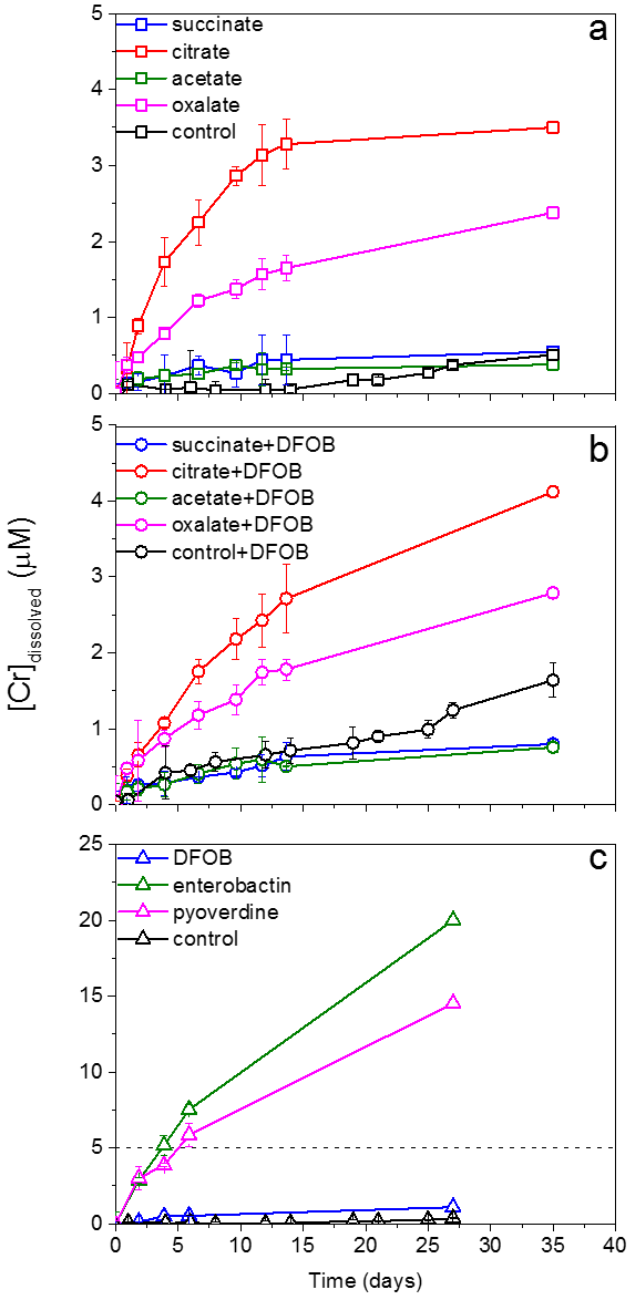

Figure 3.2 Dissolved Cr concentrations in the presence of (a) organic acids only, (b) organic acids and the siderophore, desferrioxamine B (DFOB), and (c) siderophores only. Error bars represent the deviation between replicates. The dashed line in (c) indicates the maximum value of the y-axis in (a) and (b). All dissolved Cr was determined to be in the +3 oxidation state.

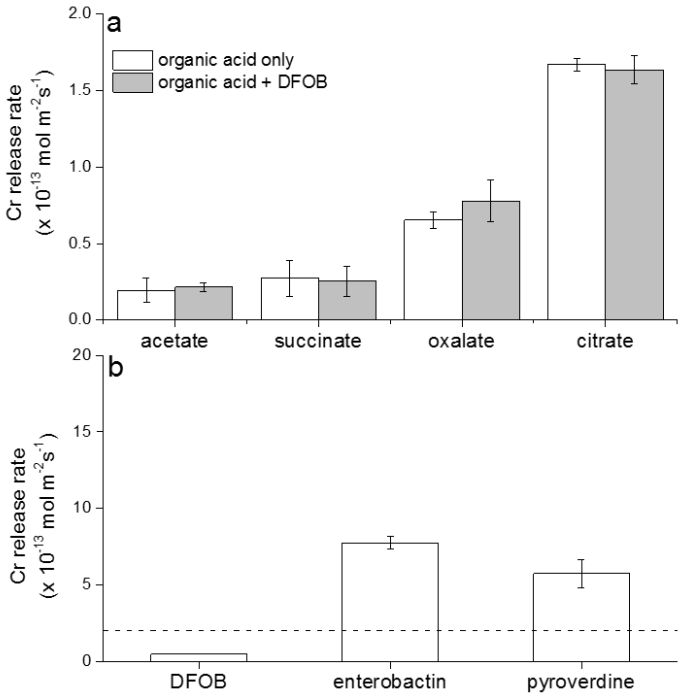

Figure 3.3 The initial surface area normalized release rates of Cr from $Cr(OH)_3$ in the presence of (a) organic acids with and without the siderophore, desferrioxamine B (DFOB) or (b) siderophores only. The dashed line in (b) is at the maximum y-value of (a). The average rates of replicates are presented with error bars reflecting deviation from replicates.

The Cr isotopic composition of the dissolved Cr(III) was also examined throughout the experiment (Figure 3.4). A wide range of $\delta^{53}Cr$ values were observed in the solubilized Cr, from +1.23 to -0.27‰. The $\delta^{53}Cr$ values varied based on ligand type and reaction extent. The isotope signature of dissolved Cr approaches that of the original solid with increasing reaction extent for the organic acids only treatments. Interestingly, though the influence of the siderophore DFOB on organic acid-promoted dissolution was relatively muted with regard to Cr(III) release rates, a significant effect of DFOB was observed on the magnitude of isotopic fractionation in combination with organic acids.

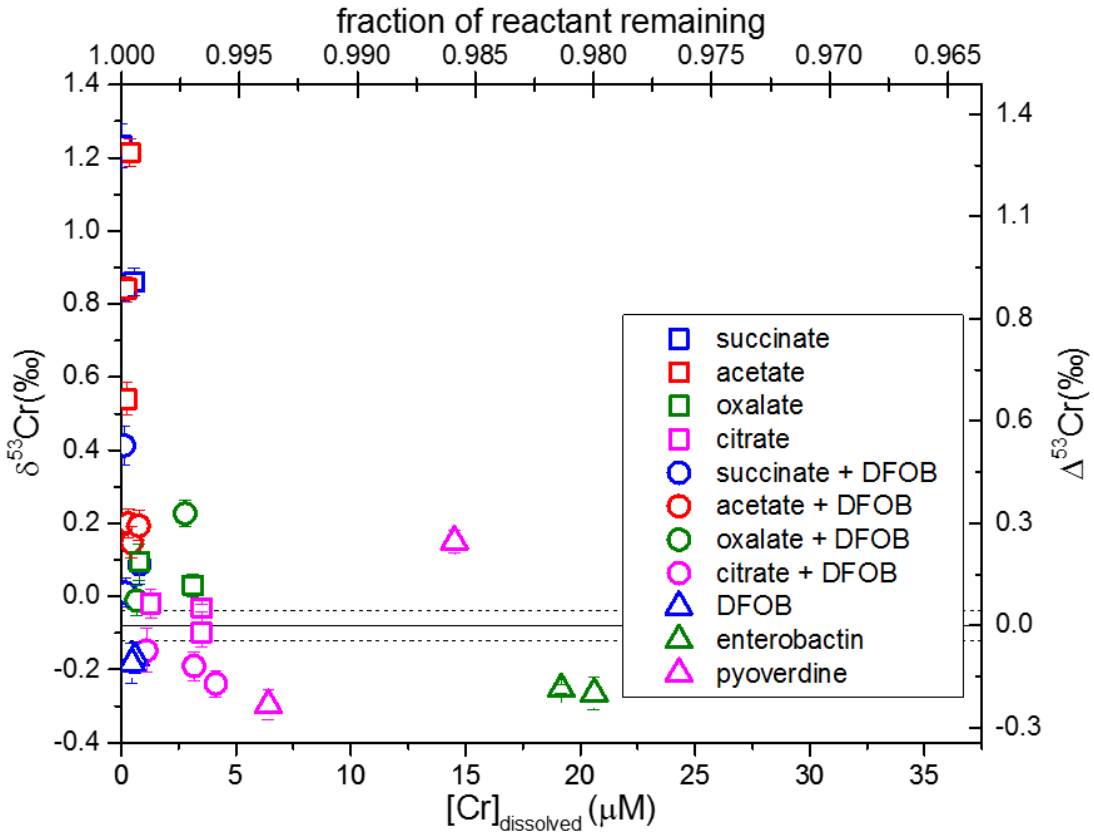

Figure 3.4 $\delta^{53}Cr$ as a function of reaction extent (either fraction of reactant remaining or concentration of Cr dissolved) for each ligand or ligand combination. $\Delta^{53}Cr$ represents $\delta^{53}Cr_{solution}$ - $\delta^{53}Cr_{initial\ solid}$ at distinct points during dissolution (similar to as presented in (Brantley et al., 2004)). The isotopic signature of the starting solid is represented by the solid line at $\delta^{53}Cr$ = 0.08 ‰ and $\Delta^{53}Cr$ = 0. The dashed lines represent ± 2σ.

3.5 Discussion

Organic ligands are known to promote the dissolution of metal oxides by forming inner sphere metal-ligand complexes at the solid-solution interface and weakening the metal-oxygen bond on the solid surface. The structure of the ligand influences the stability of both the surface and dissolved metal-ligand complexes and consequently the rate of dissolution (Stumm, 1992). The rate limiting step during ligand-promoted dissolution is

the detachment of the metal-ligand complex from the surface; thus, increasing stability of the dissolved metal-ligand complex leads to increasing dissolution rate(Furrer and Stumm, 1986). The stability constants of Cr(III)-siderophore complexes are not well established due to the slow ligand exchange rate(Hewkin and Prince, 1970), weak UV/visible absorbances (Leong and Raymond, 1975), and low reduction potentials (Latimer, 1938), all of which prevent traditional methods for the determination of stability constants (Duckworth et al., 2014). Because limited stability data are available for Cr(III)-ligand complexes for the ligands studied here, the following discussions will use the stability constants of Fe(III)-ligand complexes to estimate the potential influences of such factor on dissolution and isotope fractionation. The rationale for using Fe(III)-ligand complex stability constants as proxies is based on the similar strength of interaction between Fe(III) and Cr(III) cations and a ligand containing a hard Lewis base (e.g. the hardness of the cation) (Hernlem et al., 1996). Therefore, the ionic potential of metal cations (i.e. valence divided by ionic radius) positively correlates with the metal-ligand stability constant (e.g. Duckworth et al., 2014; Hernlem et al., 1996, and references therein). The similarity of the ionic potential of Fe(III) (ionic radius of 0.645 Å) to Cr(III) (ionic radius of 0.615 Å) (Shannon, 1976) allows for an appropriate first estimation of Cr(III)-ligand trends. Although a more complete estimation of the Cr(III)-ligand stability constants would require the metal-ligand stability constants for a greater number of metals (Duckworth et al., 2014; Hernlem et al., 1996), we suggest that substituting data for Fe(III) should allow for a useful qualitative assessment of Cr isotope fractionation trends. However, it should be noted that in some instances the measured values of Cr(III)-ligand stability, specifically for siderophores, do not necessarily follow the correlating Fe(III)-ligand stability trends, as

has been observed for rhizoferrin, an α-hydroxycarboxylate type siderophore (Carrano et al., 1996; Duckworth et al., 2014). The difference in siderophore affinity has also been previously noted between Fe(III) and Mn(III) due to the identity of the binding moiety of the siderophore and the electron configuration of the metal atoms (Harrington et al., 2012).

In the presence of organic acids, we find that dissolution rates generally increase with increasing stability constant of the corresponding Fe(III)-ligand complex (Figure 3.5). Of the organic acids utilized here, citrate, a strong chelating ligand, exhibited the greatest dissolution rate at 0.27 ± 0.01 μM d^{-1}, consistent with the previously reported rate of citrate promoted $Cr(OH)_3$ dissolution under similar experimental conditions (0.22 ± 0.09 μM d^{-1}) (Carbonaro et al., 2008). While the rates of organic acid-promoted dissolution of $Cr(OH)_3$ for oxalate, succinate, and acetate have not been reported to our knowledge, inference can be made based on the trends observed with Fe oxides. For example, similar trends of dissolution rates have been observed for organic acid-promoted ferrihydrite dissolution, which decreased in the order of citrate, oxalate, and succinate at pH 7 (Johnson and Loeppert, 2006). These trends can be described by the binding mechanism exhibited by each ligand. Citrate has been shown to adsorb to Fe oxides with each carboxyl group bound to different Fe(III) sites on the solid surface, leading to its effectiveness at dissolving metal oxides (Cornell and Schindler, 1980). Oxalate has been shown to form a bidentate mononuclear complex with Fe(III) in hematite, while succinate formed a (weaker) monodentate surface complex, leading to the observed differences in dissolution rates (Duckworth and Sposito, 2007). Acetate is a monodentate ligand, that has been shown to preferentially occupy adsorption sites on metal oxide surfaces (Carbonaro et al., 2008), though is not expected to significantly affect the dissolution rate (Martin, 2005). In general,

the trends in organic acid-promoted dissolution observed in this study are consistent with expectations.

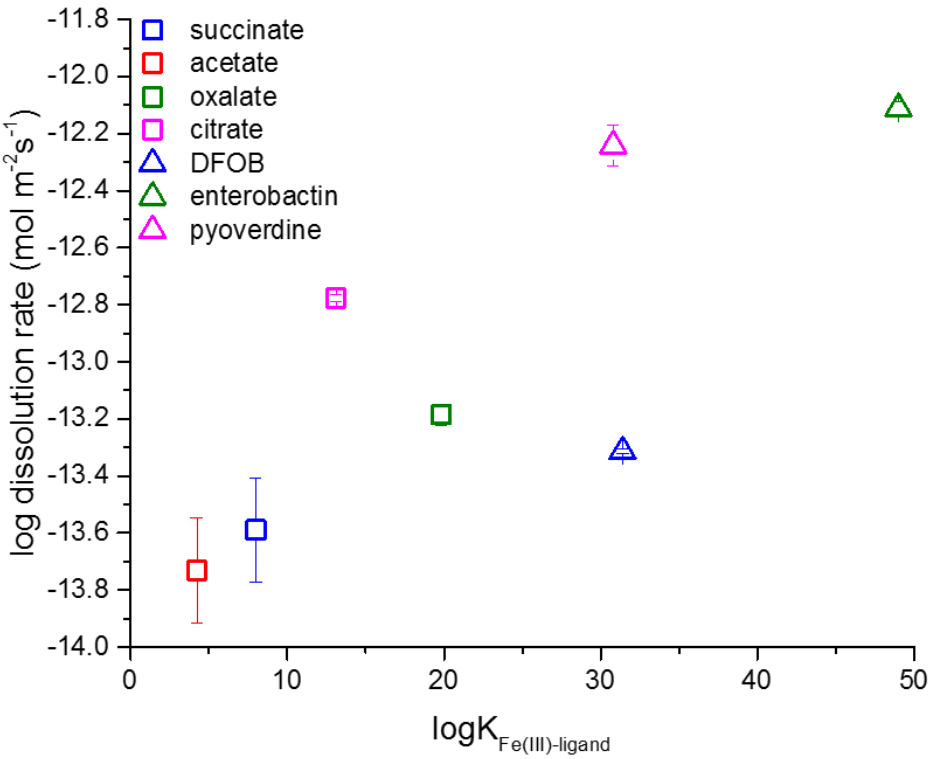

Figure 3.5 Log transformed initial dissolution rates of 0.2 g/L of $Cr(OH)_3$ (mol m^{-2} s^{-1}) at pH 7 and ionic strength of 0.1 M as a function of the stability constant of the corresponding Fe(III)-ligand complex. Stability constants are for Fe(III)-organic acid complexes (Martell and Smith 2003) predicted to be most thermodynamically stable under these conditions using MINTEQ (Gustafsson 2016). Fe(III)-siderophore stability constants are for the Fe(III)-siderophore complex with a completely unprotonated ligand (see references in Martell and Smith, 2003). This plot is presented with the caveat that not all dissolved metal may be ligand-complexed. Fe(III)-ligand stability constants are presented for consistency as Cr(III)-ligand stability constants are not available for all ligands and due to the similarity in ionic potential between Fe(III) and Cr(III).

The dissolution of $Cr(OH)_3$ by siderophores has recently been studied at several pH values by Duckworth et al.(Duckworth et al., 2014). The average surface area normalized dissolution rates at pH 7 and under similar experimental conditions were $4.3 \pm 0.7 \times 10^{-13}$ mol m^{-2} s^{-1} for DFOB and $3.0 \pm 1.7 \times 10^{-12}$ mol m^{-2} s^{-1} for protochelin (a triscatecholate type siderophore like enterobactin) (Duckworth et al., 2014), both of which are within a factor of 10 of rates observed in this experiment (Figure 3.3). The differences in observed rates may be the result of differences in properties of the initial synthesized $Cr(OH)_3$ solids and the difference in number of time points considered. Unlike organic acids, the relationship between stability constant and dissolution rate of the siderophores does not appear to be correlated (Figure 3.5), similar to what was observed in Duckworth et al. (2014). However, as mentioned previously, siderophore observations with Cr may not be explicitly comparable to the Fe(III)-siderophore stability constants. While Fe oxide dissolution rates have been shown to positively correlate to the Fe(III)-ligand stability constant (Akafia et al., 2014), Cr(III)-siderophore complexes have been shown to behave differently from their corresponding Fe(III)-siderophore complexes (Carrano et al., 1996; Duckworth et al., 2014). It is important to note that we focus here on dissolution rates rather than dissolution rate constants, which may result in some discrepancies due to siderophore adsorption affinities (Wang et al., 2015b), which were not the focus of this study.

The stability constants of the metal-ligand complexes can also be correlated with the observed isotopic fractionation factors (Figure 3.6). Metal-ligand complexes with the largest stability constants (based on stability constants for the most thermodynamically likely Fe(III)-ligand complex under these specific conditions) (Gustafsson, 2016) resulted in less positive/more negative fractionation (Figure 3.6). A similar trend has been observed

with Fe isotopes during organic acid-promoted dissolution of hornblende (Brantley et al., 2004). However, in that case the trend also encompassed greater fractionation with increasing stability constant, opposite of the observations of this study. If the predominant control is kinetic isotope fractionation, we would expect that lighter isotopes (i.e. negative $\Delta^{53}Cr$ defined as $\Delta^{53}Cr = \delta^{53}Cr_{solution} - \delta^{53}Cr_{starting\ solid}$) would enrich in solution at low dissolved Cr concentrations and approach the isotopic signature of the starting solid during continued dissolution (Johnson and Bullen, 2004). In this study, maximum isotopic fractionation was observed relatively soon after the experiment was initiated with isotope values eventually approaching the bulk solid isotope signature at greater dissolved Cr, similar to what has been previously observed with Fe isotopes during dissolution experiments on Fe oxides (e.g. Wiederhold et al., 2006). However, the enrichment of lighter isotopes in the solution during the early stages of dissolution was not evident in our system; instead positive values for $\Delta^{53}Cr$, were observed during initial dissolution (Figure 3.4). If the Cr(III)-oxygen bond(s) in the ligand is stronger than the Cr(III)-oxygen bonds in the solid, one would expect to see the observed enrichment of heavier isotopes (i.e. positive $\Delta^{53}Cr$) in the dissolved fraction (Figure 3.4). However, $\Delta^{53}Cr$ does not positively correlate to the predicted stability constant of the Fe(III)-ligand complexes, but instead generally exhibits a negative correlation (Figure 3.6). The highly positive $\Delta^{53}Cr$ values in the treatments with low stability constant ligands (e.g. acetate) may be caused by a fractionation during back reaction of weakly complexed liberated Cr(III). This process could be insignificant in more strongly bound Cr(III). Furthermore, if dissolution occurs layer-by-layer such that ligands complex and dissolve surface-Cr completely before the next layer is exposed and solubilized, a large fractionation may only be observed in the

early stages of dissolution (Johnson and Bullen, 2004). However, since $Cr(OH)_3$ only exhibits a particle size of < 10 Å and is likely a polymer of CrO_6 octahedra (e.g. Tang et al., 2010), such a "rind effect" is expected to be minimal.

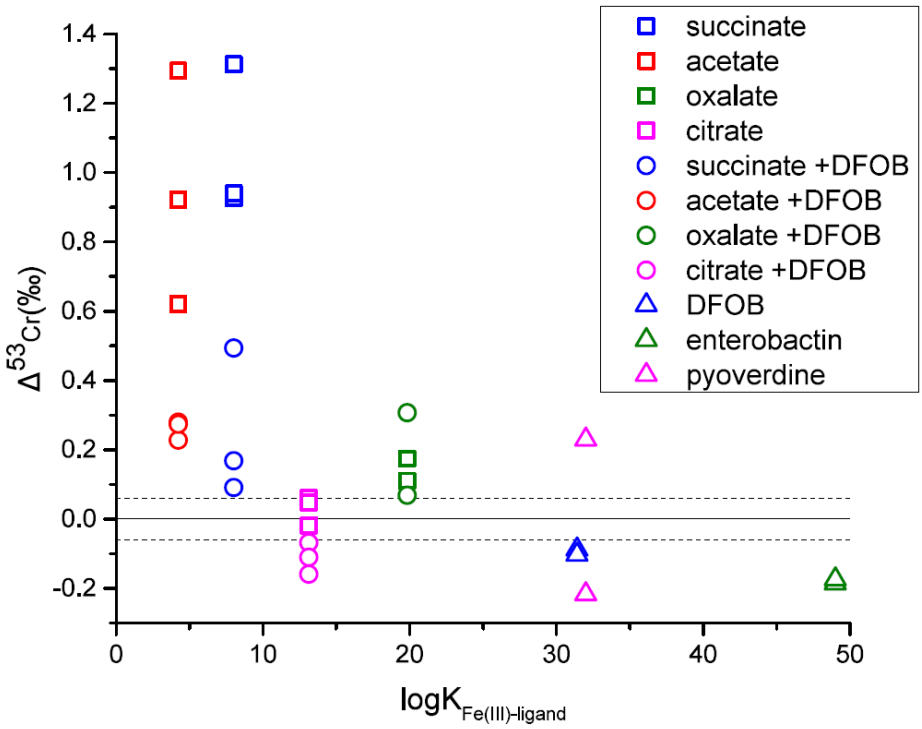

Figure 3.6 $\Delta^{53}Cr$ (defined as $\Delta^{53}Cr = \delta^{53}Cr_{solution} - \delta^{53}Cr_{starting\ solid}$) at pH 7 and ionic strength of 0.1 M as a function of the stability constant of the corresponding Fe(III)-ligand complex The data points for each condition represent complete harvests at various times throughout the experiment. Stability constants are for Fe(III)-organic acid complexes (Martell and Smith, 2003) predicted to be most thermodynamically stable under these conditions using MINTEQ (Gustafsson, 2016). Fe(III)-siderophore stability constants are for the Fe(III)-siderophore complex with a completely unprotonated ligand (see references in (Martell and Smith, 2003)). This plot is presented with the caveat that not all dissolved metal may be ligand-complexed. Fe(III)-ligand stability constants are presented for consistency as Cr(III)-ligand stability constants are not available for all ligands and due to the similarity in ionic potential between Fe(III) and Cr(III). No observed isotopic fractionation is indicated by the solid line at $\Delta^{53}Cr = 0$. The dashed lines represent ± 2σ.

3.6 Conclusions and Implications

In this study, we investigated the organic ligand-promoted dissolution of $Cr(OH)_3$ and associated Cr isotope fractionation. These results serve as the first survey study on the ligand-promoted dissolution and subsequent isotope fractionation of Cr(III), and have important implications for research using the Cr isotope system as a paleoredox and environmental tracer. Dissolution experiments were conducted at pH 7 in order to isolate the effects of ligand-promoted dissolution on Cr(OH)3 (Duckworth et al., 2014). Therefore, despite lower rates and extents of dissolution relative to proton-promoted dissolution (Duckworth et al., 2014), ligand-promoted dissolution of Cr-containing phases might contribute significantly to Cr mobilization under non-acidic conditions, such as in the marine environment. For instance, isotopically fractionated Cr(III) may be leached from dust or sourced from a benthic flux of organically complexed Cr(III). Again, the presence of ligand bound Cr(III) in the modern oceans supports organic complexation as a potentially important component of the Cr cycle (Nakayama et al., 1981; Sander and Koschinsky, 2000; Sander and Koschinsky, 2011). Terrestrial waters can also be near neutral or alkaline, suggesting the need to survey for significant ligand bound Cr(III) when using Cr isotopes to monitor Cr reduction in environmental remediation studies.

The redox-independent Cr isotope fractionations observed in this study are within the range of values previously reported to reconstruct oxygenation events (Figure 3.7 and 3.8). Therefore, the results from this study suggest that the interpretation of the Cr isotope proxy may need to be altered to account for redox-independent processes, such as the mobilization of Cr(III) by organic or inorganic complexing ligands. Some sedimentary Cr isotope archives are more likely to be affected by this process. As mentioned above, high

pH systems (e.g. marine systems) may be more likely to express the effects of ligand-promoted solubilization than low pH systems, given that proton-promoted dissolution will scale with pH. Marine systems removed from a terrestrial source (e.g. carbonate platforms) might be expected to capture variably fractionated organic bound-Cr(III). Given the high density of organic acids in the weathering realm (e.g. Neaman et al., 2005), paleosols with evidence for intense weathering may also be susceptible to expression of Cr(III)-organic isotope fractionations (e.g. Babechuk et al., 2017).

The common occurrence of organic bound-Cr(III) in modern environments and the potential for the formation of organic acids throughout Earth's history indicates that the presented results must be considered when using Cr isotopes to track Earth's oxygenation. Further, the presence of both positive and negative Δ^{53}Cr values will make it difficult to directly assess the influence of Cr(III)-ligand isotope effects in deep time studies. However, this does not require abandonment of the basic framework for using Cr isotopes as a paleoredox proxy, where analytically significant Cr isotope variations in the sedimentary records are a signal for oxidative Cr cycling that can be linked to a critical oxygen threshold (Frei et al., 2009). The common occurrence of mobile but unfractionated Cr (Cole et al., 2016; Frei et al., 2009; Planavsky et al., 2014) suggests that Cr(III) moving through Earth's surface is not ubiquitously affected by organic solubilization and ligand-induced fractionation, though some variability is observed in each of these studies. In this light, the possibility of some variable Cr isotope values should be expected in low oxygen systems (e.g. without Cr(III) oxidation), and moving forward, the paleoredox Cr isotope framework must account for this possibility. Despite this added complexity, we suggest that organic complexation is unlikely to lead to a systematic shift in the mean value of the mobile Cr

reservoir on a global scale, in contrast to extensive Cr oxidation. Therefore, sedimentary systems without Cr oxidation are likely to be characterized by mean Cr isotope values similar to crustal values. In other words, although organic complexation in terrestrial and marine systems has the potential to result in some scatter beyond the crustal range, only extensive Cr oxidation can result in consistently heavy, mobile Cr. Nevertheless, our results imply that some Cr isotope data from individual formations may lead to ambiguous conclusions about the presence of oxidative Cr cycling.

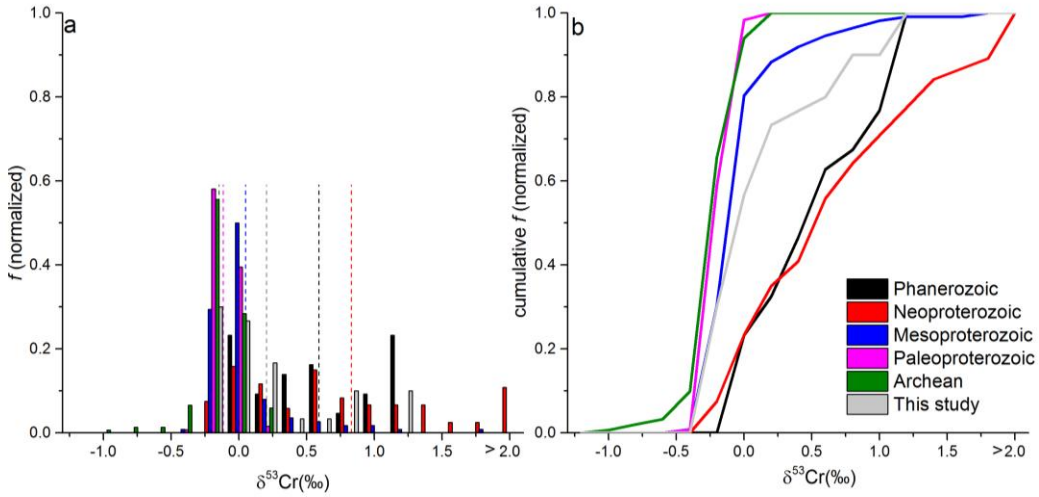

Figure 3.7 Frequency distributions (a) and cumulative frequency distributions (b) of previously observed $\delta^{53}Cr$ ranges from Phanerozoic (0.541 Ga to present), Neoproterozoic (1.0–0.541 Ga), Mesoproterozoic (1.6–1.0 Ga), Paleoproterozoic (2.48–1.6 Ga), and Archean (4–2.5 Ga) iron formations, ironstones, shales, and carbonates that have been used as evidence for surface oxygenation and data from our study (Cole et al., 2016; Crowe et al., 2013; Frei et al., 2009; Gilleaudeau et al., 2016; Planavsky et al., 2014; Reinhard et al., 2014). Dashed lines show mean $\delta^{53}Cr$ values each data set.

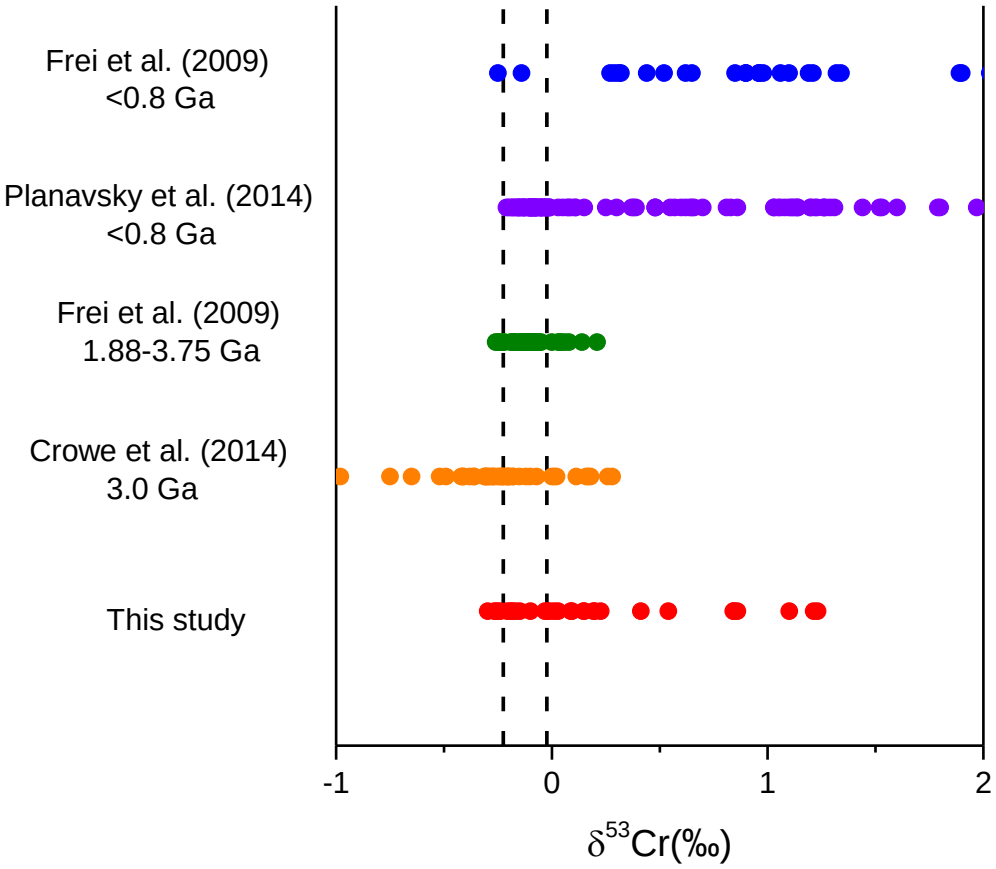

Figure 3. 8 Redox independent Cr isotope signatures observed in this study compared with previously observed δ^{53}Cr ranges iron formations and ironstones that were used as evidence for surface oxygenation. δ^{53}Cr results from this study are within similar ranges as previous results from Archean and early Proterozoic rock record, but much smaller than Neoproterozoic and Phanerozoic data. The dashed lines delineate the δ^{53}Cr ranges of igneous rocks (mainly basalts and granites).

4. UNDERSTANDING MARINE DISSOLVED ORGANIC MATTER PRODUCTION: COMPOSITIONAL INSIGHTS FROM AXENIC CULTURES OF THALASSIOSIRA PSEUDONANA

4.1 Abstract

Marine dissolved organic matter (DOM) is a key source of carbon and nutrients to microbial life in the oceans, but rapid biological utilization of labile DOM confounds its compositional characterization. In order to characterize potentially bioavailable DOM produced by phytoplankton, DOM from axenic cultures of *Thalassiosira pseudonana* cultivated in phosphorus (P) replete and low P conditions was extracted using high-recovery electrodialysis (ED) techniques, which resulted in an average dissolved organic carbon (DOC) recovery of 76 ± 7% from all cultures. Low P concentrations resulted in greater cell-normalized production of DOC relative to P replete culture controls at the same growth phase. Despite the different nutrient conditions, DOC composition and DOM molar ratios of carbon to nitrogen (C:N) were similar in all cultures. In contrast, low P concentrations influenced DOM molar carbon to phosphorus (C:P) ratios and dissolved organic phosphorus (DOP) composition. Under P replete and low P conditions, DOM C:P ratios were 130 (± 22) and 2446 (± 519), respectively. ^{31}P Nuclear Magnetic Resonance (NMR) spectroscopy identified P esters (> 90% of DOP) as the dominant P species in DOM produced under P replete conditions, with small or negligible contributions from

---

Saad EM, Longo AF, Chambers L, Huang RX, Benitez-Nelson C, Dyhrman ST, Diaz J, Tang YZ, Ingall E. Understanding marine dissolved organic matter production: Compositional insights from axenic cultures of *Thalassiosira pseudonana*. *Limnology and Oceanography*. 2016, 61, 2222-2233

phosphonates or glycerol P and polyphosphates. However, based on direct fluorometric analysis, DOP from low P cultures was greater than 8 times enriched in dissolved polyphosphate compared to DOP from replete cultures, which is consistent with the growing evidence that polyphosphate is a dynamic component of total P in low P ocean regions.

4.2 Introduction

Dissolved organic matter (DOM) is a source of bioavailable carbon (C) and nutrients, including nitrogen (N) and phosphorus (P). In the ocean, DOM supports the growth of marine bacteria (Azam et al., 1983) and phytoplankton (Bronk et al., 2007; Duhamel et al., 2010), especially in oligotrophic ocean regions (Agusti and Duarte, 2013; Ducklow et al., 1995; Fogg, 1983; Karl et al., 1998; Thomas, 1971). Furthermore, DOM composition influences marine microbial community structure (Dinasquet et al., 2013; Gomez-Consarnau et al., 2012; Nelson and Carlson, 2012; Neogi et al., 2011) and ultimately carbon remineralization and export (Letscher and Moore, 2015). Despite its critical role in ocean biogeochemistry, the composition of DOM remains poorly understood (Benner, 2002).

DOM is produced via degradation of non-living organic matter and is also actively produced by living organisms (Carlson, 2015) including phytoplankton, which are considered a source of labile DOM (Cole et al., 1982; Norrman et al., 1995). Labile DOM is preferentially utilized, predominantly by marine heterotrophs (Carlson, 2015; Jensen, 1983; Kirchman et al., 1991; Reinthaler and Herndl, 2005), over timescales of minutes to weeks (Amon et al., 2001; Carlson, 2002.). However, ambient pools of marine DOM, which are typically characterized in compositional studies (Benner, 2002), have

radiocarbon ages in the range of thousands of years (Bauer et al., 1992; Karl and Bjorkman., 2014; Loh et al., 2004; Williams and Druffel, 1987) and, thus, may not reflect freshly produced, labile DOM.

Ambient pools of marine DOM contain dissolved organic forms of C (DOC), P (DOP), and N (DON), including biomolecules and their derivatives (Repeta, 2014). Of these forms, this study focuses on DOP in order to better understand intriguing compositional observations in the ocean. Diverse regions and depths of the ocean contain relatively consistent proportions of polyphosphates (molecules with at least three P atoms joined by P-O-P bonds), 8-13% of DOP; phosphonates (direct C-P bonds), 5-10%; and P esters (P-O-C bonds), 80-85% (Young and Ingall, 2010). This uniform composition of DOP, which is distinct from that of marine organisms, has been attributed to microbial decomposition processes (Clark et al., 1998, 1999; Karl and Bjorkman., 2014; Kolowith et al., 2001; Young and Ingall, 2010). However, despite the critical role of these P forms as potential P sources (Martin et al., 2014; Van Mooy et al., 2015) and as possible drivers of climate (Diaz, 2008 #266), the composition of DOP initially produced by microorganisms remains largely unexplored.

In order to characterize the DOM fraction initially supplied to marine systems, previous studies have examined DOM produced in controlled cultures of marine phytoplankton (Hellebust, 1965; Aluwihare and Repeta, 1999; Biddanda and Benner, 1997; Biersmith and Benner, 1998; Granum et al., 2002; Myklestad, 1977; Obernosterer and Herndl, 1995). DOM compositional characterization in these studies focused on either specific compounds, such as polysaccharides, or bulk analysis of the high molecular weight fraction of DOM. Compositional differences between phytoplankton-derived DOM and

ambient ocean DOM identified in these studies were attributed to selective utilization of certain compounds by bacteria (Aluwihare and Repeta, 1999; Biddanda and Benner, 1997; Biersmith and Benner, 1998). In fact, the composition of phytoplankton-derived DOM can be altered by heterotrophic processing on timescales of days to weeks due to preferential consumption of not only specific compound classes, but also of specific molecules within compound classes (Amon et al., 2001).

Limited evidence based on analysis of specific compounds or bacterial utilization of DOM produced in culture studies suggests that nutrient availability influences the composition of phytoplankton-derived DOM (Myklestad, 1977; Myklestad and Haug, 1972; Obernosterer and Herndl, 1995; Puddu et al., 2003). For example, phytoplankton growth under low P conditions can result in the production of DOM that supports a distinct microbial community compared to DOM produced under P replete conditions (Puddu et al., 2003), which may reflect bioavailability differences and, thus, compositional differences between DOM pools produced under different P regimes. Although N is often the limiting nutrient over vast marine areas, spatial and temporal increases in N abundance may shift systems to P limitation (Karl et al., 1998; Karl et al., 1995; Moore et al., 2013). Phytoplankton alter cellular P allocation in response to P scarcity, specifically through the substitution of sulfolipids for phospholipids (Martin et al., 2011; Van Mooy et al., 2009) and modulation of cellular phosphorus pools like polyphosphate compounds (Diaz, 2015; Dyhrman et al., 2012; Martin et al., 2014). Whether these P-dependent particulate dynamics translate to similar compositional shifts within the DOP pool remain unknown.

For all DOM studies, there are difficulties associated with obtaining a representative sample for chemical analysis (Benner, 2002; Hedges, 1992). Most chemical

characterization techniques require naturally low concentrations of marine DOM (~1 ppm) to be isolated from the high salt content of seawater (~35,000 ppm) (Repeta, 2014). Isolation difficulties traditionally limit DOM studies to the analysis of a small number of molecules that can be directly measured in a high salt matrix or to the characterization of the partial DOM fractions that can be recovered. For example, many studies have isolated DOM via ultrafiltration, which recovers the high molecular weight fraction of DOM (> 1 kDa) (see references in Benner, 2002). Thus, low molecular weight, potentially bioavailable molecules typically escape characterization (Kujawinski, 2011). In fact, phytoplankton-derived DOM is dominated by low molecular weight molecules (Jensen, 1983; Lancelot, 1984), which have been suggested to have a composition distinct from molecules in the high molecular weight fraction (Benner et al., 1992; Biddanda and Benner, 1997).

Recently developed electrodialysis (ED) extraction techniques have improved DOM recoveries by approximately three times compared to ultrafiltration (Green et al., 2014; Koprivnjak et al., 2009). Higher recovery yields a final sample that is more representative of bulk DOM by diminishing the bias towards the high molecular weight DOM fraction recovered using ultrafiltration (Koprivnjak et al., 2009; Vetter et al., 2007). Thus, ED techniques offer the potential for new insights into the marine DOM composition. For example, the application of ED has recently revealed the presence of dissolved polyphosphates in diverse marine waters (Diaz et al., 2008; Young and Ingall, 2010), which typically go undetected in ultrafiltration studies (e.g. Clark et al., 1998, 1999; Kolowith et al., 2001; Sannigrahi et al., 2006).

In previous culture studies, the low DOM extraction efficiencies of ultrafiltration required processing large volumes to obtain analytically relevant quantities for studies of bulk DOM composition (Biddanda and Benner, 1997). Large volumes made it difficult to evaluate the composition of phytoplankton-derived DOM in the absence of bacteria and fungi (axenic conditions), which can consume the most bioavailable fractions on time scales of minutes to hours (Carlson, 2002.). The larger recoveries of ED permit the use of smaller culture volumes to obtain analytically useable DOM quantities for bulk compositional analyses. Additionally, smaller culture volumes simplify the creation and maintenance of axenic conditions and allow for greater levels of replication and evaluation of key influences on DOM composition, such as nutrient availability. Thus, ED offers the opportunity to characterize labile DOM that is rapidly utilized. Here, ED techniques were used to extract DOM produced under P replete and low P conditions in triplicate, axenic cultures of the marine diatom, *Thalassiosira pseudonana*, in order to provide insight into the composition of freshly produced, potentially bioavailable DOM supplied to marine systems.

4.3 Methods

4.3.1 Cultures

Axenic *Thalassiosira pseudonana* (*T. pseudonana*) CCMP1335 was obtained from the National Center for Marine Algae and Microbiota (NCMA), Bigelow Laboratories, East Boothbay, ME. *T. pseudonana* was grown in f/2 medium (Guillard and Ryther, 1962) prepared in an artificial seawater base (Kester et al., 1967). Artificial seawater without sodium biocarbonate was autoclaved before the addition of filter-sterilized (0.22 µm)

sodium bicarbonate, nutrients, vitamins, and trace metals. For P replete cultures, the phosphate and nitrate concentrations were 36 µM and 880 µM, respectively, yielding a molar N:P ratio of 24. Cultures grown under the low P conditions were cultivated with a ~30 fold reduction in inorganic P in culture media. For low P cultures, phosphate was reduced to 1 µM (N:P = 880). Cultures (2.5 L) for each nutrient regime were grown in triplicate at 22°C on a 12 h:12 h light:dark cycle at 100 µE m^{-2} s^{-1} light intensity in 4 L borosilicate glass flasks. All cultures were inoculated with cells at the same growth phase grown under nutrient replete conditions. Growth of each replicate was monitored daily by measuring chlorophyll a fluorescence (excitation: 440 nm, emission: 680 nm; Shimadzu RF-5301PC Spectrofluorophotometer) (Lorenzen, 1967). During early logarithmic phase, cell abundances were calculated using our empirically determined relationship between chlorophyll a fluorescence and direct microscopic counts. In late logarithmic phase, cells were counted directly to reduce the uncertainty associated with using chlorophyll a as a proxy for biomass under different nutrient regimes. In order to reduce the potential for differences in the rate of DOM release and DOM composition as a function of growth phase, DOM was harvested in the late logarithmic phase of growth for each nutrient condition (Figure 4.1) (Barofsky et al., 2009; Myklestad et al., 1989; Urbani et al., 2005). Harvesting in the late logarithmic phase also limits the degree of DOM recycling and alteration by *T. pseudonana*, which would likely increase late into stationary phase as inorganic nutrients are depleted and DOP hydrolytic enzymes are induced (Dyhrman et al., 2012). Specifically, alkaline phosphatase activity increases in stationary phase cultures of Emiliania huxleyi (Dyhrman and Palenik, 1999) and Escherichia coli (Chou et al., 2005), indicating a rise in the enzymatic hydrolysis of dissolved organic P, which is necessary to

avoid in the current study. Harvesting DOM at this stage of growth should also mitigate additional DOC inputs due to cell lysis during stationary phase (Puddu et al., 2003). In order to consistently sample cultures, late logarithmic phase was defined to occur 24 h before the maximum cell density was reached for each nutrient condition. This experimental design was modeled after previous work focused on examining the physiological impact of low P on phytoplankton (Dyhrman and Palenik, 1999, 2003; Wurch et al., 2014) including *T. pseudonana* (Dyhrman et al., 2012). Previous work has shown that *T. pseudonana*, grown in N:P > 800 and sampled in late logarithmic phase, exhibits a multifaceted physiological response to low P at the transcript, protein, and activity level (Dyhrman et al., 2012). Axenic conditions were confirmed for all cultures through plating on LB medium agar (de Brouwer et al., 2002) and/or inoculating the culture into the heterotrophic K-medium and incubating in the dark. A *T. pseudonana* culture grown under non-sterile conditions was used as a positive control in our tests for axenic conditions.

4.3.2 Dissolved organic matter isolation

DOM produced by *T. pseudonana* was harvested by aseptically separating biomass from the media via centrifugation (2.2 x 10^3 g, 7 min) and subsequent filtration (< 0.85 bars; Whatman GF/F, 0.7 µm nominal). This sample was then processed with ED within 24 h. This study used solely ED techniques to desalt DOM in contrast to previous studies that used ED in conjunction with reverse osmosis (Green et al., 2014; Koprivnjak et al., 2009; Vetter et al., 2007). With the system used in this study, the 2-10 L starting volume is directly freeze-dried after ED processing, removing the need for water volume reduction by reverse osmosis. Thus, DOM losses that typically occur during reverse osmosis

processing were avoided. ED was performed using Deukum electrodialysis stack (Deukum GmbH, Frickenhausen, Germany) coupled to circulation system built in our lab. To condition the ED stack for sample processing, it was first rinsed with ultrapure water (18 MΩ cm), followed by sterile f/2 media. The electrodialysis stack consists of 10 cell pairs of alternating Neosepta anion AMX and cation CMX exchange membranes (Astom Corp., Tokyo, Japan) held between a cathode and anode situated at opposite ends of the stack. The electric potential across the stack was supplied by a 1.2 kW Sorensen DCS150-8EM1 power supply. Three pumps and associated valves control the flow and pressure of the sample, referred to as the diluate, the concentrate, which is the water reservoir that receives ions from the sample, and electrode rinse, which is a sodium sulfate solution that maintains ionic balance between the cathode and anode. During the ED process, anions are pulled through the AMX membranes toward the anode, while cations are pulled through CMX membranes toward the cathode. As the ions are pulled to their respective electrodes, they move from the diluate flow into the concentrate flow. The conductivity of the sample and the applied amperage were continuously monitored to keep the system below the limiting current density, which prevents large excursions in pH during sample processing (Vetter et al., 2007; Young and Ingall, 2010). During ED processing, the concentrate was changed once when the conductivity of the sample was reduced to approximately 4.0 mS cm^{-1}. When changing the concentrate, the ED process was paused and 5/6 of the concentrate replaced with fresh, ultrapure water. This approach allows desalination to continue without causing a drastic salinity differential between the concentrate channel and the diluate channel, which improves DOM recoveries. Samples were processed from an initial conductivity ~5×10^4 μS cm^{-1} to a conductivity of ~150 μS cm^{-1}. The resulting desalinated

sample was freeze-dried, homogenized using an agate mortar and pestle, and stored at -20°C until analysis.

Extraction and concentration of DOM using ED resulted in an average DOC recovery of 76 ± 7% from all cultures. These DOC recoveries are much greater than the highest recoveries obtained using the previously applied techniques including solid phase extraction, ultrafiltration, and ED coupled with reverse osmosis (Arrieta et al., 2015; Benner et al., 1992; Dittmar et al., 2008; Green et al., 2014; Guo et al., 2000; Hertkorn et al., 2013; McCarthy et al., 1993; Stubbins et al., 2014; Walker et al., 2011). The unrecovered DOC likely consists of surface-reactive molecules that are adsorbed to ED membranes. In other studies, such surface reactive molecules are desorbed from membranes using a strong base rinse of the system (Green et al., 2014; Koprivnjak et al., 2009). Because the use of strong base confounds characterization methods and likely alters DOM composition, it was avoided in this study. ED optimization experiments testing the recovery of specific compounds dissolved in artificial seawater achieved a 90.2 ± 2.1% recovery of glucose (molecular weight 180.2 g mol^{-1}), a 67.5 ± 9.9% recovery for ethylenediamine tetraacetic acid (EDTA, molecular weight 292.2 g mol-1), and a 98.3 ± 1.6% recovery for vitamin B12 (molecular weight 1355.4 g mol-1). The difference between glucose, EDTA, and vitamin B12 recoveries is consistent with the idea that charged molecules, like EDTA, are more likely to be sorbed to ED membranes relative to neutral molecules, like glucose and vitamin B12 (at the ED operating pH).

4.3.3 Dissolved phase analysis

Sample aliquots collected at the beginning and end of ED process were characterized with several methods to quantify the recoveries associated with the desalination process. DOC was measured using high temperature catalytic oxidation on a Shimadzu TOC-V (Benner and Strom, 1993; Sharp et al., 2002). Dissolved inorganic carbon was measured with a flow injection analysis system by conductivity detection (Analytical Instruments Systems, Inc. LCC100 integrator) (Hall and Aller, 1992). Dissolved inorganic nitrogen (nitrate and nitrite) was measured using anion chromatography (Metrohm A Supp 5 150.0/ 4.0 mm) coupled to ultraviolet detection (Beckman Coulter DU 720 detector) with a sodium chloride eluent (Beckler et al., 2014). Soluble reactive phosphorus was measured by spectrophotometry (Murphy and Riley, 1962).

4.3.4 Solid phase analysis

Total carbon, nitrogen, and phosphorus were measured in freeze-dried DOM samples. Total phosphorus was measured by utilizing high temperature combustion (550^{o}C for 2 h) followed by extraction in 1 N HCl agitated for 24 h (Solorzano and Sharp, 1980) prior to spectrophotometric analysis (Murphy and Riley, 1962). Carbon and nitrogen concentrations were measured using a CHNSO analyzer (Costech instruments) (Hedges and Stern, 1984). Polyphosphate was quantified using a slightly modified version of the enzymatic extraction and fluorometric quantification method described in Martin and Van Mooy (2013). For these samples, nucleases were used to remove nucleic acid interference, as nucleic acids will also fluoresce in the presence of 4',6'-diamidino-2-phenylindole (DAPI), the fluorometric stain used to quantify polyphosphate.

4.3.5 ^{13}C NMR analysis

^{13}C cross polarized (CP) NMR spectra of freeze dried DOM samples were collected on a Bruker AVANCE III 400 spectrometer equipped with a Bruker double-channel 4-mm probe and operated at a 13C frequency of 100.6 MHz. A variable-amplitude CP (VACP) sequence pulse was used with a 1.0 ms contact time. The samples were packed into a 4 mm diameter zirconia rotor with Kel-F Caps (Wilmad, NJ) and spun at 10 kHz. Chemical shifts for ^{13}C spectra were externally referenced using adamantane. The spectrum for each sample was phased, baseline-corrected, and integrated using Bruker's Topspin 3.0 software. The ^{13}C NMR spectral data were entered into a mixing model to estimate the molecular composition of the DOM in terms of non-specific amino acid, carbohydrate, and lipid content (Nelson and Baldock, 2005; Sannigrahi et al., 2005). The relative intensity of seven chemical shift regions from the spectrum of each sample was fit and the C:N ratio of each sample was used as a constraint on compositional identifications. The fitting was performed using the average, upper, and lower limits of the C:N ratios representing the average and ± standard deviation of DOM C:N ratios from triplicate cultures.

4.3.6 ^{31}P NMR analysis

Solid-state ^{31}P NMR spectra on solid samples were recorded on a Bruker AVANCE III-HD 500 spectrometer operating at 202.489 MHz using a 1.9 mm magic angle spinning (MAS) double resonance probe. SPINAL64 (McGeorge et al., 1999) proton dipolar decoupling with a field strength of 145 kHz was applied during acquisition, and a MAS speed of 20 kHz was used. Bloch decays of 50 ms were collected with a 200 parts per million (ppm) window after 30 degree excitation pulses. The number of transients collected

varied, depending on the amount of material and ranged from 50,000 - 100,000 scans per sample (24 to 48 hours).

Spectra were fit with up to 5 Lorentzian lines at 18 to 20 ppm (phosphonate or glycerol 1,2-cyclic phosphate), 0 to 2 ppm (orthophosphate), -10 to -12 ppm (diesters), and -22 to -24 ppm (polyphosphate) to determine percentage of each compound in total P. The NMR peak observed in the 18 to 20 ppm region of the NMR spectra has been traditionally attributed to the presence of phosphonates, however some ^{31}P NMR studies of *T. pseudonana* suggest that glycerol 1,2-cyclic phosphate, a biomolecule associated with phospholipid metabolism, is also found in this spectral region (Boyd et al., 1987; Tesson et al., 2008). Values reported have a technical error of ± 5%, similar to solid-state ^{31}P NMR studies in other systems (Diaz et al., 2008).

4.4 Results

Average cell-normalized concentrations of DOC (pg cell^{-1}) in the unprocessed culture media were twice as high under low P compared to P replete control conditions: P replete, 3 (± 1) and low P, 6 (± 1). Extraction and concentration of DOM using ED resulted in an average DOC recovery of 76 (± 7)% from all cultures. DOC recoveries for P replete controls and low P cultures were 76 (± 7)% and 75 (± 9)%, respectively. The unrecovered DOC likely consists of surface-reactive molecules that are adsorbed to ED membranes (see Methods). The exact composition of surface adsorbed molecules cannot be determined, but the consistency of recovery among nutrient regimes suggests that a quantitatively and compositionally similar fraction was lost from all nutrient regimes. ED effectively removed inorganic C (> 95%), which was consistently below the detection limit (150 µM) in all

samples after ED processing. ED also removed inorganic N (99.79 ± 0.01%), and P (95.8 ± 0.9%) from all samples confirming that the material recovered by ED was dominantly composed of organic material.

DOM molar C:N ratios were similar for both the low P treatment and the control despite differences in growth (Figure 4.1). Under P replete and low P conditions, DOM molar C:N ratios were 5.2 (± 0.6) and 5.2 (± 0.4), respectively. In contrast to the C:N ratios, DOM molar C:P ratios exhibited greater variability among nutrient conditions. Under P replete and low P conditions, DOM molar C:P ratios were 130 (± 22) and 2446 (± 519), respectively.

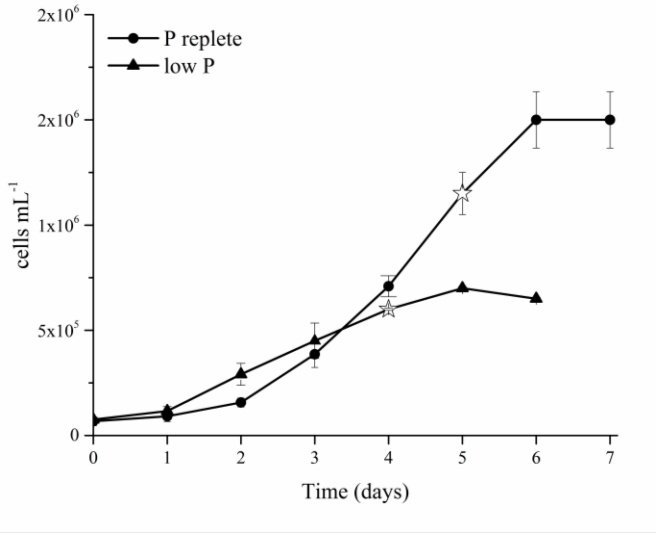

Figure 4.1 Growth curves for P replete and low P *T. pseudonana* cultures. Stars indicate the time of harvest. During early logarithmic phase, cell abundances were calculated using our empirically determined relationship between Chl *a* fluorescence and direct microscopic counts. In late logarithmic phase, cells were counted directly. Average and standard deviation cell density measurements (cells mL^{-1}) of triplicate cultures for each nutrient condition at the time of harvest were as follows: P replete ($1 \times 10^6 \pm 1 \times 10^5$) and low P ($6 \times 10^5 \pm 5 \times 10^3$). Error bars indicate standard deviation of triplicate cultures for each condition.

Under both nutrient conditions, ^{13}C NMR spectra revealed that amino acids were the dominant C-containing compound class in DOM (~70% of total C), followed by carbohydrates (~30%) and minor amounts of lipids (< 1%) (Table 4.1). With respect to P composition of P replete cultures, ^{31}P NMR spectroscopy identified P esters (90 ± 15%) as the dominant phosphorus species, followed by phosphonates or glycerol P (10 ± 15%) and polyphosphates (< 5%). In low P samples, all P compound classes were below detection under the conditions of our ^{31}P NMR analysis due to low total P content. The relative abundance of polyphosphate, which was below detection with NMR, was quantified with direct fluorometric analysis. Because the fluorometric polyphosphate quantification method cannot measure absolute quantities (i.e., molar ratios of polyphosphate:total P > 1 are possible with this technique (Martin et al. 2014)), polyphosphate is reported in units of mole equivalents (eq), similar to previous studies that have used the same method (Martin et al. 2014; Diaz et al. 2015). In DOM collected from replete cultures, polyphosphate:DOP was < 5 eq mol-1, but in low P samples, polyphosphates comprised approximately 38 eq mol-1 of DOP (Table 4.2). These results indicate that DOP was more than ~8 times enriched in polyphosphate in low P compared to P replete cultures, even though total DOP content was much lower under low P conditions.

Table 4.1 ^{13}C NMR speciation results of different biomolecules as a percent of total DOC

Biomolecule	P replete	Low P
Carbohydrates	30 ± 8	30 ± 3
Amino acids	70 ± 8	69 ± 5
Lipids	0 ± 0	<1 ± 2

Table 4.2 DOP and relative quantities of dissolved polyphosphate (polyP) content

Species	P replete	Low P
DOP (nmol mg^{-1})	13.0 ± 0.4	0.6 ± 0.4
polyP (peq mg^{-1})	548 ± 39	252 ± 27
polyP:DOP (eq mol^{-1})	4.2 ± 1.8	38 ± 8

4.5 Discussion

In this study, ED techniques were applied in order to examine the bulk composition of freshly produced DOM in *T. pseudonana* cultures from a low P treatment relative to a control. DOM production in the ocean is certainly influenced by organisms other than *T. pseudonana*, and phytoplankton-derived DOM does exhibit some species-specific compositional differences (Biddanda and Benner, 1997; Myklesta.S, 1974). In addition to compositional differences of various phytoplankton species, other DOM sources, such as the decomposition of particulate matter, grazer mediated release, and release from prokaryotes (Carlson, 2015; Thornton, 2014), may also play important roles in contributing to marine DOM composition. Nevertheless, *T. pseudonana*, a model diatom that is readily grown in culture, provides an excellent starting point to examine the composition of freshly produced, phytoplankton-derived DOM.

The C:N ratios of DOM produced from axenic cultures of *T. pseudonana* were approximately 5.2 for both the low P treatment and the control. Biddanda and Benner (1997) characterized DOM C:N ratios averaged over an entire growth curve for non-axenic cultures grown under nutrient replete conditions of several common marine phytoplankton,

Synechococcus bacillaris (4.1), Phaoecystis sp. (7.0), Emiliania huxleyi (6.3), and Skeletonema costatum (14.1), collected using ultrafiltration. C:N ratios of surface ocean DOM in diverse P replete ocean regions average 13 (± 2) (Hansell and Waterhouse, 1997), while dissolved C:N in the low P Sargasso Sea is 14 (± 2) (Hansell, 2001) (Figure 4.2a). Based on the decomposition stoichiometry of DOM from diverse ocean regions, Hopkinson and Vallino (2005) extrapolated a C:N ratio for labile DOM of 10.7 (± 2.4). The low DOM C:N ratios observed in axenic *T. pseudonana* cultures in this study are consistent with the lower ratio extrapolated for labile DOM relative to ambient surface ocean DOM. Additionally, a greater abundance of amino acids was observed in DOM produced by *T. pseudonana* (~70%) relative to ambient surface ocean DOM (~24%) (Sannigrahi et al., 2005). Enrichment in amino acids and associated low C:N ratios in DOM from our cultures relative to surface ocean DOM is consistent with the idea that N rich molecules are preferentially utilized in ocean surface waters (Hopkinson et al., 1997; Hopkinson et al., 2002; Williams et al., 1980). In fact, some freshly produced phytoplankton-derived proteins have turnover times of hours to days in marine systems, which suggests rapid utilization (Keil and Kirchman, 1993). Similarly, amino acids have been observed to have a higher utilization rate relative to carbohydrates in phytoplankton-derived DOM in various surface ocean settings (Cherrier and Bauer, 2004; Ittekkot, 1982; Williams and Yentsch, 1976).

Although C:N ratios and ^{13}C NMR DOC composition did not vary, C:P ratios and DOP composition varied between the low P treatment and control. DOM derived from *T. pseudonana* in the P replete control exhibited C:P ratios of 130 (± 22), which is lower than ratios observed in surface waters that are typically considered P replete, 299 (± 72) (Figure

4.2b) (Hopkinson and Vallino, 2005; Loh and Bauer, 2000). Based on an extrapolation of the decomposition stoichiometry of DOM from diverse ocean regions, labile DOM is hypothesized to have a mean C:P ratio of 199 (± 37) (Hopkinson and Vallino, 2005). The low DOM C:P ratios observed in axenic *T. pseudonana* cultures under P replete conditions in this study are consistent with the lower ratio extrapolated for labile DOM relative to ambient surface ocean DOM and reaffirm the suggestion that P is preferentially utilized during DOM decomposition (Hopkinson and Vallino, 2005; Kolowith et al., 2001; Letscher and Moore, 2015; Loh and Bauer, 2000). Furthermore, under P replete conditions, P esters dominated P composition of T. pseudonana-derived DOM (~90%) with smaller amounts of DOM with a chemical shift suggestive of phosphonates and/or glycerol P (~10%) and polyphosphates (< 5%). Compositional dominance of P esters has been similarly observed in the high molecular weight fraction of DOM from non-axenic cultures of *Synechococcus bacillaris*, *Phaoecystis* sp., *Emiliania huxleyi*, and *Skeletonema costatum* grown under nutrient replete conditions (Clark et al., 1999). However, ambient ocean DOP contains a higher proportion of polyphosphates (8-13%) and phosphonates (5-10%) and a lower proportion of P esters (80-85%) relative to the DOP composition observed in phytoplankton cultures (Young and Ingall, 2010). Thus, preferential utilization of dissolved P esters may produce the higher dissolved C:P ratios and higher relative proportions of dissolved polyphosphate and phosphonates observed in ambient marine DOM. This preferential utilization is consistent with previously hypothesized mechanism to explain the composition of ambient ocean DOP (Clark et al., 1999) (Kolowith et al., 2001; Young and Ingall, 2010).

Low P concentrations had a strong effect on dissolved C:P ratios and DOP composition, which, along with reduced growth rates under low P conditions (Figure 4.1), suggests that P concentrations resulted in a physiological response of *T. pseudonana*. Low P resulted in an average C:P ratio of 2446 (± 519), which is consistent with a DOM C:P ratio of approximately 2000 observed in the Sargasso Sea (Lomas, 2016), a low P region (Martin et al., 2014) (Figure 4.2b). Furthermore, low P conditions resulted in a distinct DOP composition. Based on direct fluorometric analysis, DOP contained ~8 times more polyphosphate in the low P cultures compared to P replete cultures, even though total DOP content was much lower. As a metabolic response to low P, increases in phytoplankton polyphosphate content relative to other P containing biomolecules have been observed in the particulate fraction of *T. pseuodonana* (Dyhrman et al., 2012), *Trichodesmium* (Orchard et al., 2010), and *Synechococcus* (Martin et al., 2014). The relative increase in polyphosphates may reflect substitution of molecules, such as phospholipids, with non-P-containing forms like sulfolipids (Van Mooy et al., 2009). The high relative levels of dissolved polyphosphates in DOM observed under low P conditions in our cultures may be linked to the above previously reported metabolic responses of organisms to low P availability.

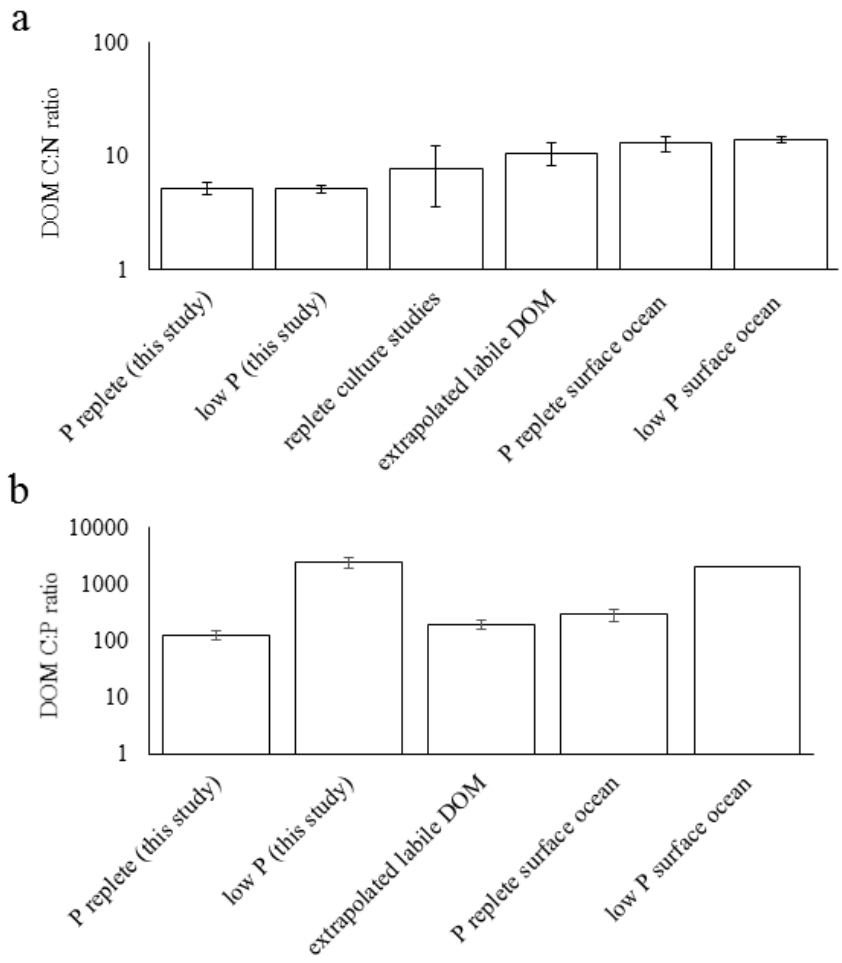

Figure 4.2 Average C:N ratios (a) and C:P ratios (b) of cultured and ambient ocean DOM. Error bars represent standard deviation around average values. Biddanda and Benner (1997) report DOM C:N ratios from the marine species *Synechococcus bacillaris*, *Phaoecystis* sp., *Emiliania huxleyi*, and *Skeletonema costatum* grown under nutrient replete conditions. The extrapolated labile DOM C:N and C:P ratios are estimated by Hopkinson and Vallino (2005) from decomposition stoichiometry of DOM from four ocean regions. Average surface ocean DOM C:N ratios are reported from P replete (Hansell and Waterhouse 1997) and low P (Hansell and Carlson 2001) regions. Average surface ocean DOM C:P ratios are reported from P replete (Loh and Bauer 2000; Hopkinson and Vallino 2005) and low P regions (Lomas 2016).

4.6 Conclusions

Nutrient ratios, DOC, and DOP composition of freshly produced, potentially bioavailable phytoplankton-derived DOM is compositionally distinct from ambient surface ocean DOM. The preferential utilization of N and P relative C during decomposition may lead to observed ambient surface ocean DOM C:N and C:P ratios. Furthermore, DOC and DOP compositional differences suggest preferential utilization of amino acids and P esters relative to other C and P containing compounds. DOM production by *T. pseudonana* is strongly altered by low P concentrations resulting in increases in the ratio of dissolved polyphosphate to DOP. This increase is consistent with growing observations of polyphosphate enrichment in marine particulates (Martin et al., 2014) and increased polyphosphate gene abundance (Temperton et al., 2011) in low P ocean regions. Forecasted shifts towards P limitation in some ocean regions (e.g., the North Pacific (Kim et al., 2014)) may lead to higher dissolved C:P ratios and dissolved polyphosphate content, which may ultimately alter the species-specific bioavailability of DOP (Diaz, 2015) and microbial species composition.

5. EFFECT OF CLEANING METHOD ON THE REACTIVITY OF DIATOM FRUSTULES

5.1 Abstract

Better constraints on biogenic silica transformation in marine sediments are of great interest for the quantification of current elemental budgets as well as the interpretation of past climate and ocean productivity records. Experimental studies characterizing the reactivity of siliceous materials require biogenic silica derived from field or cultured marine biota, which must have organic matter removed in order to simulate sedimentary conditions. Consequently, it is highly desirable to develop an effective cleaning method that imposes minimal alterations to the reactivity of the siliceous substrate. This study offers a quantitative comparison of several methods for removing organic matter associated with biogenic silica in order to assess their efficacy for use in reactivity studies. Five protocols for the removal of organic matter, including chemical treatments, baking, and low temperature ashing with an oxygen plasma, were tested and evaluated on Thalasiosira pseudonana frustules for mass recovery, organic carbon removal, elemental composition, morphology, structural order, relative abundance of silanol (Si-OH) groups, and dissolution rate in simulated sea-water. Low temperature plasma ashing was quantitatively identified as the most suitable method for organic matter removal in studies seeking to

Saad EM, Pickering-Turner, RA, Shoji K, Krause JW, Tang Y. Effect of cleaning method on the reactivity of diatom frustules. *To be submitted to Limnology and Oceanography: Methods*. In review by co-authors for addition of sediment incubation data.

constrain the reactivity of biogenic silica as it was efficient at removing organic carbon while being the least impactful on frustule reactivity.

5.2 Introduction

The global silicon (Si) cycle is strongly coupled to the carbon (C) cycle, especially through siliceous primary producers (Ragueneau et al., 2006). Diatoms are the most significant contributor to silica fixation (Treguer and De La Rocha, 2013), contributing to 40% of marine primary production (Nelson et al., 1995) and 60% of organic carbon export from the photic zone (Dugdale and Wilkerson, 1998). The siliceous cell wall of diatoms is coated with an organic material that prevents their dissolution in the ocean, which is undersaturated with respect to silica (DeMaster, 2003; Gehlen et al., 2002). After diatom death and during sinking, this organic material is subject to heterotrophic degradation (Bidle and Azam, 1999), exposing the interior silica framework and rapidly accelerating the rate of frustule dissolution (Bidle and Azam, 1999; Grill and Richards, 1964). Therefore, only ~10% of the biogenic silica produced in the photic zone actually reaches the seabed, and only 3% of this fraction is buried (Treguer and De La Rocha, 2013). The balance between dissolution and burial controls marine silica concentrations (Gehlen et al., 2002), and ultimately diatomaceous primary productivity and efficiency of the biological CO_2 pump (Laruelle et al., 2009) as well as the interpretation of the current and past Si cycle (Ragueneau et al., 2000). However, the relationship between dissolution and burial exhibits significant spatial and temporal variability (Nelson et al., 1995), which presents a major obstacle when reconstructing past environmental conditions using sedimentary records (Abelmann et al., 1990; Barker et al., 1994; De La Rocha, 2006; Koning et al., 2001; Lotter et al., 1997; McManus et al., 1995; Ragueneau et al., 2000).

In order to understand Si transport and fate, marine sedimentary processes involving biogenic silica must be better constrained (DeMaster, 2003). One increasingly recognized important diagenetic process is reverse weathering, which refers to the formation of authigenic clay minerals in marine sediments (Aller, 2014; Martin and Sayles, 2005). This process has been inferred indirectly from porewater profiles (Mackenzie and Kump, 1995; Michalopoulos and Aller, 1995), observed *in situ* on the surface of diatom frustules (Michalopoulos et al., 2000), and more recently experimentally replicated with diatom frustules (Loucaides et al., 2010b). Reverse weathering is estimated to account for up to 25% of dissolved silica removal from the ocean (Holland, 2005). In Amazon delta sediments, authigenic clay mineral phases were estimated to form at a rate as high as 280 μmol Si cm^{-2} yr^{-1} (Michalopoulos and Aller, 2004). However, the kinetics and mechanisms of this process are still not well understood, and very few laboratory studies have been conducted to elucidate the reaction mechanisms involved.

Because the transformation of biogenic silica under sedimentary conditions (i.e. during the reverse weathering process) is thought to initially involve the dissolution of frustules, controlled laboratory studies must first remove the organic coating of biogenic silica. The cleaning procedure should be efficient, but not significantly alter the silica surface. Silica reactivity is inherently linked to its dissolution; Strong correlations between surface structure and chemical reactivity have been shown (Loucaides et al., 2010a). Once exposed, the dissolution kinetics of biogenic silica are intimately linked to the chemical structure at the solid-aqueous solution interface (Van Cappellen et al., 2002). The reactivity of silica is determined by surface activity, which is determined by the concentration, distribution, and composition of surface silanol groups (Si-OH), siloxane groups (Si-O-Si),

and the porous structure of the silica (Zhuravlev, 2000). Furthermore, as evidenced by the formation of surface precipitates during reverse weathering, the integrity of the surface structure of the silica must be maintained during the organic matter removal process.

The most frequently employed cleaning methods are high temperature baking, hydrogen peroxide, acid, and sodium dodecyl sulfate (SDS)/ethylenediaminetetraacetic acid (EDTA) treatment (e.g. Boyle et al., 1984; Dean, 1974; Tesson et al., 2008; Van der Werff, 1955). Harsh treatments, such as nitric acid and hydrogen peroxide, are thought to cause selective etching of the frustule surface, whereas gentle methods may not effectively remove sufficient organic matter (Van Eynde et al., 2014). Furthermore, the solubility of biogenic silica can be affected by the adsorption of cations on its surface (Lewin, 1961), which is why acid cleaned biogenic silica commonly has a more rapid dissolution rate than those from natural siliceous assemblages of phytoplankton (Lawson et al., 1978). However, reactivity alterations after cleaning treatments are not well compared or characterized.

Comparisons of frustule cleaning methods are primarily limited to microscopic and composition (e.g. stable isotope, element ratio) applications (e.g. Blanco et al., 2008; Morales et al., 2013; Tyler et al., 2007; Xiong et al., 2012). In addition, with the recent interest in material and nanotechnological applications of biogenic silica, a few laboratory studies have quantitatively compared frustule pore size, surface area, and composition under several cleaning conditions (e.g. Van Eynde et al., 2014). A recent study quantitatively compared and assessed several cleaning methods for the isotopic determination of diatom frustule-bound nitrogen for the potential application of this system as a paleoproxy for marine productivity (Morales et al., 2013). Among all available methods for preparing diatom frustules for reactivity tests, one promising method is low

temperature plasma ashing (Koning et al., 2007; Loucaides et al., 2010b). This method was originally proposed as a gentle and efficient method of removing organic matter of diatom species with delicate frustule structures for taxonomic identification (Watanabe et al., 2010). However, no quantitative assessment of this cleaning process and resulting frustule composition, structure, and reactivity is currently available.

The employed organic removal method must keep in mind the ultimate utility of the material. For use in reactivity studies, the ideal cleaning method will remove organic matter and loosely adsorbed cations while not significantly affecting the structure and reactivity of the silica. In this study, several cleaning methods were employed on two representative diatom species, and the treated materials were compared to assess the suitability of these methods in biogenic silica reactivity studies.

5.3 Materials and Methods

5.3.1 Biomass Cleaning

Thalassiosira pseudonana (*T. pseudonana*) was procured from Reed Mariculture Inc. for cleaning method comparison. The raw biomass was stored at -20 °C until use. All cleaning procedures using different methods were performed in the same week. Prior to use, biomass was thawed and repeatedly rinsed with deionized water (DI, 18 MΩ cm) to remove residual growth media. Rinsing involved suspending ~1 g of wet biomass in 50 mL of DI, followed by repeated shaking and centrifugation (2.2×10^3 g, 5 min) until the conductivity of the supernatant was constant and similar to that of deionized water (DI, < 20 μS cm^{-1}). This rinsed material was then freeze-dried and gently ground for organic matter removal by a survey of commonly employed methods (Table 5.1), including

hydrochloric acid and high temperature baking (HCl + baking), high temperature baking only (baking only), heated hydrogen peroxide (H_2O_2), heated nitric acid (HNO_3), hydrogen peroxide and heated HCl (H_2O_2 + HCl), and a low temperature plasma ashing (LTP) treatments. Each treatment was performed in duplicate. After each cleaning method, samples were repeatedly rinsed in DI until the conductivity of the supernatant was similar to (DI < 20 $\mu S\ cm^{-1}$), and freeze-dried for subsequent characterizations. A portion of the initial, uncleaned material (raw material) was preserved for subsequent analyses.

5.3.2 Characterization of the raw and cleaned material

Freeze dried raw and cleaned material was characterized for composition, morphology, and structural properties. Organic carbon content was measured by combustion using a CHNSO analyzer (Costech Instruments) after acid fuming over night (Hedges and Stern 1984). A portion of the solids were also digested using 0.2 M NaOH for 15 min at 100 ^oC (Krausse et al., 1983) and analyzed for magnesium (Mg), potassium (K), calcium (Ca), aluminum (Al), and iron (Fe) concentrations using inductively coupled plasma-mass spectrometry (ICP-MS, Agilent 7500a). Silica content in digests was quantified following the molybdenum blue spectrophotometric method (Strickland and Parsons, 1972) using an UV-vis spectrophotometer (Agilent Cary 60). Morphology of the solid was characterized using scanning electron microscopy (SEM; Hitachi SU-8230). Solid structure and phase characterization was conducted using X-ray diffraction (XRD, PANalytical Empyrean, Cu Kα source). Order and relative abundance of silanol and siloxane groups was elucidated using attenuated total reflect mode-Fourier transformed infrared (ATR-FT-IR) spectroscopy (Bruker Equinox 55).

Table 5.1 Summary of organic matter removal techniques compared

Treatment	Method Description	Reference
HCl+baking	• 1 g (dry weight) suspended in 50 mL of 15% hydrochloric acid (HCl, trace metal grade, Sigma-Aldrich) in a 500 mL beaker, boiled for 1 h while continuously stirring, allowed to cool • Transferred to a 50 mL centrifuge tube, repeatedly rinsed by centrifugation and resuspension in DI until the pH of the supernatant was similar to that of DI (~ 6) • Supernatant was decanted, and solid was dried at 120 ^{o}C until completely dry • Heated in a furnace at 600 ^{o}C for 6 h	Jiang et al. 2014
Baking	• 1 g (dry weight) evenly spread into a thin layer in 500 mL beaker • Heated in a furnace at 600 ^{o}C for 6 h	Jiang et al. 2014
H_2O_2	• 0.5 g (dry weight) suspended in 50 mL of 15% hydrogen peroxide (H_2O_2, trace metal grade, Sigma-Aldrich), heated at 60^{o}C for 48 h in a 500 mL beaker • Transferred to a 50 mL centrifuge tube, repeatedly rinsed by centrifugation and resuspension in DI until the pH of the supernatant was similar to the pH of DI (~ 6)	Van Eynde et al. 2014
HNO_3	• 1 g (dry weight) suspended in 50 mL of 30% nitric acid (HNO_3, trace metal grade, Sigma-Aldrich) in a 500 mL beaker, heated at 60^{o}C for 48 h • Transferred to a 50 mL centrifuge tube, repeatedly rinsed by centrifugation and resuspension in DI until the pH of the supernatant was similar to the pH of DI (~ 6)	Van Eynde et al. 2014
H_2O_2+HCl	• 0.5 g (dry weight) suspended in 50 mL of 30% H_2O_2 overnight • Transferred to a 50 mL centrifuge tube, repeatedly rinsed by centrifugation and resuspension in DI until the pH of the supernatant was similar to the pH of DI (~ 6) • Resuspended in 6 M HCl at 110 ^{o}C for 20 h • Transferred to a 50 mL centrifuge tube, repeatedly rinsed by centrifugation and resuspension in DI until the pH of the supernatant was similar to the pH of DI (~ 6)	Abramson et al. 2009
LTP	0.2 g material placed in glass petri dishes and treated by low temperature plasma ashing (Plasma-Therm RIE) at 350 W, 25 ^{o}C, O_2 flow rate = 60 sccm for 7 h)	Watanabe et al. 2010

5.3.3 Reactivity test of cleaned material

The reactivity of the cleaned materials, as probed by dissolution rate and extent, was characterized in controlled laboratory conditions by incubating cleaned biogenic silica with simulated seawater. Thermodynamically predicted solubility of amorphous silica under the same experimental condition was also calculated using the software MINEQL (Gustafsson, 2016). Cleaned *T. pseudonana* biomass from each duplicate treatment (0.1 g/L) were suspended in filter sterilized (0.2 μm, cellulose acetate) artificial seawater (Kester et al., 1967) buffered with 15 mM 4-(2-hydroxyethyl)-1-piperazineethanesulfonic acid (HEPES, high purity grade) at pH 7. Suspensions were constantly agitated on a shaker table in the dark. Aliquots of each sample were collected throughout a time series, syringe filtered (0.2 μm, PTFE, VWR), and analyzed for dissolved silica using the molybdenum blue spectrophotometric method (Strickland and Parsons, 1972). pH was also monitored at each time point and readjusted to 7.0 ± 0.1 as they tended towards pH 7.3 ± 0.1 during dissolution. No microbial growth was observed throughout the experiment. Dissolution rates were determined by fitting a regression line through the dissolution profile over the same time frame (7 days) for each treatment and normalizing to initial Si content of the solid. Replicates of one sample from each treatment were also conducted, and the error associated with the dissolution experiment alone was significantly less than that of the duplicates of each treatment. The presented errors associated with each average are a result of the propagation of error associated with duplicate cleaning methods as with duplicate dissolution experiments.

5.3.4 Natural sediment incubations

In addition to controlled laboratory experiments, biogenic silica was also incubated with natural sediments for 5 months to assess the short- and long-term effects on the solubility, reactivity, and transformation of diatom-derived biogenic silica under simulated sedimentary conditions. Organic matter associated with biogenic silica derived from *Thalassiosira weissfloggi* (*T. weissfloggi*) was removed by LTP (as described above) or HNO_3 (Hasle, 1978). Sediments were collected with a box core from 20 m isobath on the Mississippi-Alabama coastal shelf in the northern Gulf of Mexico. Sediments were homogenized using wire mesh sieves to first separate the < 63 μm size fraction, then sieved down to < 20 μm. The < 2 μm size fraction (clay suspensions) were created through centrifugation.

Sediments and cleaned biogenic silica were suspended in filtered Gulf of Mexico sea-water (0.2 μm filtered, collected from the same location as the sediments), buffered with HEPES to pH 7, and placed in custom-built PVC reactors in two different chambers separated by a dialysis membrane (12–14 kD, 47 mm; Spectra/Por®). A hole was drilled at the end of each chamber, which was sealed with silicone vial stoppers and epoxy. All materials were acid washed and UV sterilized prior to use. The reactors were placed in a rotating wheel (2 rpm) and sampled using a 1 mm needle through the silicone stoppers. Evolution of dissolved silica was monitored along a time series for 5 months.

5.4 Assessment

5.4.1 Controlled laboratory experiments

Parameters used for comparing different treatment methods include mass recovery, organic carbon content, concentrations of other elements, morphological alteration,

structural alteration, and reactivity as probed by dissolution. These parameters were quantitatively compared for *T. pseudonana* biomass cleaned under different conditions (Section 5.3.1 and Table 5.1).

Mass recovery was used as an indicator of method efficiency, since biogenic silica is often limited for natural samples and significant losses in sample quantity might affect data interpretation (Watanabe et al., 2010; Xiong et al., 2012). Mass recovery can assess efficiency in terms of operator error (e.g. mass loss during transfer) as well as potential mass loss due to dissolution of the solid during the cleaning process (Watanabe et al., 2010). The organic carbon content of the raw material was 28.1 ± 0.9 wt% (Table 5.2); thus, mass recovery less than ~70% can be attributed to mass loss due to sample handling and the cleaning process. The highest mass recoveries resulted from baking, LTP, and HNO_3 treatments (> 30% recovery) and the lowest from HCl + baking and H_2O_2 treatments (< 30%). In addition, the precision of the treatments can provide some insights into the robustness of the method. The methods resulting in the lowest percent relative standard deviation (RSD) were the LTP and HNO_3 treatments (1% RSD), followed by HCl + baking, baking only, and H_2O_2 treatments (8-10%), followed finally by H_2O_2 + HCl treatment (20%).

Table 5.2 Characteristics of raw and cleaned *T. pseudonana*

Treatment	Mass Recovery (%)	Organic Carbon (wt%)	Fe (wt%)
Raw material	-	28.9 ± 0.4	0.7 ± 0.1
HCl+baking	27 ± 3	0.07 ± 0.03	BDL
Baking	38 ± 3	0.08 ± 0.01	1.4 ± 0.5
H_2O_2	26 ± 3	1.1 ± 0.07	0.4 ± 0.2
HNO_3	37 ± 0	2.2 ± 0.42	BDL
H_2O_2+HCl	32 ± 6	10.1 ± 0.60	BDL
LTP	34 ± 0	1.0 ± 0.09	0.4 ± 0.1

Note: BDL (below detection limit of 0.13 wt%).

Organic carbon content was used to evaluate method efficacy. Of the recovered cleaned material, the lowest organic carbon content resulted from both baking treatments (< 0.1 %), followed by LTP and H_2O_2 (~ 1%), HNO_3 (2.2%), and H_2O_2 + HCl treatment (10%). Mg, Ca, K, and Al were not found to be associated with the raw or cleaned material after the initial DI rinsing (detection limit of Mg, Ca, and K: ~1%; Al: ~ 0.1%). However, Fe was detected in the initial material and remained present in the materials cleaned by methods that did not involve acid (Table 5.2). It is likely that the Fe came from the growth medium and was associated within the frustule structure as Fe has been previously shown to incorporate into *T. pseudonana* diatom frustules during growth (Ellwood and Hunter, 2000).

Solid phase characterizations were also performed to assess the potential alteration of diatom frustules by different cleaning methods. SEM analyses revealed no difference in morphology or porosity at the micrometer scale by different cleaning methods (Figure 5.1), though random fragmentation to some extent was observed in samples from each treatment, most likely due to the repeated rinsing both before and after cleaning. XRD analysis revealed that after treatment, all material was characterized as opal-A (amorphous silica), as evidenced by the presence of only a broad peak at ~15–30^o 2θ (Figure 5.2) (DeMaster, 2003).

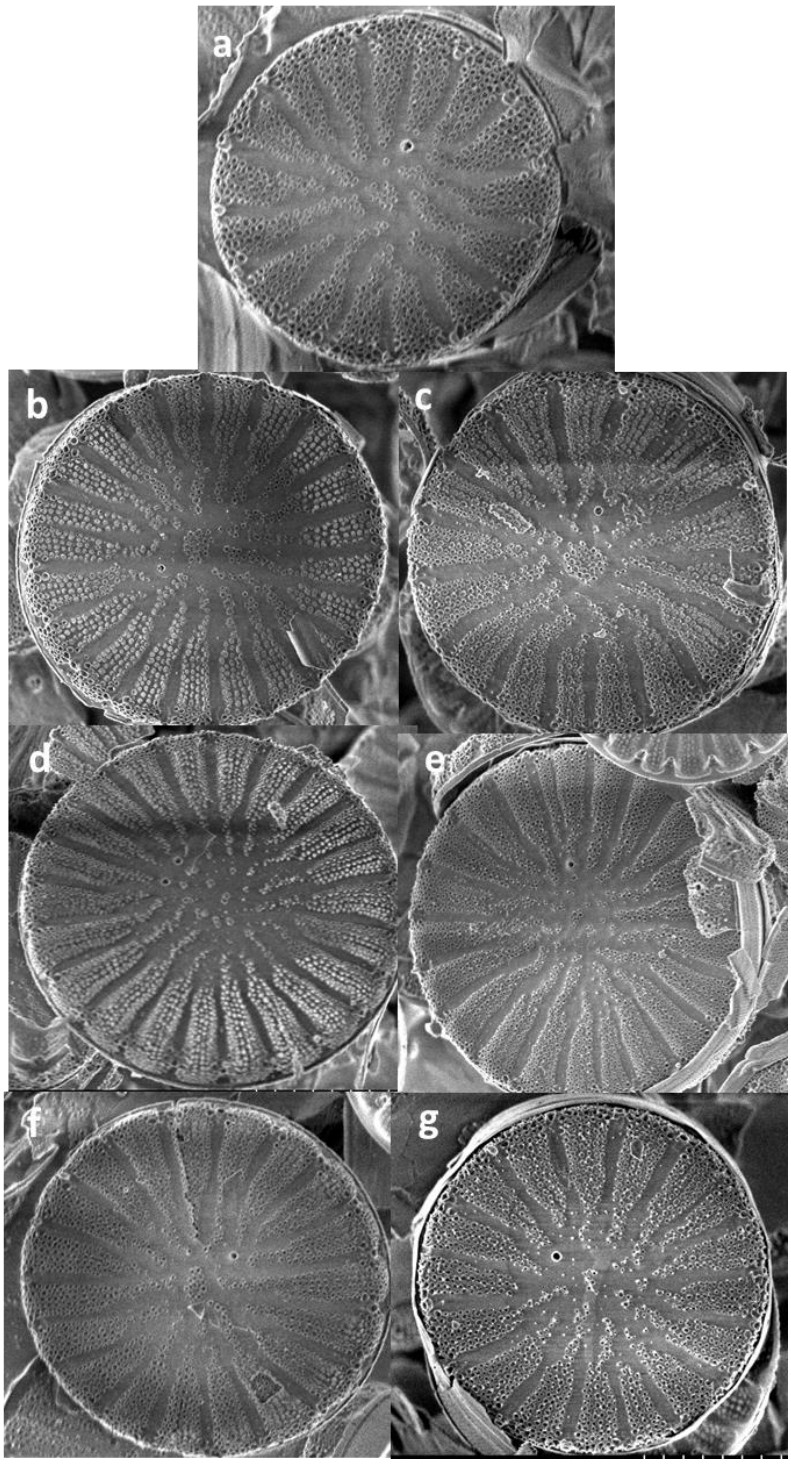

Figure 5.1 Representative SEM images of *T. pseudonana* frustules (a) before cleaning and after (b) HCl + baking, (c) baking only, (d) H_2O_2, (e) HNO_3, (f) H_2O_2 + HCl, (g) LTP treatments

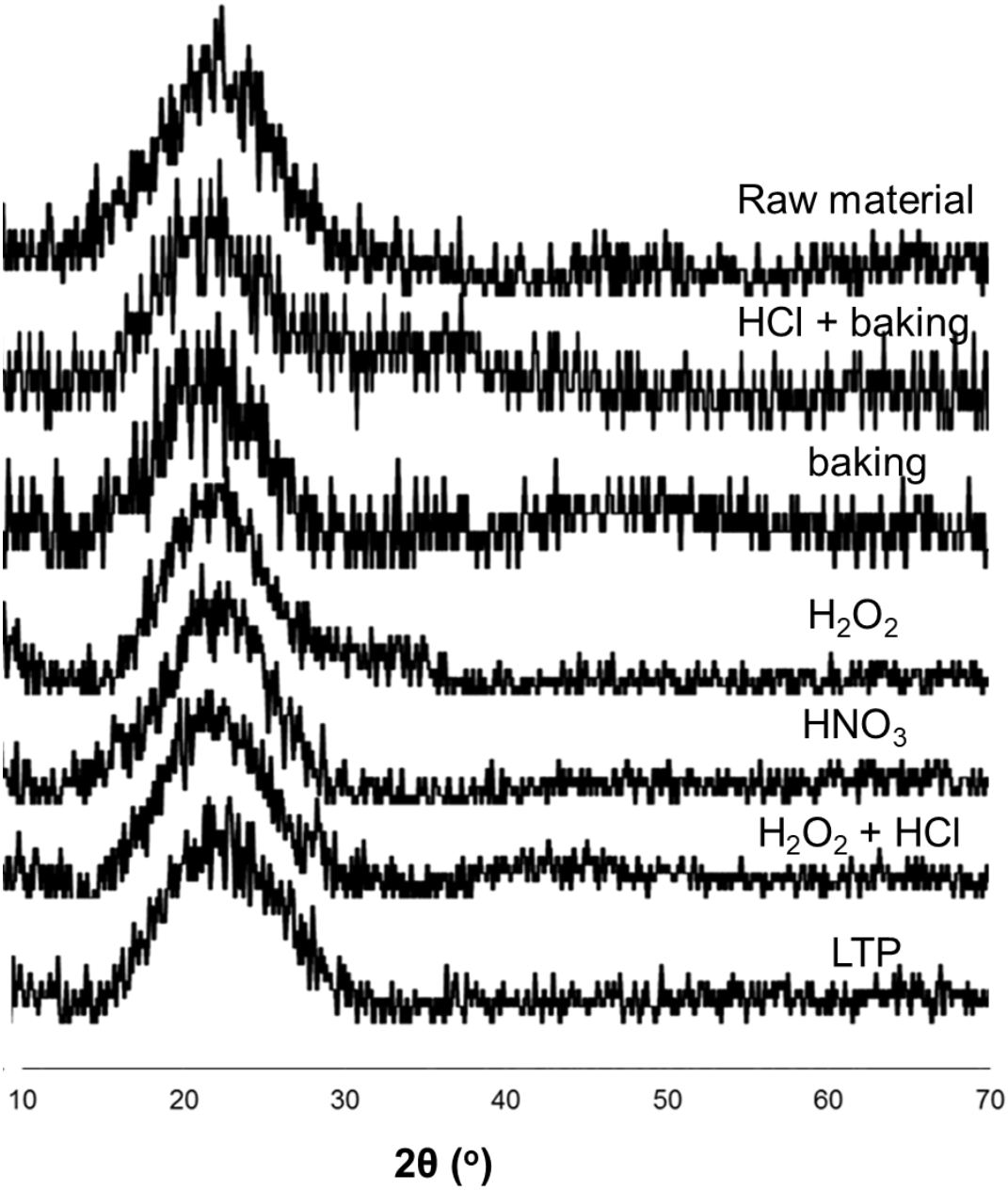

Figure 5.2 XRD patterns of biogenic silica of *T. pseudonana* before and after cleaning, all in amorphous silica phases as indicated by the broad peak at ~15–30° 2θ.

The potential for reactivity of the silica substrates was probed by FT-IR in order to elucidate relative abundances of silanol (Si-OH) and siloxane (Si-O-Si) groups, as well as overall structural order (Zhuravlev, 2000). FT-IR revealed the three vibration bands within the scan range that are indicative of amorphous silica (Figure 5.3) (Iler, 1979; Legrand, 1998). The vibration bands at ~1100, ~950, and ~800 cm^{-1} are attributed to the stretching vibration mode of the SiO_4 tetrahedron, the Si-O stretching of the Si-OH groups, and the bending vibration of inter-tetrahedral Si-O-Si bonds, respectively (Iler, 1979; Legrand, 1998). Ratios of the integrated absorption intensities at these energies can be used to elucidate the structural and molecular characterization of the solid (Table 5.3). The ratio of the integrated intensities of the 800 and 1100 cm^{-1} absorption bands (A_{800}/A_{1100}) has been used to indicate the degree of ordering in the SiO_2 framework (Gendron-Badou et al., 2003) while the ratio of the integrated intensities of the 950 and 800 cm^{-1} absorption bands (A_{950}/A_{800}) has been used to indicate the relative abundance of silanol group (Si-OH) (Schmidt et al., 2001). The A_{800}/A_{1100} ratio was lowest for the raw material and LTP treatment (0.03), followed by H_2O_2 (0.05), then HCl+baking, HNO_3, and H_2O_2 + HCl treatments (0.06), and finally by the baking only treatment (0.07). The A_{950}/A_{800} ratio decreased from that of the raw material (1.70), to LTP (1.50), HNO_3 (1.47), H_2O_2 (1.18), H_2O_2 + HCl (1.14), baking only (0.08), and finally HCl + baking (0) (Table 5.3).

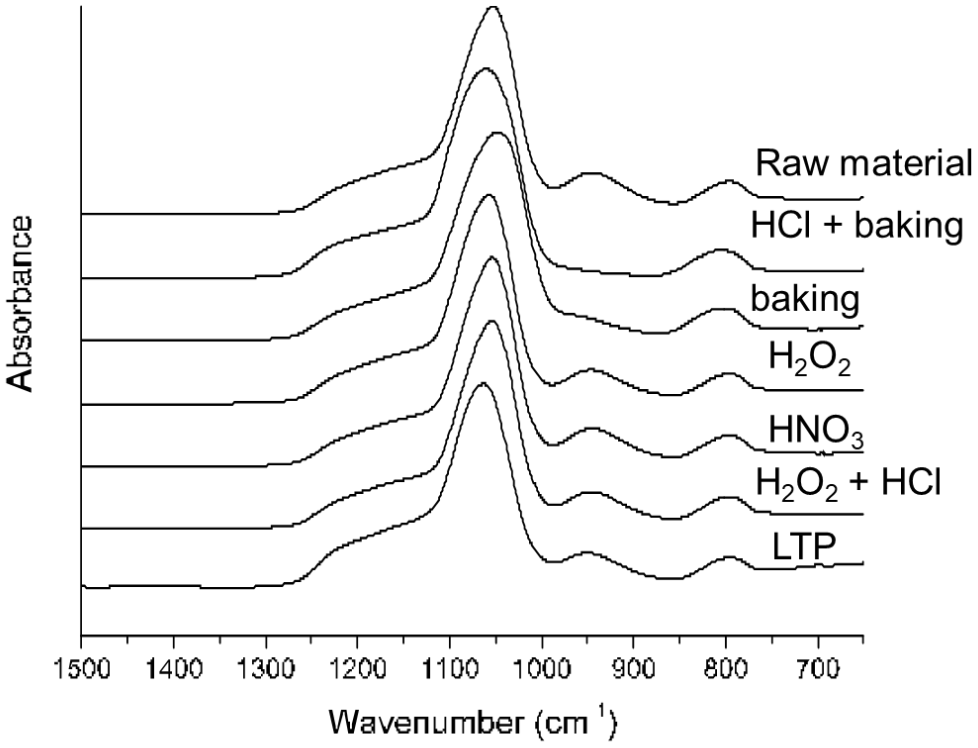

Figure 5.3 FT-IR spectra of biogenic silica of *T. pseudonana* before and after cleaning.

Table 5.3 Band intensity ratios for the FTIR spectra shown in Figure 5.3. The A_{800}/A_{1100} ratio is a measure of the degree of ordering of the SiO2 framework. The A_{950}/A_{800} ratio is a measure of the relative abundance of silanol (Si-OH) groups

Treatment	A_{800}/A_{1100}	A_{950}/A_{800}
Raw material	0.03±0.01	1.70±0.21
HCl+baking	0.06±0.01	0.00±0.00
Baking	0.07±0.01	0.08±0.06
H_2O_2	0.05±0.01	1.18±0.05
HNO_3	0.06±0.01	1.47±0.09
H_2O_2+HCl	0.06±0.01	1.14±0.05
LTP	0.03±0.01	1.50±0.16

The reactivity, as probed by solubility, of the cleaned materials varied greatly (Figure 5.4). After ~30 days, HNO_3 treatment reached the greatest extent of dissolved silica (~1600 µM), followed by H_2O_2 + HCl (~1400 µM), H_2O_2 and HCl + baking (~1100 µM), baking only (~800 µM), LTP (~600 µM), and the raw material (~400 µM). Initial dissolution rates normalized to initial Si content in solid revealed similar trends (Figure 5.5).

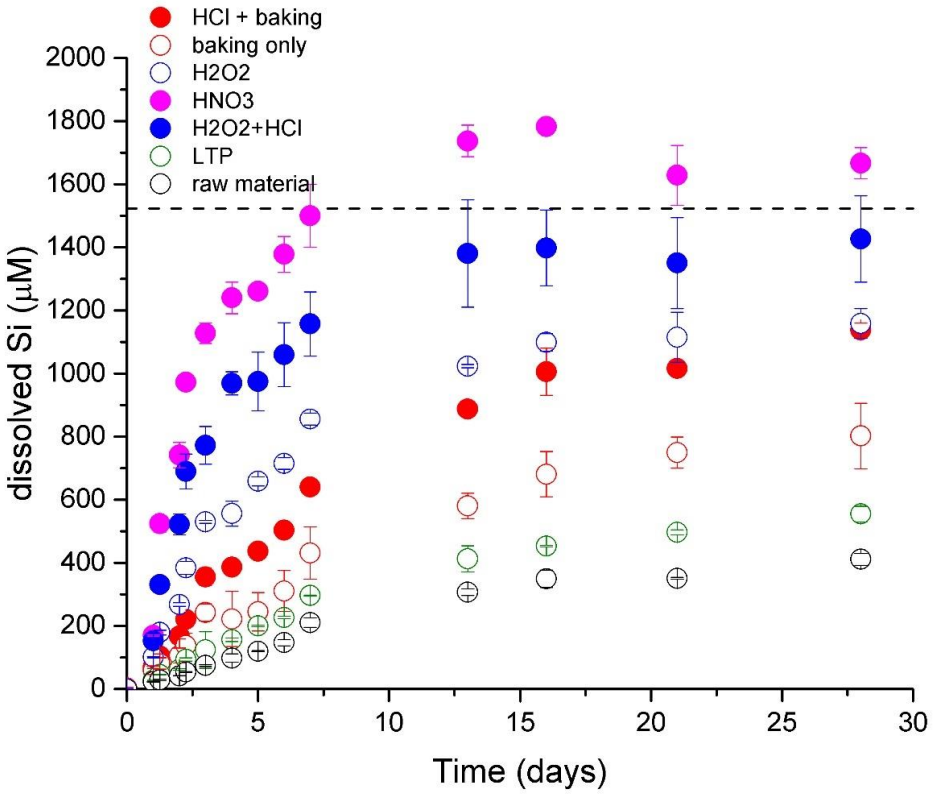

Figure 5.4 Dissolution profile of *T. pseudonana*-derived biogenic silica(0.1 g/L) in artificial sea water (pH 7, 15 mM HEPES). Dashed line indicates the thermodynamically predicted solubility of amorphous silica under the same experimental condition using MINEQL (Gustafsson 2016). Error bars represent variation between duplicates for each treatment.

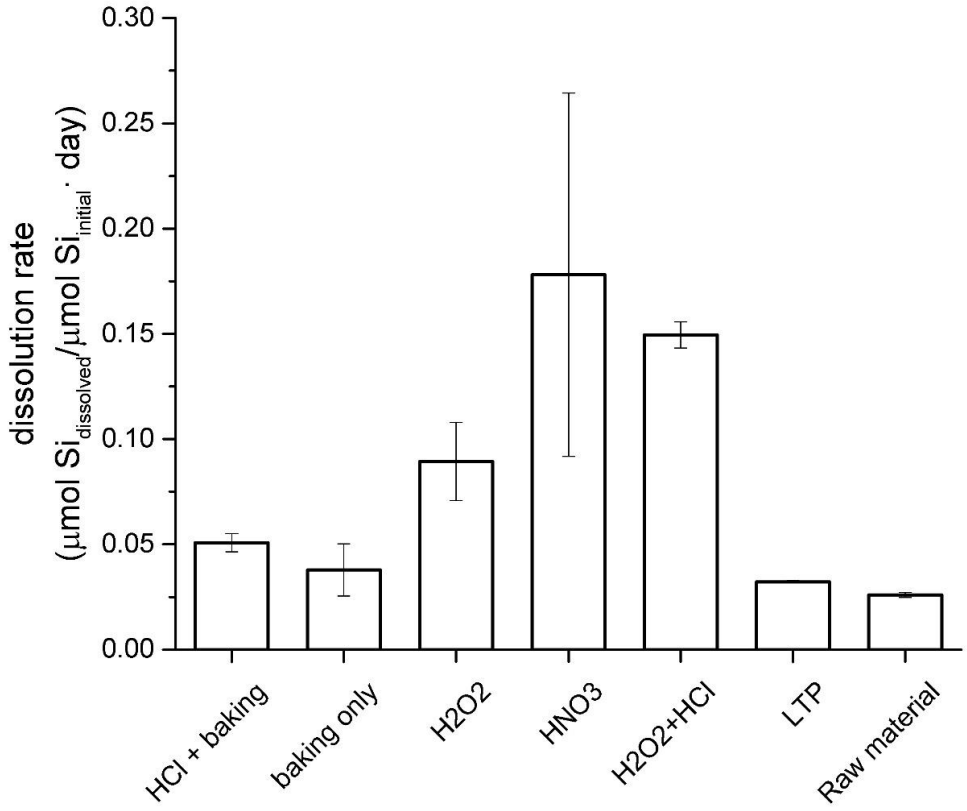

Figure 5.5 Initial rate of dissolution for *T. pseudonana* (0.1 g/L) suspended in artificial sea water buffered to pH 7 with 15 mM HEPES. Dissolution rates were determined by fitting a regression line through the dissolution profile over the same time frame (7 days) for each treatment and normalizing to initial Si content in the solid. Data is presented as averages and standard deviations of duplicates for each treatment.

5.4.2 Sediment incubations

Incubations of natural marine sediments with *T. weissflogii*, which had organic matter removed either by LTP or HNO_3, were also used to probe the influence of cleaning method on the reactivity of biogenic silica under sediment conditions. LTP resulted in a lower dissolution rate and a longer amount of time to reach steady state relative to HNO_3 cleaning. However, after 5 months of reaction, the extent of dissolution was the same for both cleaning methods (data not shown).

5.5 Discussion

In order to quantitatively characterize the reactivity of biogenic silica from a controlled laboratory perspective, the starting material must have the organic coating removed, while imposing minimal chemical and physical alterations of the surface. Thus, the cleaning method employed must not artificially modify the reactivity of the biogenic silica. Furthermore, the method must be able to be robustly employed.

In this study, samples cleaned with chemical treatments overall exhibited enhanced dissolution rates relative to the LTP treatment when normalized to the initial silica content of the material (Figure 5.4). The consistency in porosity revealed by SEM (Figure 5.1) and phase revealed by XRD (Figure 5.2) suggest that the increased dissolution rates are not likely due to enhanced porosity of the solid or a change in phase. Lack of variation in morphology and porosity as a function of cleaning method has been previously reported for similar treatment methods (Abramson et al., 2009; Van Eynde et al., 2014). Dissimilarly, FT-IR reveals slight differences in structure order as and relative abundance of silanol groups (Figure 5.3, Table 5.3). The slight increase in the A_{800}/A_{1100} ratio in the order raw material ~ LTP < H_2O_2 < HCl + baking ~ HNO_3 ~ H_2O_2+HCl < baking only indicates a slight increase in overall order of the solid (Gendron-Badou et al., 2003). The apparent absence or near absence of the absorption band at 950 cm^{-1} in both baking treatments suggests that the surface area of the material had been significantly changed as this band only becomes visible with specific surface areas greater than 200 m^2g^{-1} (Gun'ko et al., 2005). Furthermore, the A_{950}/A_{800}, and thus the relative abundance of silanol groups, ratios decreased in the order of raw material > LTP > HNO_3 > H_2O_2 ~ H_2O_2+HCl > baking only > HCl + baking (Table 5.3). Thus, the enhanced reactivity suggested by the enhanced

dissolution rates is likely due to alterations in the surface concentration, distribution, and composition of the surface functional groups (e.g. hydroxyl groups) (Zhuravlev, 2000) as well as changes in structural order. While the cleaning method may not impact frustule reactivity over extended time periods, the initial reactivity is significantly impacted by cleaning method, most likely due to surface structure alterations (Loucaides et al., 2010a).

In addition to the initial dissolution rate, the mass recovery associated with LTP was at the higher end of the recoveries of the cleaning treatments (Table 5.2) and consistently removed ~99% of the organic matter associated with the frustule (Table 5.2). Furthermore, this technique was performed in 7 h, which is the least amount of time associated with any of the cleaning methods employed (Table 5.1). Therefore, the recommended protocol for the cleaning of diatom frustules for reactivity studies is LTP.

5.6 Comments and Recommendations

Preparing diatom frustules for use in laboratory-based reactivity experiments, such as those that seek to constrain diagenetic processes of biogenic silica, should limit the amount of chemical alteration to the frustule. In our recommended cleaning method, low temperature plasma ashing, outer organic matter is efficiently removed while not significantly impacting the reactivity or surface structure of the frustule. Additionally, LTP offers itself as a promising method of organic matter removal for a variety of biominerals (e.g. manganese oxides, iron oxides, etc.), since they are often conglomerates of both inorganic and organic materials and sensitive to chemical treatments.

6. TRANSFORMATION KINETICS OF BIOGENIC SILICA DURING EARLY DIAGENESIS: INSIGHTS FROM SIMULATED SEDIMENT INCUBATIONS

6.1 Abstract

Controls and mechanisms of authigenic clay formation during early diagenesis of biogenic silica remain poorly constrained. This study sought to elucidate the mechanisms and kinetics of the transformation of diatom-derived biogenic silica under anoxic, controlled laboratory conditions, as well as the roles of iron (Fe) and aluminum (Al) containing phases in this process. Biogenic silica derived from *Thalasiosira pseudonana* was incubated with Fe- and Al-containing minerals in anoxic artificial seawater in the presence of varied concentrations of dissolved Fe(II). Fe(II) and Al were found to suppress the rate and extent of biogenic silica dissolution. After one month of reaction, Fe(II)- and Al-enriched silicate phases were identified. Results from this study, including the rate of biogenic silica transformation, controlling factors, and the (trans)formation product(s), can be used to inform biogeochemical models for better constraint of the marine Si cycle.

Saad EM, Pickering-Turner RA, Xu W, Liu P, Sun J, Taillefert M, Chen S, Kruase JW, Tang Y. Transformation kinetics of biogenic silica during early diagenesis: Insights from simulated sediment incubations. In preparation for *Limnology and Oceanography*.

6.2 Introduction

The major sink of silica in marine reservoir is the burial and early diagenesis of biogenic silica in marine sediments (Aller, 2014). Early diagenetic behavior of silica exerts a major control over oceanic productivity through diatom growth, as well as the paleoceanographic record of ancient productivity (Misra and Froelich, 2012). Early diagenesis of biogenic silica is characterized by complex interplay among dissolution, surface alteration, and precipitation reactions (Michalopoulos and Aller, 2004). Although the major sedimentary storage mode for biogenic silica is as opaline or slightly altered opaline silica, multiple alternative diagenetic reaction pathways also occur that can result in partial or complete conversion of silica into authigenic aluminosilicate minerals (e.g. Cole, 1985; Hein et al., 1979; Hurd, 1973; Odin and Fröhlich, 1988). Consistent with observations of solids phases, profiles of pore water dissolved silica also suggest controls by authigenic aluminosilicate formation during early diagenesis (Dixit et al., 2001; King et al., 2000; Rabouille et al., 1997; VanBeusekom et al., 1997; VanCappellen and Qiu, 1997a, b). Pore waters in a wide range of deltaic and estuarine environments typically exhibit stoichiometric relationships between dissolved aluminum (Al) and silicon (Si), indicative of rapid early diagenetic formation of authigenic aluminosilicates (Mackin, 1986; Mackin and Aller, 1984, 1986).

The involvement of biogenic silica in the formation of aluminosilicate phases represents a reverse weathering process (Mackenzie and Garrels, 1966; Michalopoulos and Aller, 1995). These reactions can be generally expressed as:

$$\text{biogenic silica} + Al(OH)_4^- + (Fe^{2+}, Fe^{3+}, Mg^{2+}, K^+, Li^+) + HCO_3^- \rightarrow \text{aluminosilicates} + CO_2 \quad (6)$$

Reverse weathering reactions can result in the formation of cation-rich aluminosilicate phases at the expense of biogenic silica and clays during early diagenesis. These reactions have been proposed as a significant component of oceanic elemental mass balances of magnesium (Mg^{2+}), potassium (K^+), bicarbonate (HCO_3^-), and dissolved silica (H_4SiO_4) to compensate as the missing sink for these elements (Mackenzie and Garrels, 1966; Michalopoulos and Aller, 1995). However, this process remains poorly constrained (Aller, 2014). Specifically, the exact roles of the reactants and identification of the (trans)formation product(s) are currently poorly constrained. During these reactions, biogenic silica acts as a source of dissolved silica, and potentially also as nucleation sites for subsequent mineral formation (Loucaides et al., 2010). The potential roles of Fe species in the transformation process also remain elusive, despite the common association of Fe and the formed aluminosilicates phases (Loucaides et al., 2010). Direct *in situ* evidence supporting reverse weathering reactions had been challenging to collect as some of the same clay mineral types formed in sediments may also be of detrital origin (Libes, 2009). Furthermore, these authigenic clay phases are small in size and are usually found in the fine-grained sediment fraction (Arvidson et al., 2006). Consequently, detection requires tedious size segregation methods, and traditional analytical methods for the characterization of such small particles failed to provide evidence of this process (Drever, 1971; Russell, 1970). Finally, alternative elemental sinks such as hydrothermal systems resulted in a tendency to overlook reverse weathering (Aller, 2014). Both trends in pore water solute stoichiometry (Mackin and Aller, 1984; Rude and Aller, 1994) and marine

lithium (Li) isotope systematics, which require the formation of these authigenic clay minerals in order to account for the isotopically heavy sea water Li signature (Misra and Froelich, 2012), indirectly support the occurrence of the reverse weathering process. The formation of authigenic silicates (e.g. green marine clays) on continental shelves has been well documented, but the timescales of formation, such as those inferred from the deep sea, were traditionally estimated to be in the order of 10^3–10^6 years (Odin and Fröhlich, 1988). Recent experimental and field studies of deltaic sediments (such as Amazon, Mississippi, and Congo deltas) have directly demonstrated the existence of rapid, early diagenetic reverse weathering reactions in deposits with extremely high sediment accumulation rates. These studies indicate spatial variability of this process. In Fe- and Al-oxide rich environments (such as deltaic systems), reactive biogenic silica availability may be limiting (Ehlert et al., 2016; Ku and Walter, 2003; Loucaides et al., 2010b; Michalopoulos and Aller, 1995, 2004; Presti and Michalopoulos, 2008); whereas in regions that have low sediment accumulation rates (such as the Southern Ocean), Al- and Fe-oxide availability may be limiting (Aplin, 1993; VanCappellen and Qiu, 1997b). Experiments with unaltered Amazon delta sediments were found to contain authigenic aluminosilicate minerals (Michalopoulos and Aller, 1995). Minerals formed and found *in situ* in Amazon shelf sediments were spectroscopically characterized to be K- and Fe-rich mica type clays (Michalopoulos et al., 2000). Furthermore, cation and metal rich aluminosilicate coatings on diatom frustules have also been observed in Amazon river delta sediments (Michalopoulos and Aller, 2004). These studies all suggested that the reverse weathering process must be reconsidered as a significant Si diagenetic process.

In environments with high sediment accumulation rates such as deltas, the alteration of biogenic silica and formation of authigenic silicates can increase net storage of silica by factors of 2–3 (Mississippi delta) or 5–10 (Amazon delta) relative to consideration of biogenic silica transformation to opaline products (Michalopoulos and Aller, 2004; Presti and Michalopoulos, 2008). When diagenetic transformation of biogenic silica to aluminosilicates is incorporated into global budgets for Si, the continental margins increase in importance for biogenic silica storage (Laruelle et al., 2009). Using published transects along salinity gradients, DeMaster (2002) estimated that 0.6×10^{12} mol Si yr^{-1} is removed in estuaries. As shallow water columns prevent extensive dissolution before deposition to the sediments (DeMaster, 2002), reverse weathering is most significant in deltaic sediments where authigenic minerals compose up to 40% of the total sink for reactive silica (Treguer and De La Rocha, 2013). In fact, accounting for the fluxes of K^+ and other relevant ions, stoichiometry of clays, and diagenesis of biogenic silica, reverse weathering may remove 20–25% of the total riverine Si input (Holland, 2005).

Because of the coupling between C and Si, better constraints on the oceanic Si cycle is required, as it relates to both the biologic pump of organic carbon to the deep ocean (Dugdale et al., 1995) and the potential influence on ocean pH through the production of CO_2 during reverse weathering process (Mackenzie and Garrels, 1966). Moreover, reverse weathering and the associated Si cycle is coupled not only to the C cycle, but also to the biogeochemical cycles of other key elements (though through poorly characterized interactions) (Loucaides et al., 2012). Although reverse weathering has been demonstrated to occur in certain coastal sediments, it is still rarely included in budgets and modelling of biogeochemical cycles (Treguer and De La Rocha, 2013). Furthermore, though cases of

site-specific data have been calculated, global application to deltaic sediments is not yet possible (Berner and Berner, 2012). Direct estimates of Si retention on continental shelves are still lacking, even with the aid of both solid phase and solution analyses. The aforementioned recent field and laboratory evidences also suggest that reverse weathering (Mackenzie and Garrels, 1966) be revisted as an important process affecting ocean chemistry (Martin and Sayles, 2005). However, very few laboratory studies have been conducted to elucidate the reaction mechanisms and kinetics of the reverse weathering process. The extent of the reaction is still unknown (Ragueneau et al., 2010). Furthermore, the mechanism is not constrained, but is thought to involve dissolution and reprecipitation. Both direct and indirect evidence suggested the participation of Al, Si, and cations (e.g. Mg and Fe) in the formation of these authigenic clay phases (Loucaides et al., 2010b; Michalopoulos and Aller, 1995; Arvidson et al., 2006).

This study seeks to constrain the mechanism of authigenic clay formation in simulated sedimentary conditions in order to further elucidate the roles of Fe and Al in this process.

6.3 Methods

6.3.1 Solid phase synthesis and characterization

Ferrihydrite (hereafter $Fe(OH)_3$), amorphous Al hydroxide (hereafter $Al(OH)_3$), were synthesized following previous procedures (Isobe et al., 2003; Tang et al., 2010), as the Fe- and Al-containing solid substrates, respectively (Figure 6.1). Biogenic silica (hereafter $bSiO_2$) was produced from the marine diatom *Thalassiosira pseudonana* (*T. pseudonana,* procured from Reed Mariculture Inc.) and stored at -20 °C until use. Prior to

use, *T. pseudonana* biomass was thawed and repeatedly rinsed with deionized water (DI, 18 MΩ cm) to remove residual growth media. Rinsing involved suspending ~1 g of wet biomass in 50 mL of DI, shaking very well, and centrifuging (2.2×10^3 g, 5 min) until the conductivity of the supernatant was constant and similar to deionized water (< 20 μS cm^{-1}). This rinsed material was then freeze dried and gently ground for organic matter removal by low temperature plasma ashing. 0.2 g of solid was placed in glass petri dishes and treated by low temperature plasma ashing (Plasma-Therm RIE at 350 W, 25 ^oC, O_2 flowrate = 60 sccm for 7 h). This material was characterized by X-ray diffraction (XRD, PANalytical Empyrean, Cu Kα source) and elemental composition. The organic carbon content was measured by combustion using a CHNSO analyzer (Costech Instruments) after acid fuming over night (Hedges and Stern, 1984). Mg, K, Ca, Al, and Fe contents were analyzed on material digested using 0.2 M NaOH for 15 min at 100 °C (Krausse et al., 1983) by inductively coupled plasma-mass spectrometry (ICP-MS, Agilent 7500a). All three solid phases were confirmed to be X-ray amorphous (Figure 6.1). bSiO_2 contained 1.0 ± 0.09 wt% organic carbon and 0.4 ± 0.1 wt % Fe; all other elements were below the detection limits (1% for Mg, Ca, and K: ~0.1% for Al).

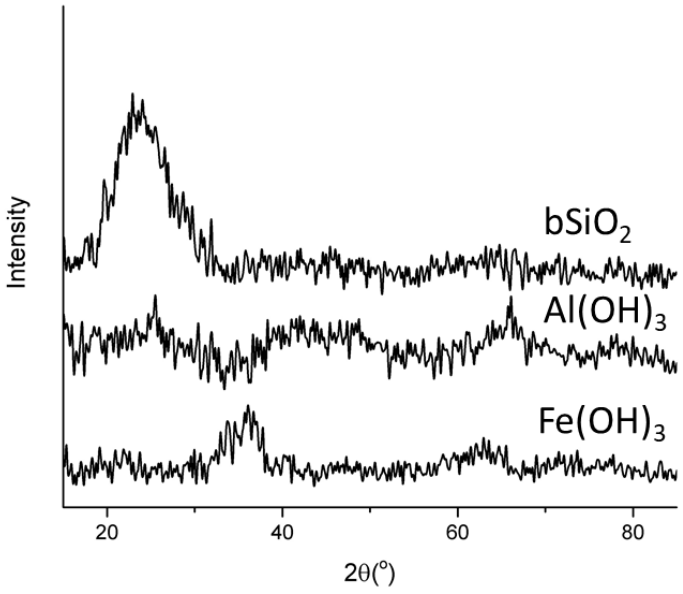

Figure 6.1 XRD patterns of initial solid substrates (Cu Kα source; λ = 1.5418 Å).

6.3.2 Batch experiments

Batch experiments under simulated sedimentary conditions were conducted using $Fe(OH)_3$, $Al(OH)_3$, and/or $bSiO_2$, each at 0.1 g/L, suspended in filter-sterilized (0.2 μm, cellulose acetate) anoxic artificial seawater (Kester et al., 1967) buffered with 15 mM 4-(2-hydroxyethyl)-1-piperazineethanesulfonic acid (HEPES, high purity grade) at pH 7.5, similar to the pH of Amazon sediment pore waters (Michalopoulos and Aller, 1995). Pore waters were simulated by the addition of 150 μM dissolved Si from Na_2SiO_3 (ACS grade), which is similar to the observed dissolved silica concentration for upper 100 cm of Amazon Delta sediments (Michalopoulos and Aller, 1995) and Mississippi sediments (Presti and Michalopoulos, 2008). Dissolved Fe(II) was also added ($FeCl_2$, ACS grade) to the reaction solution to simulate pore water conditions, at either 100 μM (e.g upper 100 cm of Amazon

Delta sediments (Aller et al., 1996)) or 1000 μM (e.g. upper 20 cm of Congo River fan sediments (Beckler et al., 2016)).

Experiments were conducted inside an anoxic glove box (Coy; 95/5 N_2/H_2) in custom-built PVC reactors (3 inch) with two chambers separated by a dialysis membrane (12–14 kD, 47 mm; Spectra/Por®). Each chamber has a hole at the end, which was sealed with silicone vial stoppers and epoxy. All materials were acid washed and UV sterilized prior to use. Treatment conditions are shown in Table 6.1. The $bSiO_2$ substrate was contained in one chamber, and the $Al(OH)_3$ and/or $Fe(OH)_3$ in the other chamber, such that any transformation involving Al and/or Fe solid phases could be attributed to a dissolution-reprecipitation reaction. This also allowed the sampling and structural characterization of transformation products of $bSiO_2$ without interference from the Al and/or Fe solid phases. An additional control was added that included only dissolved phases: 150 μM silica (as Na_2SiO_3, ACS grade), 100 μM Fe(II) (as $FeCl_2$, ACS grade), and 30 μM Al^{3+} (as $AlCl_3$, ACS grade).

Sample-loaded reactors were constantly agitated on a shaker table. Aliquots of the suspensions were collected using a 1 mm needle through the silicone stoppers and syringe filtered (0.1 μm, PTFE, VWR). Evolution of the aqueous phase was monitored along a time series for the duration of the experiment (details in Section 6.3.3). At the end of reactions, final solid phases were harvested, repeatedly rinsed with anoxic DI water under vacuum filtration, dried in the glove box, and characterized for morphological and structural features (details in Section 6.3.4).

Table 6.1 Summary of treatment conditions. The matrix is anoxic artificial seawater (Kester et al. 1967) buffered with 15 mM HEPES at pH 7.5 with 150 µM dissolved Si.

$[Fe(II)]_{aq}$ (µM)	No solid phase	$bSiO_2$ only	$Fe(OH)_3$ only	$Al(OH)_3$ only	$Fe(OH)_3$ + $Al(OH)_3$	$bSiO_2$ + $Fe(OH)_3$	$bSiO_2$ + $Al(OH)_3$	$bSiO_2$ + $Fe(OH)_3$ + $Al(OH)_3$
0	xx	xx	xx	xx	xx	xx	xx	xx
100	xx	xx	xx	xx	xx	xx	xx	xx
1000	xx	xx	xx	xx	xx	xx	xx	xx

6.3.3 Aqueous phase analyses

At each point, total dissolved iron (Fe_T) and dissolved Fe(II) were quantified using the ferrozine spectrophotometric method either with or without hydroxylamine, respectively (Stookey, 1970). Dissolved silica was quantified using the molybdenum blue spectrophotometric method (Strickland and Parsons, 1972). Concentrations of dissolved Al were measured by ICP-MS (Agilent 7500a). Dissolved inorganic carbon (DIC) was measured at the beginning and end of experiments using a flow injection analysis system by conductivity detection (Analytical Instruments Systems, Inc. LCC100 integrator) (Hall and Aller, 1992).

6.3.4 Solid Phase analyses

Initial $bSiO_2$, $Fe(OH)_3$, and $Al(OH)_3$ were freeze dried. Reacted solids were dried on filter membranes inside the glove box. Solid phases were characterized for morphology using scanning electron microscopy (SEM; Hitachi SU-8230) and associated elemental maps were constructed using energy dispersive X-ray spectroscopy (EDX). A portion of the solids were also sealed into glass capillaries inside the glove box for synchrotron XRD measurements at Beamline 17-BM-B (λ = 0.39433 Å) at Advanced Photon Source (APS) at Argonne National Laboratory (Lemont, IL).

6.4 Results

6.4.1 Solution phase evolution

In the absence of Fe(II) and other solids, the concentration of dissolved silica reaches ~1000 μM, similar to the thermodynamically predicted solubility value of amorphous silica under these conditions (Figure 6.2) (Gustafsson, 2016). Treatments containing $Al(OH)_3$ most significantly reduced the extent of Si release at the concentration plateau ($Al(OH)_3$ alone: 16±4%, $Fe(OH)_3$ + $Al(OH)_3$: 28±9%) while $Fe(OH)_3$ alone did not exert as much of an influence (9±1%). In the presence of Fe(II), the extent of dissolved Si was also reduced compared to treatments without Fe(II). In the 100 μM Fe(II) treatments, dissolved Si concentrations at the end of the experiment were reduced by 13±5% for the control, 20±4% for the $Fe(OH)_3$ + $Al(OH)_3$ treatment, 20±9% for the $Fe(OH)_3$ treatment, and 29±6% for the $Al(OH)_3$ treatment relative to the experiments without Fe(II). In the presence of 100 μM Fe(II), all Fe(II) was removed from solution (Figure 6.2), consistent with thermodynamic prediction that the system was oversaturated with respect to Fe(II)-silicate phases (Gustafsson, 2016), as well as the appearance of newly formed green solid phase(s). In the treatments with 1000 μM Fe(II), dissolved Si concentrations at the end of the experiment were reduced by 36±7% for the control, 54±2% for the $Fe(OH)_3$ + $Al(OH)_3$ treatment, 31±10% for the $Fe(OH)_3$ treatment, and 43±4% for the $Al(OH)_3$ treatment relative to the experiments without Fe(II). Green solids were observed at the end of the experiment associated with the $bSiO_2$ and the $Al(OH)_3$. Additionally, in the presence of Fe(II), treatments with $Al(OH)_3$ exhibited the most deviation of Si dissolution extent relative to the control (Figure 6.2). Initial Si release rates

were also influenced by Fe(II) concentration; the presence of Fe(II) decreased the initial Si release rate relative to the treatments without Fe(II) (Figure 6.3).

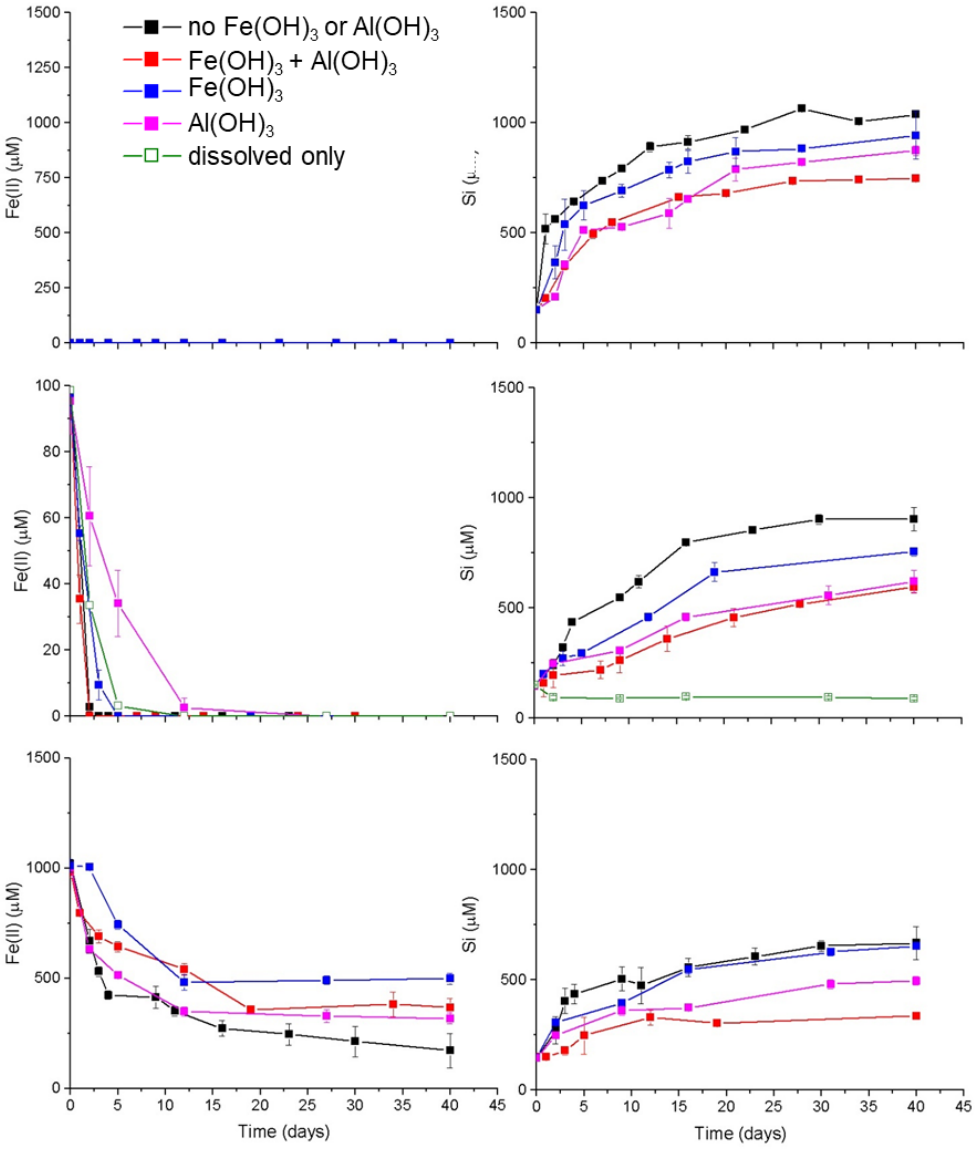

Figure 6.2 Time evolution of dissolved Fe(II) (left panels) and dissolved Si (right panels) in treatments with 0 µM Fe(II) (top panels), 100 µM Fe(II) (middle panels), and 1000 µM Fe(II) (bottom panels). Error bars represent deviation amongst duplicate treatments.

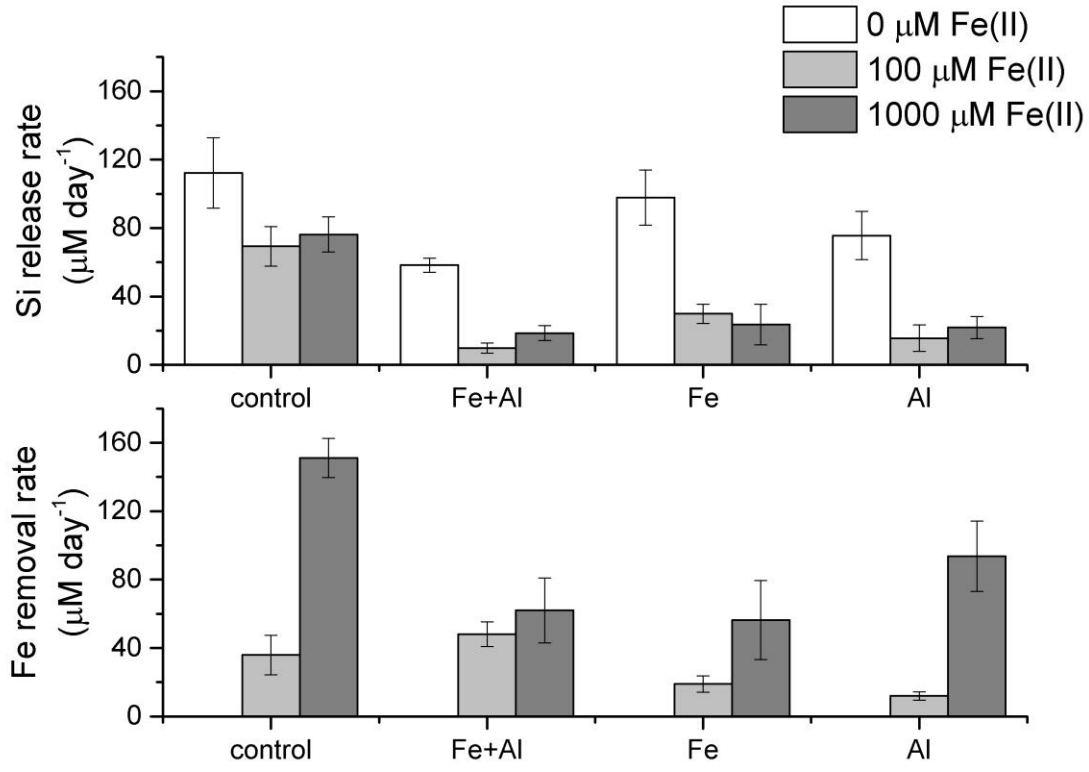

Figure 6.3 Initial dissolution rates of biogenic SiO_2 and removal rates of dissolved Fe(II) ($\mu M\ day^{-1}$). Labels are as follows: Control = $bSiO_2$ only; Fe+Al = $bSiO_2$+ $Fe(OH)_3$+$Al(OH)_3$; Fe = $bSiO_2$+ $Fe(OH)_3$; Al = $bSiO_2$ +$Al(OH)_3$. Rates were determined by fitting a regression line through the concentration evolution over the same time frame (~ 7 days). Error bars represent error associated with duplicates of each treatment.

In the absence of biogenic silica, similar trends were observed (Figure 6.4). Regardless of initial Fe(II) concentration, in the presence of other solids, $Al(OH)_3$ exerted the strongest control over Si dissolution extent as evidenced by deviation from the control. In the presence of Fe(II), concentrations of dissolved Si were reduced relative to those observed in the absence of Fe(II) for each treatment. In the 100 μM Fe(II) treatments, dissolved Si concentrations at the end of the experiment were reduced by 39±6% for the control, 26±4% for the $Fe(OH)_3$ + $Al(OH)_3$ treatment, 47±9% for the $Fe(OH)_3$ treatment,

and 75±5% for the $Al(OH)_3$ treatment relative to their respective unamended treatments. In the 1000 μM Fe(II) treatments, Si concentrations at the end of the experiment were reduced by 38±6% for the control, 26±5% for the $Fe(OH)_3$ + $Al(OH)_3$ treatment, 66±10% for the $Fe(OH)_3$ treatment, and 65±8% for the $Al(OH)_3$ treatment relative to their respective unamended treatments. Additionally, the control experiment containing only dissolved Fe(II), Si, and Al resulted in complete removal of Fe(II) (Figure 6.3) and Al (within 1 day, data not shown) from solution consistent with thermodynamic predictions of oversaturation with respect to Fe(II)-silicates, Al-silicates, and amorphous Al-solids under these conditions (Gustafsson, 2016).

Dissolved inorganic carbon was measured before and after reactions (Figure 6.5). In general, treatments containing biogenic silica contained less DIC at the end of the experiment, compared to those with only dissolved Si. The control with dissolved Si only did not result in significant removal of DIC from solution. Changes in solution Mg, Ca, and K were not detected. Furthermore, dissolved Al was intermittently detected throughout the experiment, but not with any noticeable trend (data not shown), most likely due to the formation of colloids that may not pass through 0.1 μm filters (Gehlen et al., 2003).

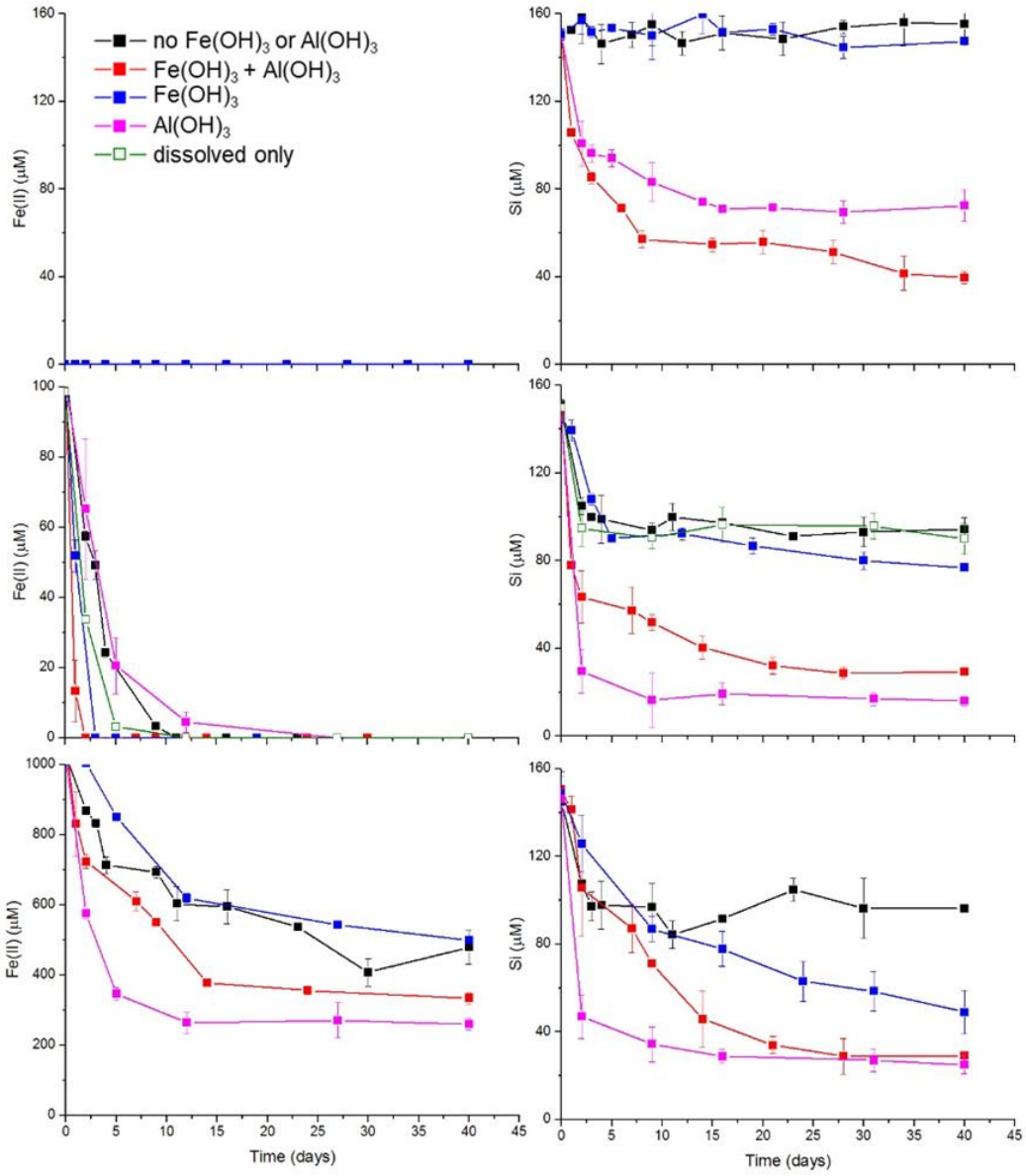

Figure 6.4 Time evolution of dissolved Fe(II) (left panels) and dissolved Si (right panels) in treatments with 0 µM Fe(II) (top panels), 100 µM Fe(II) (middle panels), and 1000 µM Fe(II) (bottom panels). No treatments contain biogenic SiO_2. Error bars represent deviation amongst duplicate treatments.

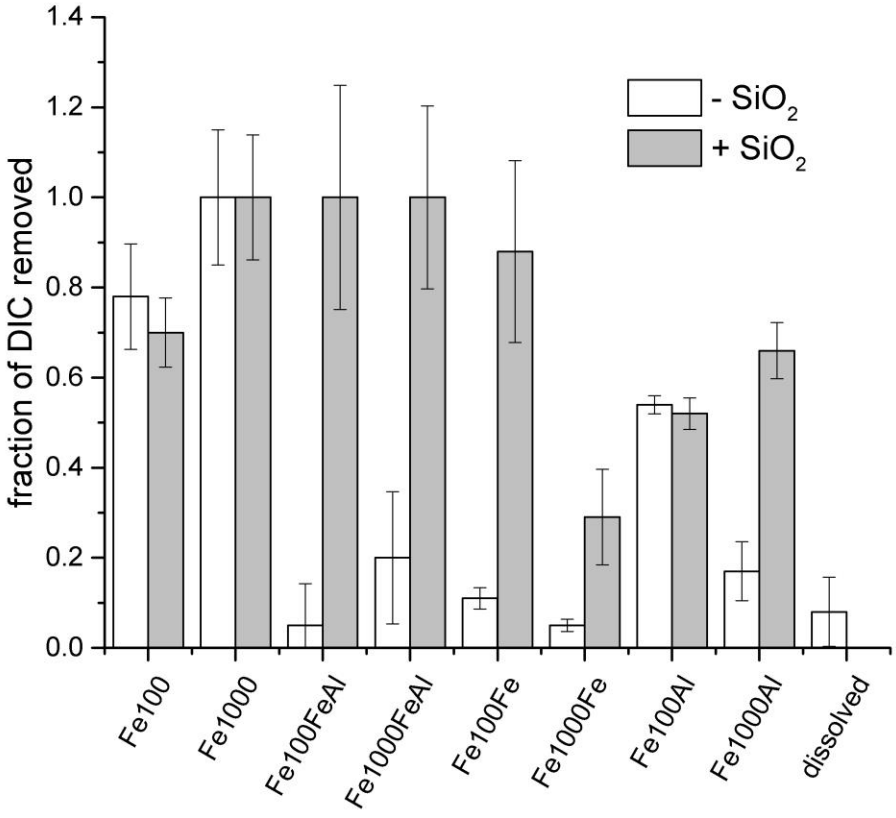

Figure 6.5 Fraction of initial DIC removed from solution at the end of the experiment (~40 days). Labels are as follows: Fe100 = 100 μM Fe(II); Fe1000 = 1000 μM Fe(II); FeAl = $Fe(OH)_3$ + $Al(OH)_3$; Fe = $Fe(OH)_3$; Al = $Al(OH)_3$.

6.4.2 Solid phase characterization

XRD analysis revealed that after reaction, biogenic silica remained amorphous in the majority of the treatments (Figure 6.6). The treatment with 1000 μM Fe(II) and $Al(OH)_3$ showed the appearance of new peaks (~8^o and 14^o 2θ) , suggesting formation of phase(s). Additional subtle peaks were also present in the 1000 μM Fe(II) and $Fe(OH)_3$ + $Al(OH)_3$ treatments. Furthermore, SEM/EDX analysis revealed that in the absence of Fe(II), the biogenic silica did not undergo morphological transformations (Figure 6.7). However, in the presence of 1000 μM Fe(II), the biogenic silica revealed significant morphological

transformation with significant destruction of biogenic silica and formation of secondary layered solid phases (Figure 6.8). EDX analyses indicate that the newly formed phase(s) were Fe-rich. Furthermore, in the presence of $Al(OH)_3$, the biogenic silica revealed evidence of Fe- and Al-rich silicate phases (Figure 6.9).

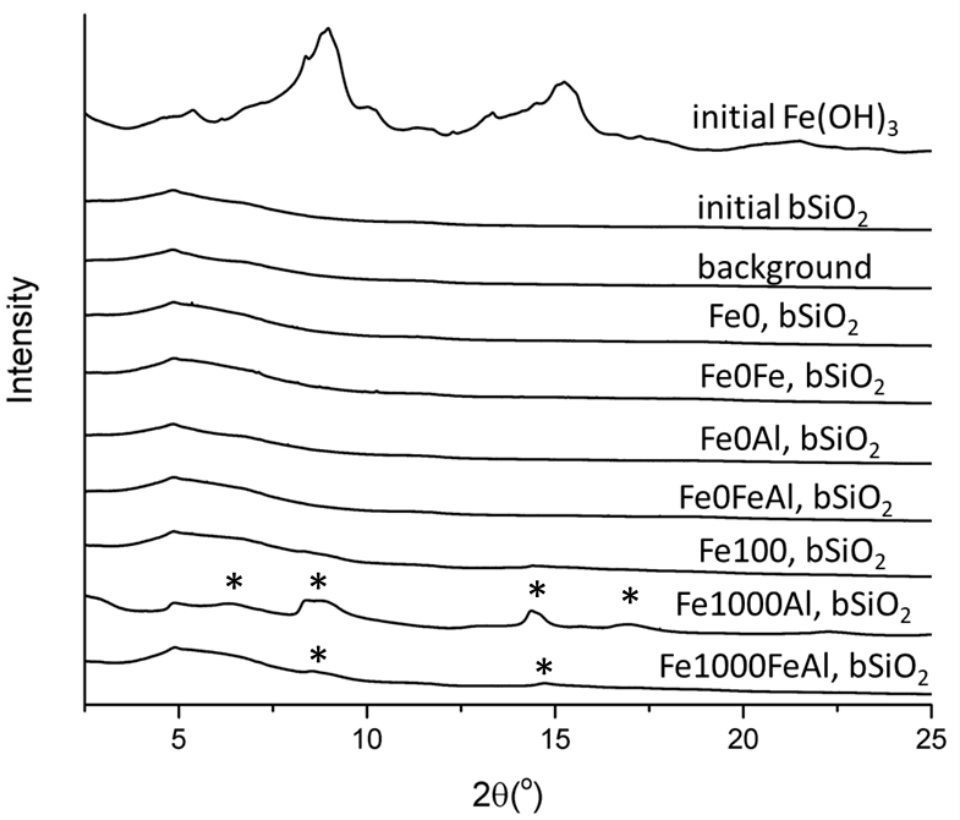

Figure 6.6 Synchrotron XRD patterns (λ = 0.39433 Å) of initial bSiO2 and $Fe(OH)_3$ as well as reacted bSiO2. Labels are as follows: Fe0 = 0 µM Fe(II); Fe100 = 100 µM Fe(II); Fe1000 = 1000 µM Fe(II); FeAl = $Fe(OH)_3$+$Al(OH)_3$; Fe = $Fe(OH)_3$; Al = $Al(OH)_3$.

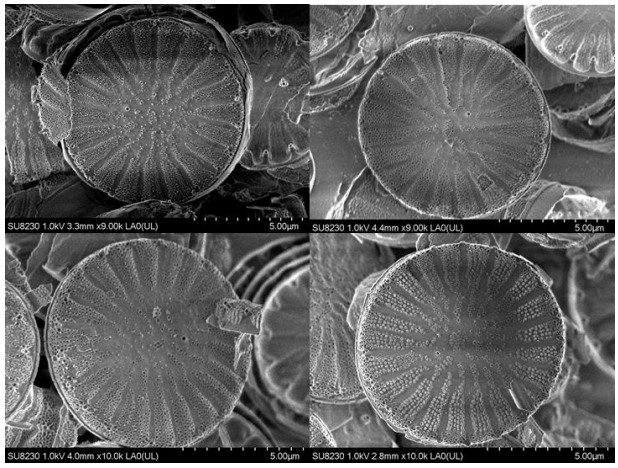

Figure 6.7 Representative images of $bSiO_2$ after reaction with 0 µM Fe(II) for 40 days. No changes in morphology were observed.

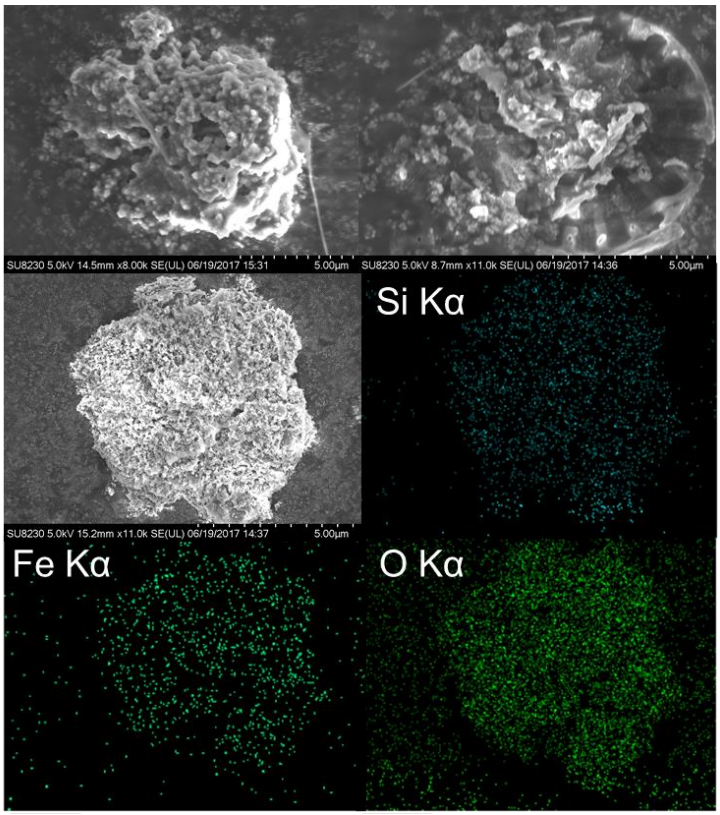

Figure 6.8 Representative SEM images and corresponding EDX maps of $bSiO_2$ after reaction with 1000 µM Fe(II) for 40 days. Morphological and elemental association changes were observed.

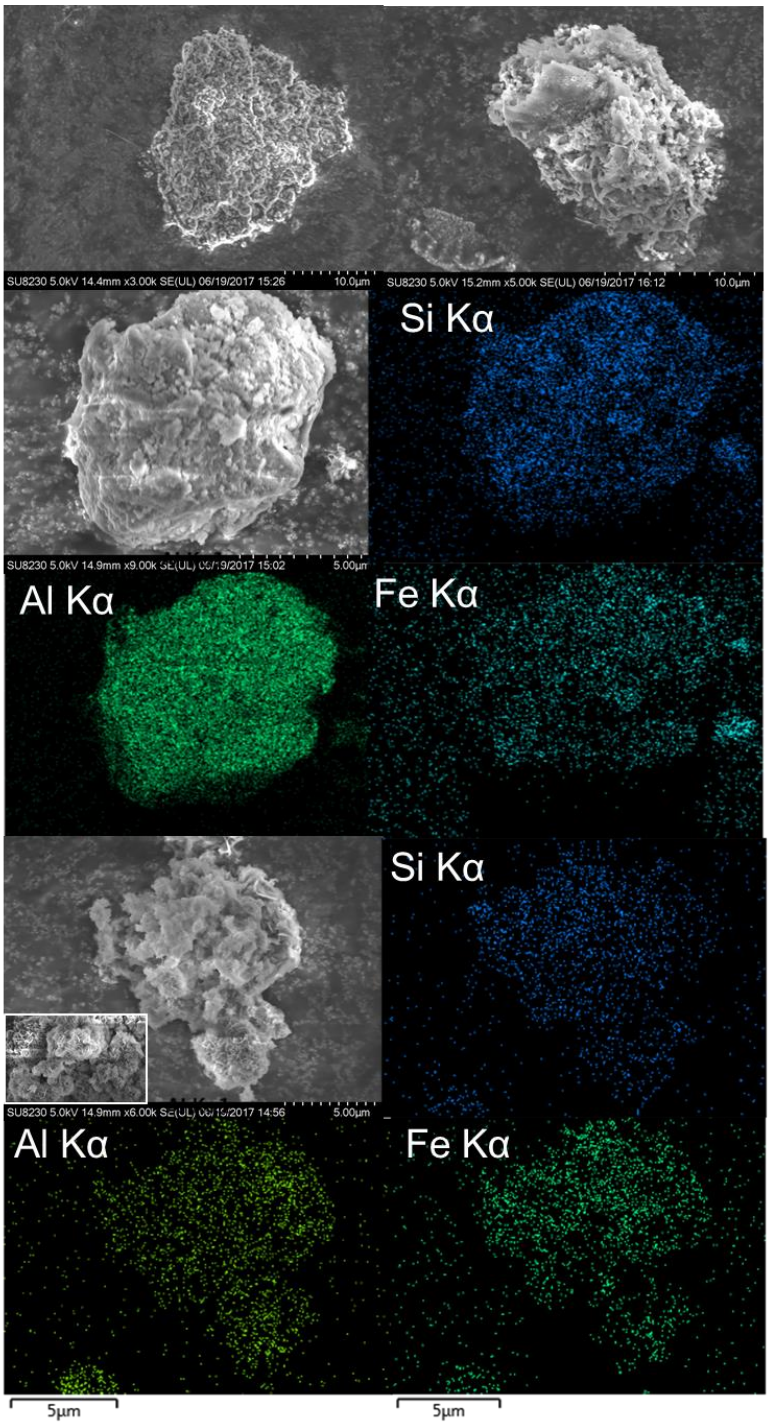

Figure 6.9 Representative SEM images and associated EDX maps of reacted biogenic silica with 1000 µM Fe(II) with $Al(OH)_3$ for 40 days. Insert in white box is a close-up of altered precipitates. Morphological and elemental association changes were observed.

6.5 Discussion

The discrepancy between expected and actual efficiency of biogenic silica recycling and preservation in marine systems requires constraint of factors controlling biogenic silica diagenesis (Van Cappellen et al., 2002; Ragueneau et al., 2006). This study demonstrates a decrease in silica dissolution in simulated sedimentary conditions in the presence of Fe- and Al-containing solids (Figures 6.2 and 6.3). A similar decrease in silica solubility was previously observed when biogenic silica was incubated with kaolinite or basalt with compositions proportional to the mass ratio of lithogenic material (Dixit et al., 2001). This decrease in $bSiO_2$ solubility mimics the inverse relationship of pore water dissolved silica concentrations with abundance of lithogenic minerals relative to biogenic silica observed in Southern Ocean sediments (VanCappellen and Qiu, 1997a). Furthermore, a decrease in silica solubility in the presence of sediments has been correlated to the uptake of additional ions in the biogenic silica (Loucaides et al. 2010).

The influence of Al-containing solids on the dissolution of biogenic silica was evident in the present system (Figure 6.2). Furthermore, SEM/EDX of the biogenic silica reacted with $Al(OH)_3$ indicates that the enhanced association of Al with the silica phase must have resulted from a dissolution-reprecipitation reaction as our experimental design separated the two solid phases with a dialysis membrane. Al has been shown to be associated strongly with diatom frustules during early diagenesis in Congo Fan sediments (Vanbennekom et al., 1989). Al sorption onto biogenic silica has been shown to reduce the solubility and dissolution kinetics of biogenic silica (Iler, 1979; Vanbennekom et al., 1989). In fact, previous incubations of diatom frustules with sediments found Al strongly associated with the biogenic silica as secondary precipitates (Loucaides et al., 2010b).

This study also demonstrated that, under our experimental conditions, Fe(II), more-so than Fe(III)-containing solids, was a major control of biogenic silica transformation. Fe(II) has been shown to suppress the dissolution rate of silica, while Fe(III) was not found to have any affect (Lewin, 1961). Conversely, Fe(III) oxides have been shown to accelerate the dissolution of biogenic silica, perhaps because of their ability to adsorb dissolved silica, consequently removing Si from solution and allowing for further dissolution (Mayer et al., 1991). In fact, Loucaides et al. (2010) observed Fe associated with diatom frustules incubated in Congo Fan sediments, but not in their laboratory-incubated diatom frustules. They attributed this deviation to the fact that their laboratory experiments took place in oxic conditions (Loucaides et al., 2010b), which perhaps suppressed possible anaerobic respiration processes that can produced Fe(II).

6.6 Conclusions

The interaction between biogenic silica and lithogenic minerals (e.g. Al- and Fe-oxides) can remove reactive silica from the marine system through authigenic transformation and sedimentary burial. However, these processes are rarely considered in elemental budgets and biogeochemical cycle models (Loucaides et al., 2010b). This study demonstrated the transformation of biogenic silica after 1 month of reaction in the presence of Al- and Fe-containing phases that are representative of initial stages of early diagenesis of biogenic silica in marine sediments. Specifically, Fe(II) and Al were identified as the primary drivers of this transformation.

More complementary non-destructive techniques should be employed to further constrain the transformation products in these experiments. Fe-K-edge X-ray absorption

spectroscopy (XAS) can be used to provide information on the the oxidation state and structural associate of Fe with the solid phases (i.e. incorporated or adsorbed). Because the biogenic silica was separated from the Fe-containing solid phase, bulk XAS may be sufficient in characterizing the Fe association with the silica. However, because of the small sample amount and low concentration of Fe associated with the solid phase, it may be necessary to utilize a synchrotron beamline with microprobe capabilities. Identification of the Fe-silicate phase can also be elucidated by indexing the peaks in the diffraction pattern from the 1000 μM Fe(II) + $Al(OH)_3$ treatments (Figure 6.6). Additionally, high resolution transmission electron microscopy (HRTEM) coupled to EDX mapping and selected area electron diffraction (SAED) can be employed to identify the morphology, structure, elemental compositions of the reacted silica phases. Elemental composition *(e.g.* Mg, Ca, Na, K, Fe, Al) of the reacted solids can also be determined by ICP-MS on digested materials *(*according to (Reitz et al., 2004)), which will help construct the stoichiometric dissolution-precipitation reactions involving the starting materials and final products.

7. CONCLUSIONS

This dissertation investigated the degree to which microbes participate in mineral weathering reactions and associated impacts on the rates and extent of mineral dissolution, as well as the composition, structure, and stability of the (trans)formation product(s). The rate, extent, and speciation of mineral dissolution was assessed by solution phase analyses. Characterization of the (trans)formation product(s) was performed using a suite of complementary solid phase techniques. By using these approaches under controlled laboratory settings, gaps in knowledge regarding two model systems were bridged, as discussed below and with recommendations for future research directions.

7.1 The chromium system

The role of organic ligands on the redox-independent solubilization and isotopic fractionation of Cr has been generally overlooked and poorly constrained. This dissertation presents evidence that microbial exudates that are ubiquitous in the environment can promote the dissolution of Cr(III) from common Cr sinks, Cr(III)-Fe(III)-(oxy)hydroxides, via two mechanisms: (1) direct ligand-promoted solubilization of Cr(III) from the Cr(III)-Fe(III)-(oxy)hydroxide solid phases, as well as (2) increased solubility of the secondary solid phases resulted from incongruent dissolution of the starting solid phases. The rate and extent of redox-independent Cr solubilization mechanisms must be assessed in addition to redox-dependent pathways in order to better simulate complex environmental settings. In addition to abiotic experiments, biotic experiments can also be conducted using model organisms and under controlled laboratory conditions to assess the roles of redox-independent mechanisms and their interplay with redox-dependent mechanisms. For

example, the weathering of Cr-containing solids can be examined using model bacteria and fungi species that are capable of producing Mn oxides in addition to organic acids and ligands, which can provide assessments of multiple solubilization pathways. This dissertation further provides evidence that interaction of Cr(III) (oxy)hydroxide with microbial exudates can induce a redox-independent isotopic fractionation of Cr. While the isotope signatures of the dissolved Cr(III) species varied based on ligand and reaction extent, the observed trends suggest that isotope fractionation may be dependent on Cr(III)-ligand stability. Future work involving theoretical modeling based on calculating vibrational frequencies of the initial and final Cr(III) species can be used to gain a mechanistic understanding of the factors controlling observed fractionations.

7.2 The silica system

The composition of freshly produced, diatom-derived DOM has remained elusive. Using a high recovery DOM extraction technique and axenic diatom cultures, this thesis demonstrates that the DOM initially supplied to marine systems by diatoms is compositionally distinct from ambient surface ocean composition and provides further insights into the preferential utilization of certain DOM components by marine heterotrophs. Additionally, P limitation was demonstrated to significantly influence the DOP pool, which suggests that forecasted shifts towards P limitation may ultimately alter species-specific bioavailability of DOP. This study represented a starting point for examining the composition of freshly produced, phytoplankton-derived DOM. However, future work could use this approach on DOM derived from various marine phytoplankton and/or prokaryote species in order to obtain a more holistic view of the composition of DOM initially supplied to marine systems. In addition to growing microbes under P

limitation, DOM composition during growth under N and Fe limitation would provide further insights into ocean systems that might experience spatial and temporal variations in nutrient regime.

The diagenetic transformation of diatom-derived biogenic silica was also investigated under controlled laboratory settings in order to elucidate the rate, extent, and final products of the transformation process, as well as the roles of Fe and Al containing minerals. Transformation of biogenic silica in the presence of Fe(II) and Al oxides was found to occur after 1 month of reaction in anoxic simulated sea-water. Al and Fe, as Fe(II) specifically, were found to provide a major control on the reaction rate, extent, and transformation product(s). While this study utilized a separate Al source (i.e. to mimic detrital Al), future work should further constrain the role of Al in this sedimentary process by examining the impact of frustule associated-Al (i.e. through Al presence during diatom growth or death before exposure to Fe(II)). Furthermore, the role of the biogenic silica substrate should also be further constrained in order to assess its potential roles as a nucleation site for secondary precipitation in addition to the source of dissolved silica for this transformation. The tight coupling between this transformation and Fe also suggests that the balance between reverse weathering and anaerobic respiration processes must be assessed. Finally, the intriguing HCO_3^- results suggest that future work is necessary to identify the role of carbonate budget in reverse weathering, especially as it may relate to ocean acidification.

APPENDIX A. SUPPLEMENTARY INFORMATION FOR CHAPTER 2

A.1 Results and discussion for experimental treatments with 0.1 mM oxalate and 0.1 mM DFOB

Relative to the control experiment, the presence of 0.1 mM oxalate resulted in similar Cr(III) dissolution extent (up to ~1 μM by Cr10), but reached near steady state much faster (within 10 days) (Figures A.2 and 2.1). Furthermore, the increase in oxalate concentration from 0.1 to 1 mM approximately doubled the rate of Cr release (Figures 2.1C and A.2A, Tables A.3 and A.4). Compared to DFOB alone, the presence of 0.1 mM oxalate caused changes of Fe release extent of ~52% increase for Fe10, ~70% increase for Cr2Fe8, ~31% decrease for Cr5Fe5, and ~6% decrease for Cr8Fe2. This is consistent with a previous study on goethite dissolution, where an increase in Fe release was related to the increase in oxalate concentration (Reichard et al. 2007). For Cr release extent compared to DFOB alone, the presence of 0.1 mM oxalate caused changes of ~18% decrease for Cr10, ~24% increase for Cr8Fe2, ~100% increase for Cr5Fe5, and ~70% decrease for Cr2Fe8 (Figures A.2 and 2.1). Similar to the case of Fe/Cr dissolution extent, the addition of 0.1 mM oxalate had either positive, negative, or no effect on Fe and Cr release rates, depending on solid composition. Compared to DFOB alone, the presence of 0.1 mM oxalate caused changes of Fe release rate of ~30% decrease for Fe10, ~60% increase for Cr2Fe8, ~13% decrease for Cr5Fe5, and ~53% increase for Cr8Fe2. For Cr release rate compared to DFOB alone, the presence of 0.1 mM oxalate caused changes of ~5% decrease for Cr10, ~9% increase for Cr8Fe2, >100% increase for Cr5Fe5, and ~50% decrease for Cr2Fe8.

Table A.1 Sample label, metal ratio, and approximate composition used for PDF normalization of the pristine and reacted solids based on elemental compositions and hydration states from our previous study (Tang et al. 2010).

Sample	Target Cr:Fe mole ratio	Actual Cr:Fe mole ratio	BET specific surface area (g m^{-2})	Approximate Composition for PDF normalization
Cr10	100:0	100:0	95	$Cr_2O_3 \cdot 10H_2O$
Cr8Fe2	80:20	77:23	154	$Cr_{0.8}Fe_{0.2} \cdot 10H_2O$
Cr5Fe5	50:50	43:57	99	$Cr_{0.5}Fe_{0.5} \cdot 8.8H_2O$
Cr2Fe8	20:80	16:84	129	$Cr_{0.2}Fe_{0.8} \cdot 4.1H_2O$
Fe10	0:100	0:100	107	$Fe_2O_3 \cdot 2.5H_2O$

Table A.2 Surface area-normalized Fe and Cr release rates (mol m^{-2} s^{-1}) as determined from the slope of the linear region of the dissolution profiles for each treatment (~21 days). The uncertainty was determined based on the standard error of the regression analysis.

Sample	Metal-ligand release rate (mol m^{-2} s^{-1})									
	0.1 mM oxalate		1 mM oxalate		0.1 mM DFOB		0.1 mM DFOB + 0.1 mM oxalate		0.1 mM DFOB + 1 mM oxalate	
	Fe	Cr	Fe	Cr	Fe	Cr	Fe	Cr	Fe	Cr
Fe10	BDL	-	BDL	-	$1.51\pm0.05\times10^{-12}$	-	$1.06\pm0.03\times10^{-12}$	-	$1.82\pm0.03\times10^{-12}$	-
Cr2Fe8	BDL	$7.03\pm1.45\times10^{-15}$	BDL	$2.10\pm0.48\times10^{-14}$	$9.02\pm0.87\times10^{-14}$	$1.28\pm0.12\times10^{-14}$	$1.47\pm0.17\times10^{-13}$	$5.95\pm1.29\times10^{-15}$	$4.01\pm0.43\times10^{-13}$	$2.75\pm0.41\times10^{-14}$
Cr5Fe5	BDL	$1.53\pm0.60\times10^{-14}$	BDL	$4.71\pm1.12\times10^{-14}$	$7.53\pm0.50\times10^{-13}$	$1.69\pm0.11\times10^{-14}$	$6.50\pm0.75\times10^{-13}$	$4.35\pm0.66\times10^{-14}$	$9.93\pm1.08\times10^{-13}$	$6.54\pm0.57\times10^{-14}$
Cr8Fe2	BDL	$1.51\pm0.35\times10^{-14}$	BDL	$2.92\pm0.52\times10^{-14}$	$2.16\pm0.22\times10^{-13}$	$1.05\pm0.35\times10^{-14}$	$3.31\pm0.39\times10^{-13}$	$1.41\pm0.26\times10^{-14}$	$2.67\pm0.26\times10^{-13}$	$3.25\pm0.33\times10^{-14}$
Cr10	-		-	$4.47\pm0.52\times10^{-14}$	-	$2.86\pm0.35\times10^{-14}$	-	$2.73\pm0.32\times10^{-14}$	-	$4.44\pm0.54\times10^{-14}$

Note: BDL (below detection limit, ~0.1 µM for Fe, ~0.01 µM for Cr).

Table A.3 Mass-normalized Fe and Cr release rates (µmol g^{-1} day^{-1}) as determined from the slope of the linear region of the dissolution profiles for each treatment (~21 days). The uncertainty was determined based on the standard error of the regression analysis.

Sample	Metal-ligand release rate (µmol g^{-1} day^{-1})									
	0.1 mM oxalate		1 mM oxalate		0.1 mM DFOB		0.1 mM DFOB + 0.1 mM oxalate		0.1 mM DFOB + 1 mM oxalate	
	Fe	Cr	Fe	Cr	Fe	Cr	Fe	Cr	Fe	Cr
Fe10	BDL	-	BDL	-	13.98±0.46	-	9.82±0.27	-	16.89±0.26	-
Cr2Fe8	BDL	0.08±0.02	BDL	0.23±0.05	1.00±0.10	0.14±0.01	1.64±0.19	0.07±0.01	4.46±0.47	0.31±0.05
Cr5Fe5	BDL	0.13±0.05	BDL	0.40±0.10	6.43±0.42	0.14±0.01	5.56±0.64	0.48±0.07	8.48±0.92	0.56±0.05
Cr8Fe2	BDL	0.20±0.05	BDL	0.39±0.07	2.88±0.29	0.14±0.05	2.72±0.32	0.16±0.03	3.55±0.34	0.43±0.04
Cr10	-	0.25±0.05	-	0.37±0.06	-	0.23±0.03	-	0.30±0.04	-	0.36±0.04

Note: BDL (below detection limit, ~0.1 µM for Fe, ~0.01 µM for Cr)

Table A. 4 Calculated logKsp values for pristine and reacted solids based on the data and relationship from Sass and Rai (1987).

Sample	Solid phase composition and properties	Reaction condition (pH 7, ~30 days)					
		Control	0.1 mM oxalate	1 mM oxalate	0.1 mM DFOB	0.1 mM DFOB + 0.1 mM oxalate	0.1 mM DFOB + 1 mM oxalate
Cr2Fe8	Cr/metal ratio (% change)	0.6% ↓	1.4% ↓	2.6% ↓	0.3%↑	2.7% ↑	6.9% ↑
	Fe/metal ratio (% change)	0.1% ↑	0.3% ↑	0.5% ↑	0.04%↑	0.5% ↑	1.3% ↑
	Log Ksp (pristine=2.46)	2.46 (0.2% ↓)	2.45 (0.5% ↓)	2.44 (1.0% ↓)	2.47 (0.1% ↑)	2.49 (1.0% ↑)	2.53 (2.6% ↑)
Cr5Fe5	Cr/metal ratio (% change)	0.7% ↓	1.5% ↓	2.1% ↓	20.0%↑	15.5% ↑	29.3% ↑
	Fe/metal ratio (% change)	0.5% ↑	1.1% ↑	1.5% ↑	14.5%↑	11.3% ↑	21.3% ↑
	Log Ksp (pristine=3.52)	3.52 (0.2% ↓)	3.51 (0.5% ↓)	3.5 (0.7% ↓)	3.72 (5.6% ↑)	3.68 (4.4% ↑)	3.8 (7.7% ↑)
Cr8Fe2	Cr/metal ratio (% change)	0.7% ↓	0.9% ↓	0.5% ↓	7.7% ↑	7.7% ↑	10.6% ↑
	Fe/metal ratio (% change)	2.2% ↑	2.9% ↑	1.5% ↑	24.6%↑	24.8% ↑	34.1% ↑
	Log Ksp (pristine=4.08)	4.08 (0.1% ↓)	4.08 (0.2% ↓)	4.08 (0.1% ↓)	4.13 (1.2% ↑)	4.13 (1.2% ↑)	4.15 (1.5% ↑)

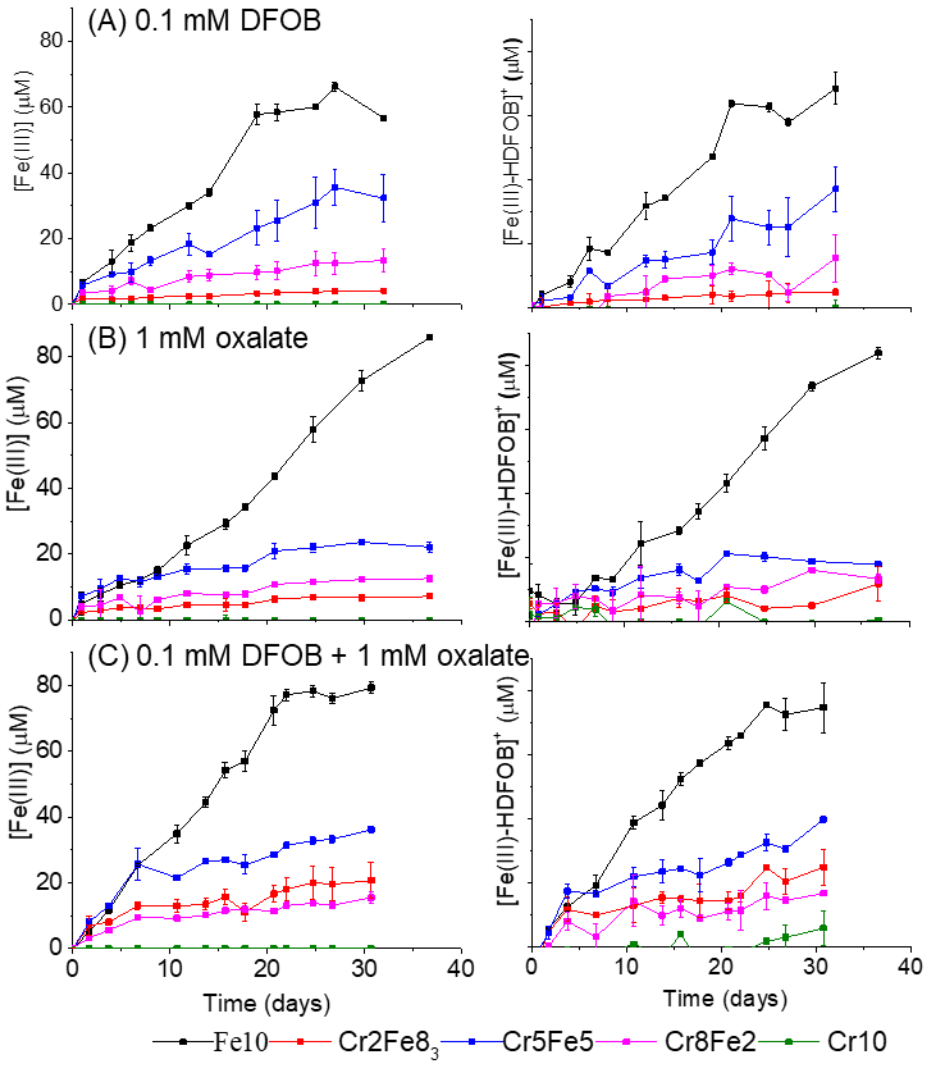

Figure A.1 Concentrations of dissolved Fe(III) (left panels) and [Fe(III)-HDFOB]+ complex (right panels) as a function of time in the presence of (A) 0.1 mM DFOB, (B) 0.1 mM DFOB + 0.1 mM oxalate, and (C) 0.1 mM DFOB + 1 mM oxalate.

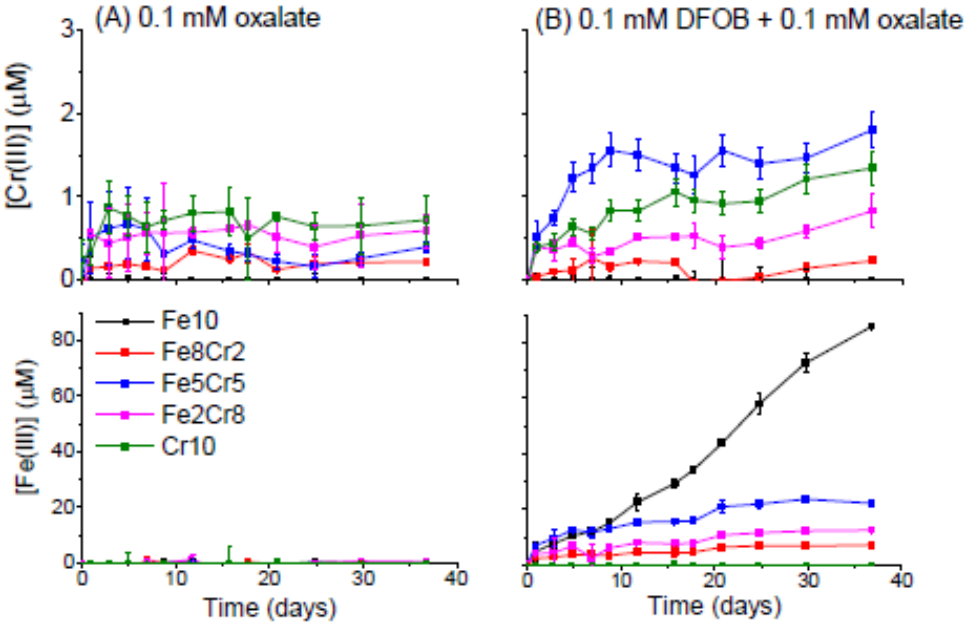

Figure A.2 Concentrations of dissolved Cr and Fe from the $Cr_xFe_{1-x}(OH)_3$ phases using ten-fold lower oxalate concentrations than in Figure 1 in the presence of (A) 0.1 mM oxalate and (B) 0.1 mM DFOB + 0.1 mM oxalate

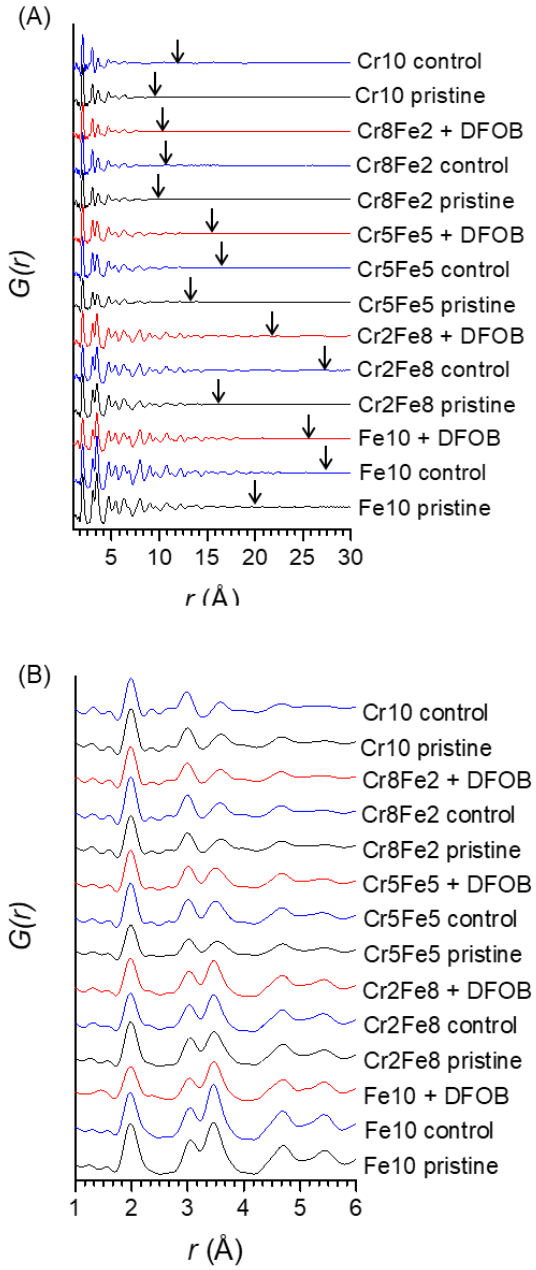

Figure A.3 PDFs, G(r), of the solid phases under pristine (unreacted), control (no DFOB, no oxalate), and 0.1 mM DFOB conditions with an *r* range of (A) 30 Å and (B) 6 Å. The arrows in (A) correspond to approximate end of oscillations, indicating loss of structure

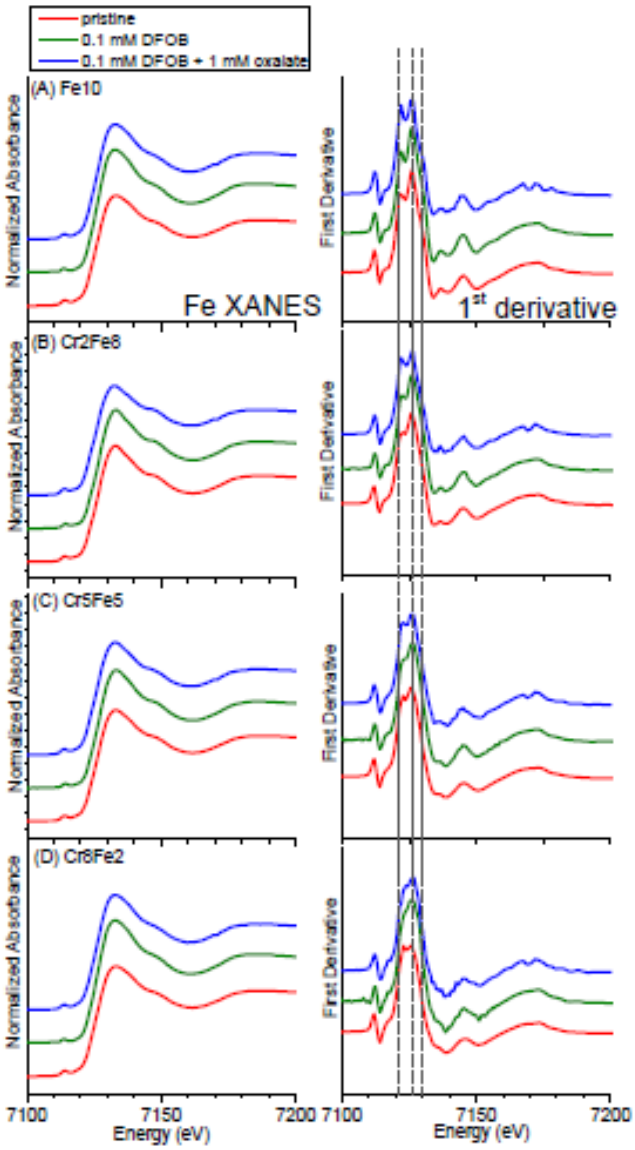

Figure A.4 Fe K-edge XANES spectra (left panels) and corresponding 1st derivatives (right panels) of (A) Fe10, (B) Cr2Fe8, (C) Cr5Fe5, and (D) Cr8Fe2 under pristine, control, 0.1 mM DFOB only, and 0.1 mM DFOB + 1 mM oxalate conditions. Vertical lines indicate regions where gradual transformations are observed.

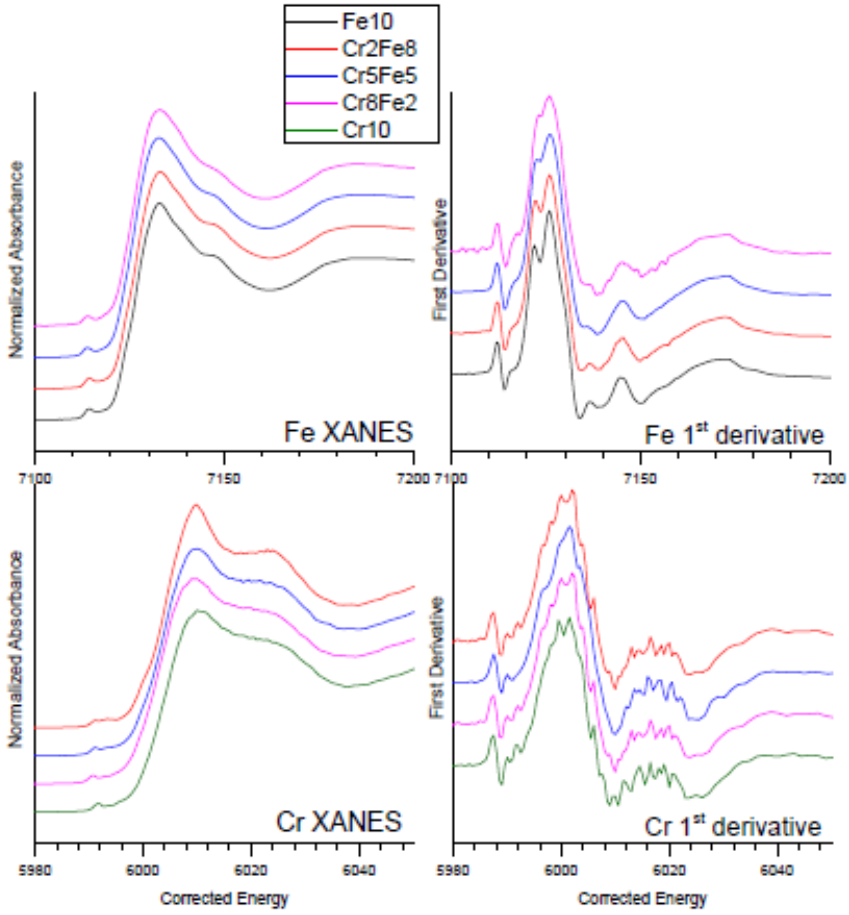

Figure A.5 Fe (top) and Cr (bottom) K-edge XANES spectra (left panels) and corresponding 1st derivatives (right panels) of control $Cr_xFe_{1-x}(OH)_3$ phases (i.e. reacted in solution with no DFOB and no oxalate).

REFERENCES

Abelmann, A., Gersonde, R. and Spiess, V. (1990) Pliocene — Pleistocene Paleoceanography in the Weddell Sea — Siliceous Microfossil Evidence, in: Bleil, U., Thiede, J. (Eds.), Geological History of the Polar Oceans: Arctic versus Antarctic. Springer Netherlands, Dordrecht, pp. 729-759.

Abramson, L., Wirick, S., Lee, C., Jacobsen, C. and Brandes, J.A. (2009) The use of soft X-ray spectromicroscopy to investigate the distribution and composition of organic matter in a diatom frustule and a biomimetic analog. Deep-Sea Research Part I-Topical Studies in Oceanography 56, 1369-1380.

Agusti, S. and Duarte, C.M. (2013) Phytoplankton lysis predicts dissolved organic carbon release in marine plankton communities. Biogeosciences 10, 1259-1264.

Ahern, F., Eckert, J.M., Payne, N.C. and Williams, K.L. (1985) Speciation of chromium in sea water. Anal. Chim. Acta 175, 147-151.

Ahmed, E. and Holmstrom, S.J.M. (2014) Siderophores in environmental research: roles and applications. Microb. Biotechnol. 7, 196-208.

Akafia, M.M., Harrington, J.M., Bargar, J.R. and Duckworth, O.W. (2014) Metal oxyhydroxide dissolution as promoted by structurally diverse siderophores and oxalate. Geochimica Et Cosmochimica Acta 141, 258-269.

Albrecht-Gary, A.M. and Crumbliss, A.L. (1998) Coordination chemistry of siderophores: Thermodynamics and kinetics of iron chelation and release. Metal Ions in Biological Systems, Vol 35 35, 239-327.

Aller, R.C. (2014) Sedimentary Diagenesis, Depositional Environments, and Benthic Fluxes, in: H.D., H., K.K., T. (Eds.), Treatise on Geochemistry, Second Edition. Elsevier, Oxford, pp. 293-334.

Aller, R.C., Blair, N.E., Xia, Q. and Rude, P.D. (1996) Remineralization rates, recycling, and storage of carbon in Amazon shelf sediments. Continental Shelf Research 16, 753-786.

Altman, C. and King, E.L. (1961) The Mechanism of the Exchange of Chromium(III) and Chromium(VI) in Acidic Solution1-3. Journal of the American Chemical Society 83, 2825-2830.

Aluwihare, L.I. and Repeta, D.J. (1999) A comparison of the chemical characteristics of oceanic DOM and extracellular DOM produced by marine algae. Marine Ecology Progress Series 186, 105-117.

Amacher, M.C. and Baker, D.E. (1982) Redox reactions involving chromium, plutonium, and manganese in soils, in: Resources, Institute for Research on Land and Water Resources, Las Vegas, Nevada, p. 166.

Amon, R.M.W., Fitznar, H.P. and Benner, R. (2001) Linkages among the bioreactivity, chemical composition, and diagenetic state of marine dissolved organic matter. Limnology and Oceanography 46, 287-297.

Anschutz, A.J. and Penn, R.L. (2005) Reduction of crystalline iron(III) oxyhydroxides using hydroquinone: Influence of phase and particle size. Geochemical Transactions 6, 60-66.

Aplin, A.C. (1993) The composition of authigenic clay minerals in recent sediments: Links to the supply of unstable reactants, in: DAC, M., PL, H., CR, H. (Eds.), Geochemistry of Clay-Pore Fluid Interactions. Chapman and Hall, London, pp. 81-106.

Arrieta, J.M., Mayol, E., Hansman, R.L., Herndl, G.J., Dittmar, T. and Duarte, C.M. (2015) Dilution limits dissolved organic carbon utilization in the deep ocean. Science 348, 331-333.

Arvidson, R.S., Mackenzie, F.T. and Guidry, M. (2006) MAGic: A Phanerozoic model for the geochemical cycling of major rock-forming components. Am. J. Sci. 306, 135-190.

Azam, F., Fenchel, T., Field, J.G., Gray, J.S., Meyerreil, L.A. and Thingstad, F. (1983) The ecological role of water-column microbes in the sea. Marine Ecology Progress Series 10, 257-263.

Babechuk, M.G., Kleinhanns, I.C. and Schoenberg, R. (2017) Chromium geochemistry of the ca. 1.85 Ga Flin Flon paleosol. Geobiology 15, 30-50.

Ball JW, Nordstrom DK (1998) Critical evaluation and selection of standard state thermodynamic properties for chromium metal and its aqueous ions, hydrolysis species, oxides, and hydroxides. J Chem Eng Data 43:895–918.

Banik, S. and Dey, B.K. (1982) Available phosphate content of an alluvial soil as influenced by inoculation of some isolate phosphate-solubilizing mircorganisms. Plant Soil 69, 353-364.

Barker, P., Fontes, J.C., Gasse, F. and Druart, J.C. (1994) Experimental dissolution of diatom silica in concentrated salt-solutions and implications for paleoenvironmental reconstruction. Limnology and Oceanography 39, 99-110.

Barofsky, A., Vidoudez, C. and Pohnert, G. (2009) Metabolic profiling reveals growth stage variability in diatom exudates. Limnology and Oceanography-Methods 7, 382-390.

Bartlett, R. and James, B. (1979) Behavior of chromium in soils. 3. Oxidation. Journal of Environmental Quality 8, 31-35.

Bartlett, R.J. and James, B.R. (1988) Mobility and bioavailibility of chromium in soils, in: Nriagu, J.O., Nieboer, E. (Eds.), Chromium in the natural and human environments. Wiley, New York, pp. 267-304.

Baskaran, M. (2012) Environmental Isotope Geochemistry: Past, Present and Future, in: Baskaran, M. (Ed.), Handbook of Environmental Isotope Geochemistry: Vol I. Springer Berlin Heidelberg, Berlin, Heidelberg, pp. 3-10.

Bauer, J.E., Williams, P.M. and Druffel, E.R.M. (1992) C-14 activity of dissolved organic carbon fractions in the north-central Pacific and Sargasso Sea. Nature 357, 667-670.

Beckler, J.S., Kiriazis, N., Rabouille, C., Stewart, F.J. and Taillefert, M. (2016) Importance of microbial iron reduction in deep sediments of river-dominated continental-margins. Mar. Chem. 178, 22-34.

Beckler, J.S., Nuzzio, D.B. and Taillefert, M. (2014) Development of single-step liquid chromatography methods with ultraviolet detection for the measurement of inorganic anions in marine waters. Limnology and Oceanography-Methods 12, 563-576.

Benner, R. (2002) Chemical composition and reactivity., in: D. Hansell, a.C.C. (Ed.), Biogeochemistry of marine dissolved organic matter. Academic Press, pp. 59-90.

Benner, R., Pakulski, J.D., McCarthy, M., Hedges, J.I. and Hatcher, P.G. (1992) Bulk chemical characteristics of dissolved organic matter in the ocean. Science 255, 1561-1564.

Benner, R. and Strom, M. (1993) A critical evaluation of the analytical blank associated with DOC measurements by high-temperature catalytic oxidation. Mar. Chem. 41, 153-160.

Berna, E.C., Johnson, T.M., Makdisi, R.S. and Basui, A. (2010) Cr Stable Isotopes As Indicators of Cr(VI) Reduction in Groundwater: A Detailed Time-Series Study of a Point-Source Plume. Environmental Science & Technology 44, 1043-1048.

Berner, E.K. and Berner, R.A. (2012) The Oceans, in: 2 (Ed.), Global Environment: Water, Air, and Geochemical Cycles. Princeton University Press, pp. 339-386.

Berner, R.A., Lasaga, A.C. and Garrels, R.M. (1983) The carbonate-silicate geochemical cycle and its effect on atmospheric carbon dioxide over the pas 100 million years. Am. J. Sci. 283, 641-683.

Bi, Y.Q., Hesterberg, D.L. and Duckworth, O.W. (2010) Siderophore-promoted dissolution of cobalt from hydroxide minerals. Geochimica Et Cosmochimica Acta 74, 2915-2925.

Biddanda, B. and Benner, R. (1997) Carbon, nitrogen, and carbohydrate fluxes during the production of particulate and dissolved organic matter by marine phytoplankton. Limnology and Oceanography 42, 506-518.

Bidle, K.D. and Azam, F. (1999) Accelerated dissolution of diatom silica by marine bacterial assemblages. Nature 397, 508-512.

Biersmith, A. and Benner, R. (1998) Carbohydrates in phytoplankton and freshly produced dissolved organic matter. Mar. Chem. 63, 131-144.

Blanco, S., Alvarez, I. and Cejudo, C. (2008) A test on different aspects of diatom processing techniques. Journal of Applied Phycology 20, 445-450.

Blowes, D. (2002) Environmental chemistry - Tracking hexavalent Cr in groundwater. Science 295, 2024-2025.

Boenigk, J., Wodniok, S. and Glücksman, E. (2015) Biodiversity and Earth History. Springer, New York.

Bondietti, G., Sinniger, J. and Stumm, W. (1993) The reactivity of Fe(II) (hydr)oxides- Effects of ligands in inhibiting the dissolution. Colloids and Surfaces a-Physicochemical and Engineering Aspects 79, 157-167.

Bonnand, P., Parkinson, I.J., James, R.H., Karjalainen, A.M. and Fehr, M.A. (2011) Accurate and precise determination of stable Cr isotope compositions in carbonates by double spike MC-ICP-MS. Journal of Analytical Atomic Spectrometry 26, 528-535.

Boyd, R.K., Defreitas, A.S.W., Hoyle, J., McCulloch, A.W., McInnes, A.G., Rogerson, A. and Walter, J.A. (1987) Glycerol 1,2-cyclic phosphate in centric diatoms- observations by P-31 NMR in vivo, isolation, and structural determination. J. Biol. Chem. 262, 12406-12408.

Boyle, J.A., Pickettheaps, J.D. and Czarnecki, D.B. (1984) Valve morphogenesis in the pennate diatom Achanthes coarctata. Journal of Phycology 20, 563-573.

Brantley, L.S. (2008) Kinetics of Mineral Dissolution, in: Brantley, L.S., Kubicki, D.J., White, F.A. (Eds.), Kinetics of Water-Rock Interaction. Springer New York, New York, NY, pp. 151-210.

Brantley, S.L., Liermann, L.J., Guynn, R.L., Anbar, A., Icopini, G.A. and Barling, J. (2004) Fe isotopic fractionation during mineral dissolution with and without bacteria. Geochimica Et Cosmochimica Acta 68, 3189-3204.

Bronk, D.A., See, J.H., Bradley, P. and Killberg, L. (2007) DON as a source of bioavailable nitrogen for phytoplankton. Biogeosciences 4, 283-296.

Brown, G.E., Calas, G., Waychunas, G.A. and Petiau, J. (1988) X-ray absorption spectroscopy and its applications in mineralogy and geochemistry. Reviews in Mineralogy 18, 431-512.

Brunauer, S., Emmett, P.H. and Teller, E. (1938) Adsorption of gases in multimolecular layers. Journal of the American Chemical Society 60, 309-319.

Budzikiewicz, H., Georgias, H. and Taraz, K. (2002) Diastereomeric pyoverdin-chromium(III) complexes. Z.Naturforsch.(C) 57, 954-956.

Carbonaro, R.F., Gray, B.N., Whitehead, C.F. and Stone, A.T. (2008) Carboxylate-containing chelating agent interactions with amorphous chromium hydroxide: Adsorption and dissolution. Geochimica Et Cosmochimica Acta 72, 3241-3257.

Carbonaro, R.F. and Stone, A.T. (2015) Oxidation of Cr-III aminocarboxylate complexes by hydrous manganese oxide: products and time course behaviour. Environ. Chem. 12, 33-51.

Carlson, C.A. (2002.) Production and removal processes, in: Carlson, C.A., Hansell D. A. (Ed.), Biogeochemistry of marine dissolved organic matter., 2 ed. Academic Press., pp. 91-151.

Carlson, C.A., D.A. Hansell. (2015) DOC Sources, Sinks, Reactivity, and Budgets, in: D.A. Hansell, D. A., Carlson, C. A. (Ed.), Biogeochemistry of Marine Dissolved Organic Matter, 2 ed. Academic Press, pp. 65-126.

Carrano, C.J., Drechsel, H., Kaiser, D., Jung, G., Matzanke, B., Winkelmann, G., Rochel, N. and AlbrechtGary, A.M. (1996) Coordination chemistry of the carboxylate type siderophore rhizoferrin: The iron(III) complex and its metal analogs. Inorg. Chem. 35, 6429-6436.

Casey, W.H., Westrich, H.R., Banfield, J.F., Ferruzzi, G. and Arnold, G.W. (1993) Leaching and reconstruction at the surfaces of dissolving chain-silicate minerals. Nature 366, 253-256.

Cervini-Silva, J. and Sposito, G. (2002) Steady-state dissolution kinetics of aluminum-goethite in the presence of desferrioxamine-B and oxalate ligands. Environmental Science & Technology 36, 337-342.

Cheah, S.F., Kraemer, S.M., Cervini-Silva, J. and Sposito, G. (2003) Steady-state dissolution kinetics of goethite in the presence of desferrioxamine B and oxalate ligands: implications for the microbial acquisition of iron. Chemical Geology 198, 63-75.

Cherrier, J. and Bauer, J.E. (2004) Bacterial utilization of transient plankton-derived dissolved organic carbon and nitrogen inputs in surface ocean waters. Aquatic Microbial Ecology 35, 229-241.

Chou, J., J. , Morse, S., Omeis and Venos, E.S. (2005) Escherichia coli C29 alkaline phosphatase enzyme activity and protein level in exponential and stationary phases. J. Exp. Microbiol. Immunol. 7, 1-6.

Chou, L. and Wollast, R. (1984) Study of the weathering fo albite at room-temperature and pressure with a fluidized-bed reactor. Geochimica Et Cosmochimica Acta 48, 2205-2217.

Clark, L.L., Ingall, E.D. and Benner, R. (1998) Marine phosphorus is selectively remineralized. Nature 393, 426-426.

Clark, L.L., Ingall, E.D. and Benner, R. (1999) Marine organic phosphorus cycling: Novel insights from nuclear magnetic resonance. Am. J. Sci. 299, 724-737.

Cole, D.B., Reinhard, C.T., Wang, X.L., Gueguen, B., Halverson, G.P., Gibson, T., Hodgskiss, M.S.W., McKenzie, N.R., Lyons, T.W. and Planavsky, N.J. (2016) A shale-hosted Cr isotope record of low atmospheric oxygen during the Proterozoic. Geology 44, 555-558.

Cole, J.J., Likens, G.E. and Strayer, D.L. (1982) Photosynthetically produced dissolved organic carbon- An important carbon source for plantonic bacteria. Limnology and Oceanography 27, 1080-1090.

Cole, T.G. (1985) Composition, oxygen isotope geochemistry, and origin of smectite in the metalliferous sediments of the Bauer Deep, Southeast Pacific. Geochimica Et Cosmochimica Acta 49, 221-235.

Cornell, R.M. and Schindler, P.W. (1980) Infrared study of the adsorption of hydroxycarboxylic acids on alpha-FeOOH and amorphous Fe(III)hydroxide. Colloid and Polymer Science 258, 1171-1175.

Cotton, F.A. and Wilkinson, G. (1972) Advanced Inorganic Chemistry, Third ed. Interscience Publishers, New York.

Crowe, S.A., Dossing, L.N., Beukes, N.J., Bau, M., Kruger, S.J., Frei, R. and Canfield, D.E. (2013) Atmospheric oxygenation three billion years ago. Nature 501, 535-+.

Dalai, P., Kaddour, H. and Sahai, N. (2016) Incubating Life: Prebiotic Sources of Organics for the Origin of Life. Elements 12, 401-406.

Davis, J.A. and Leckie, J.O. (1978) Surface ionixation and complexation at oxide-water interface. 2. Surface properties of amorphous iron oxyhydroxide and adsorption of metal-ions. Journal of Colloid and Interface Science 67, 90-107.

De Brouwer, J.F.C., Wolfstein, K. and Stal, L.J. (2002) Physical characterization and diel dynamics of different fractions of extracellular polysaccharides in an axenic culture of a benthic diatom. European Journal of Phycology 37, 37-44.

De La Rocha, C.L. (2006) Opal-based isotopic proxies of paleoenvironmental conditions. Global Biogeochemical Cycles 20.

Dean, W.E. (1974) Determination of carbonate and organic matter in calcareous sediments and sedimenatry rocks by loss on ignition- Comparison with other methods. Journal of Sedimentary Petrology 44, 242-248.

Degenhardt, J. and McQuillan, A.J. (1999) Mechanism of oxalate ion adsorption on chromium oxide-hydroxide from pH dependence and time evolution of ATR-IR spectra. Chem. Phys. Lett. 311, 179-184.

DeMaster, D.J. (2002) The accumulation and cycling of biogenic silica in the Southern Ocean: revisiting the marine silica budget. Deep-Sea Research Part Ii-Topical Studies in Oceanography 49, 3155-3167.

DeMaster, D.J. (2003) 7.04 - The Diagenesis of Biogenic Silica: Chemical Transformations Occurring in the Water Column, Seabed, and Crust A2 - Holland, Heinrich D, in: Turekian, K.K. (Ed.), Treatise on Geochemistry. Pergamon, Oxford, pp. 87-98.

Deng, B.L. and Stone, A.T. (1996) Surface-catalyzed chromium(VI) reduction: Reactivity comparisons of different organic reductants and different oxide surfaces. Environmental Science & Technology 30, 2484-2494.

Diaz, J., Ingall, E., Benitez-Nelson, C., Paterson, D., de Jonge, M.D., McNulty, I. and Brandes, J.A. (2008) Marine polyphosphate: A key player in geologic phosphorus sequestration. Science 320, 652-655.

Diaz, J.M., Björkman, K. M., Haley, S. T., Ingall, E. D., Karl, D. M., Longo, A. F. and Dyhrman, S. T. (2015) Polyphosphate dynamics at Station ALOHA, North Pacific subtropical gyre. Limnol. Oceanography.

Dinasquet, J., Kragh, T., Schroter, M.L., Sondergaard, M. and Riemann, L. (2013) Functional and compositional succession of bacterioplankton in response to a gradient in bioavailable dissolved organic carbon. Environmental Microbiology 15, 2616-2628.

Dittmar, T., Koch, B., Hertkorn, N. and Kattner, G. (2008) A simple and efficient method for the solid-phase extraction of dissolved organic matter (SPE-DOM) from seawater. Limnology and Oceanography: Methods 6, 230-235.

Dixit, S., Van Cappellen, P. and van Bennekom, A.J. (2001) Processes controlling solubility of biogenic silica and pore water build-up of silicic acid in marine sediments. Mar. Chem. 73, 333-352.

Drever, J.I. (1971) Early diagensis of clay minerals in Rio-Ameca Basin, Mexico. Journal of Sedimentary Petrology 41, 982-&.

Ducklow, H.W., Carlson, C.A., Bates, N.R., Knap, A.H. and Michaels, A.F. (1995) Dissolved organic carbon as a component of the biological pump in the north-Atlantic ocean. Philosophical Transactions of the Royal Society of London Series B-Biological Sciences 348, 161-167.

Duckworth, O.W., Akafia, M.M., Andrews, M.Y. and Bargar, J.R. (2014) Siderophore-promoted dissolution of chromium from hydroxide minerals. Environ. Sci.-Process Impacts 16, 1348-1359.

Duckworth, O.W., Bargar, J.R., Jarzecki, A.A., Oyerinde, O., Spiro, T.G. and Sposito, G. (2009) The exceptionally stable cobalt(III)-desferrioxamine B complex. Mar. Chem. 113, 114-122.

Duckworth, O.W. and Martin, S.T. (2001) Surface complexation and dissolution of hematite by C-1-C-6 dicarboxylic acids at pH=5.0. Geochimica Et Cosmochimica Acta 65, 4289-4301.

Duckworth, O.W. and Sposito, G. (2007) Siderophore-promoted dissolution of synthetic and biogenic layer-type Mn oxides. Chemical Geology 242, 497-508.

Dugdale, R.C. and Wilkerson, F.P. (1998) Silicate regulation of new production in the equatorial Pacific upwelling. Nature 391, 270-273.

Dugdale, R.C., Wilkerson, F.P. and Minas, H.J. (1995) The role of a silicate pump in driving new production. Deep-Sea Research Part I-Oceanographic Research Papers 42, 697-719.

Duhamel, S., Dyhrman, S.T. and Karl, D.M. (2010) Alkaline phosphatase activity and regulation in the North Pacific Subtropical Gyre. Limnology and Oceanography 55, 1414-1425.

Dyhrman, S.T., Jenkins, B.D., Rynearson, T.A., Saito, M.A., Mercier, M.L., Alexander, H., Whitney, L.P., Drzewianowski, A., Bulygin, V.V., Bertrand, E.M., Wu, Z.J., Benitez-Nelson, C. and Heithoff, A. (2012) The Transcriptome and Proteome of the Diatom Thalassiosira pseudonana Reveal a Diverse Phosphorus Stress Response. Plos One 7, 10.

Dyhrman, S.T. and Palenik, B. (1999) Phosphate stress in cultures and field populations of the dinoflagellate Prorucentrum minimum detected by a single-cell alkaline phosphatase assay. Appl. Environ. Microbiol. 65, 3205-3212.

Dyhrman, S.T. and Palenik, B. (2003) Characterization of ectoenzyme activity and phosphate-regulated proteins in the coccolithophorid Emiliania huxleyi. Journal of Plankton Research 25, 1215-1225.

Eary, L.E. and Rai, D. (1988) Chromate removal from aqueous wastes by reduction with ferrous iron. Environmental Science & Technology 22, 972-977.

Ehlert, C., Doering, K., Wallmann, K., Scholz, F., Sommer, S., Grasse, P., Geilert, S. and Frank, M. (2016) Stable silicon isotope signatures of marine pore waters - Biogenic opal dissolution versus authigenic clay mineral formation. Geochimica Et Cosmochimica Acta 191, 102-117.

Ehrlich, H.L. (1996) How microbes influence mineral growth and dissolution. Chemical Geology 132, 5-9.

Ehrlich, H.L. (1998) Geomicrobiology: its significance for geology. Earth-Science Reviews 45, 45-60.

Eick, M.J., Peak, J.D. and Brady, W.D. (1999) The effect of oxyanions on the oxalate-promoted dissolution of goethite. Soil Sci. Soc. Am. J. 63, 1133-1141.

Ellis, A.S., Johnson, T.M. and Bullen, T.D. (2002) Chromium isotopes and the fate of hexavalent chromium in the environment. Science 295, 2060-2062.

Ellis, A.S., Johnson, T.M. and Bullen, T.D. (2004) Using chromium stable isotope ratios to quantify Cr(VI) reduction: Lack of sorption effects. Environmental Science & Technology 38, 3604-3607.

Ellwood, M.J. and Hunter, K.A. (2000) The incorporation of zinc and iron into the frustule of the marine diatom Thalassiosira pseudonana. Limnology and Oceanography 45, 1517-1524.

EPA, U.S. (2000) *In situ* treatment of soil and groundwater contaminated with chromium, Office of Research and Development.

Fan, T.W.M., Lane, A.N., Pedler, J., Crowley, D. and Higashi, R.M. (1997) Comprehensive analysis of organic ligands in whole root exudates using nuclear magnetic resonance and gas chromatography mass spectrometry. Analytical Biochemistry 251, 57-68.

Fendorf, S.E. (1995) Surface-reactions of chromium in soils and waters. Geoderma 67, 55-71.

Fendorf, S.E. and Zasoski, R.J. (1992) Chromium(III) oxidations by delta-MnO2. 1. Characterization. Environmental Science & Technology 26, 79-85.

Fogg, G.E. (1983) The ecological signficance of extracellular products of phytoplankton photosynthesis. Botanica Marina 26, 3-14.

Fortin, D. and Langley, S. (2005) Formation and occurrence of biogenic iron-rich minerals. Earth-Science Reviews 72, 1-19.

Fox, T.R. and Comerford, N.B. (1990) Low-molecular-weight organic-acids in selected forest soils of the southeastern USA. Soil Sci. Soc. Am. J. 54, 1139-1144.

Francis, C.A., Obraztsova, A.Y. and Tebo, B.M. (2000) Dissimilatory metal reduction by the facultative anaerobe Pantoea agglomerans SP1. Appl. Environ. Microbiol. 66, 543-548.

Fredrickson, J.K., Kostandarithes, H.M., Li, S.W., Plymale, A.E. and Daly, M.J. (2000) Reduction of Fe(III), Cr(VI), U(VI), and Tc(VII) by Deinococcus radiodurans R1. Appl. Environ. Microbiol. 66, 2006-2011.

Frei, R., Gaucher, C., Poulton, S.W. and Canfield, D.E. (2009) Fluctuations in Precambrian atmospheric oxygenation recorded by chromium isotopes. Nature 461, 250-U125.

Frommer, J., Nachtegaal, M., Czekaj, I. and Kretzschmar, R. (2010) The Cr X-ray absorption K-edge structure of poorly crystalline Fe(III)-Cr(III)-oxyhydroxides. American Mineralogist 95, 1202-1213.

Furrer, G. and Stumm, W. (1986) The coordination chemistry of weathering. 1. Dissolution kinetics of delta-Al2O3 and BeO. Geochimica Et Cosmochimica Acta 50, 1847-1860.

Gadd, G.M. (2000) Bioremedial potential of microbial mechanisms of metal mobilization and immobilization. Curr. Opin. Biotechnol. 11, 271-279.

Gadd, G.M. (2007) Geomycology: biogeochemical transformations of rocks, minerals, metals and radionuclides by fungi, bioweathering and bioremediation. Mycological Research 111, 3-49.

Gadd, G.M. (2010) Metals, minerals and microbes: geomicrobiology and bioremediation. Microbiology-(UK) 156, 609-643.

Gehlen, M., Beck, L., Calas, G., Flank, A.M., Van Bennekom, A.J. and Van Beusekom, J.E.E. (2002) Unraveling the atomic structure of biogenic silica: Evidence of the structural association of Al and Si in diatom frustules. Geochimica Et Cosmochimica Acta 66, 1601-1609.

Gehlen, M., Heinze, C., Maier-Reimer, E. and Measures, C.I. (2003) Coupled Al-Si geochemistry in an ocean general circulation model: A tool for the validation of oceanic dust deposition fields? Global Biogeochemical Cycles 17.

Gendron-Badou, A., Coradin, T., Maquet, J., Frohlich, F. and Livage, J. (2003) Spectroscopic characterization of biogenic silica. Journal of Non-Crystalline Solids 316, 331-337.

Gerard, F., Francois, M. and Ranger, J. (2002) Processes controlling silica concentration in leaching and capillary soil solutions of an acidic brown forest soil (Rhone, France). Geoderma 107, 197-226.

Gilleaudeau, G.J., Frei, R., Kaufman, A.J., Kah, L.C., Azmy, K., Bartley, J.K., Chernyavskiy, P. and Knoll, A.H. (2016) Oxygenation of the mid-Proterozoic atmosphere: clues from chromium isotopes in carbonates. Geochemical Perspectives Letters 2, 178-186.

Ginder-Vogel, M. and Sparks, D.L. (2010) The Impacts of X-Ray Absorption Spectroscopy on Understanding Soil Processes and Reaction Mechanisms, in: Balwant, S., Markus, G. (Eds.), Developments in Soil Science. Elsevier, pp. 1-26.

Gomez-Consarnau, L., Lindh, M.V., Gasol, J.M. and Pinhassi, J. (2012) Structuring of bacterioplankton communities by specific dissolved organic carbon compounds. Environmental Microbiology 14, 2361-2378.

Goudie, A.S. (1996) Organic agency in calcrete development. Journal of Arid Environments 32, 103-110.

Granum, E., Kirkvold, S. and Myklestad, S.M. (2002) Cellular and extracellular production of carbohydrates and amino acids by the marine diatom Skeletonema costatum: diel variations and effects of N depletion. Marine Ecology Progress Series 242, 83-94.

Green, N.W., Perdue, E.M., Aiken, G.R., Butler, K.D., Chen, H.M., Dittmar, T., Niggemann, J. and Stubbins, A. (2014) An intercomparison of three methods for the large-scale isolation of oceanic dissolved organic matter. Mar. Chem. 161, 14-19.

Grill, E.V. and Richards, F.A. (1964) Nutrient regeneration from phytoplankton decompositng in seawater. Journal of Marine Research 22, 51-69.

Gueguen, B., Reinhard, C.T., Algeo, T.J., Peterson, L.C., Nielsen, S.G., Wang, X.L., Rowe, H. and Planavsky, N.J. (2016) The chromium isotope composition of reducing and oxic marine sediments. Geochimica Et Cosmochimica Acta 184, 1-19.

Guillard, R.R. and Ryther, J.H. (1962) Studies of marine planktonic diatoms. 1. Cyclotella nana hustedt and detonula confervacea (cleve) gran. Canadian Journal of Microbiology 8, 229-&.

Gun'ko, V.M., Mironyuk, I.F., Zarko, V.I., Voronin, E.F., Turov, V.V., Pakhlov, E.M., Goncharuk, E.V., Nychiporuk, Y.M., Vlasova, N.N., Gorbik, P.P., Mishchuk, O.A., Mishchuk, O.A., Chuiko, A.A., Kulik, T.V., Palyanytsya, B.B., Pakhovchishin, S.V., Skubiszewska-Zieba, J., Janusz, W., Turov, A.V. and Leboda, R. (2005) Morphology and surface properties of fumed silicas. Journal of Colloid and Interface Science 289, 427-445.

Guo, L.D., Wen, L.S., Tang, D.G. and Santschi, P.H. (2000) Re-examination of cross-flow ultrafiltration for sampling aquatic colloids: evidence from molecular probes. Mar. Chem. 69, 75-90.

Gustafsson, J.P. (2016) Visual MINTEQ, 3.1 ed, Stockholm.

Gustafsson, J.P., Persson, I., Oromieh, A.G., van Schaik, J.W.J., Sjöstedt, C. and Kleja, D.B. (2014) Chromium(III) Complexation to Natural Organic Matter: Mechanisms and Modeling. Environmental Science & Technology 48, 1753-1761.

Hall, P.O. and Aller, R.C. (1992) Rapid, small volume, flow injection analysis for sigma-CO2 and NH4+ in marine and freshwaters. Limnology and Oceanography 37, 1113-1119.

Hammersley, A.P. (1998) "Fit2D" V. 9.129 Reference Manual V. 3.1, ESRF Internal Report.

Hammersley, A.P., Svensson, S.O., Hanfland, M., Fitch, A.N. and Hausermann, D. (1996) Two-dimensional detector software: From real detector to idealised image or two-theta scan. High Pressure Research 14, 235-248.

Hansel, C.M., Wielinga, B.W. and Fendorf, S.R. (2003) Structural and compositional evolution of Cr/Fe solids after indirect chromate reduction by dissimilatory iron-reducing bacteria. Geochimica Et Cosmochimica Acta 67, 401-412.

Hansell, D.A., C.A. Carlson (2001) Marine dissolved organic matter and the carbon cycle. Oceanography 14, 41-49.

Hansell, D.A. and Waterhouse, T.Y. (1997) Controls on the distributions of organic carbon and nitrogen in the eastern Pacific Ocean. Deep-Sea Research Part I-Oceanographic Research Papers 44, 843-857.

Harrington, J.M., Bargar, J.R., Jarzecki, A.A., Roberts, J.G., Sombers, L.A. and Duckworth, O.W. (2012) Trace metal complexation by the triscatecholate siderophore protochelin: structure and stability. Biometals 25, 393-412.

Hedges, J.I. (1992) Global biogechemical cycles-Progress and Problems. Mar. Chem. 39, 67-93.

Hedges, J.I. and Stern, J.H. (1984) Carbon and nitrogen determinations of carbonate-containing solids. Limnology and Oceanography 29, 657-663.

Hein, J.R., Yeh, H.W. and Alexander, E. (1979) Origin of iron-rich montmorillonite from the manganese nodule belt of the North Equatorial Pacific. Clays and Clay Minerals 27, 185-194.

Helgeson, H.C. and Mackenzi.Ft (1970) Silicate-sea water equilibria in ocean system. Deep-Sea Research 17, 877-&.

Hernlem, B.J., Vane, L.M. and Sayles, G.D. (1996) Stability constants for complexes of the siderophore desferrioxamine B with selected heavy metal cations. Inorganica Chimica Acta 244, 179-184.

Hertkorn, N., Harir, M., Koch, B.P., Michalke, B. and Schmitt-Kopplin, P. (2013) High-field NMR spectroscopy and FTICR mass spectrometry: powerful discovery tools for the molecular level characterization of marine dissolved organic matter. Biogeosciences 10, 1583-1624.

Hewkin, D.J. and Prince, R.H. (1970) The mechanism of octahedral complex formation by labile metal ions. Coordination Chemistry Reviews 5, 45-73.

Holdren, G.R. and Speyer, P.M. (1985) PH dependent changes in the rates and stoichiometry of dissolution of an alakali feldspar at room-temperature. Am. J. Sci. 285, 994-1026.

Holland, H.D. (2005) Sea level, sediments and the composition of seawater. Am. J. Sci. 305, 220-239.

Hopkinson, C.S., Fry, B. and Nolin, A.L. (1997) Stoichiometry of dissolved organic matter dynamics on the continental shelf of the northeastern USA. Continental Shelf Research 17, 473-489.

Hopkinson, C.S. and Vallino, J.J. (2005) Efficient export of carbon to the deep ocean through dissolved organic matter. Nature 433, 142-145.

Hopkinson, C.S., Vallino, J.J. and Nolin, A. (2002) Decomposition of dissolved organic matter from the continental margin. Deep-Sea Research Part Ii-Topical Studies in Oceanography 49, 4461-4478.

Humborg, C., Ittekkot, V., Cociasu, A. and VonBodungen, B. (1997) Effect of Danube River dam on Black Sea biogeochemistry and ecosystem structure. Nature 386, 385-388.

Hurd, D.C. (1973) Interactions of biogenic opan, sediment, and seater in Central Equatorial Pacific. Geochimica Et Cosmochimica Acta 37, 2257-&.

Icopini, G.A. and Long, D.T. (2002) Speciation of aqueous chromium by use of solid-phase extractions in the field. Environmental Science & Technology 36, 2994-2999.

Iler, R.K. (1979) The Chemistry of Silica. Wiley- Interscience, New York.

Isobe, T., Watanabe, T., de la Caillerie, J.B.D., Legrand, A.P. and Massiot, D. (2003) Solid-state H-1 and Al-27 NMR studies of amorphous aluminum hydroxides. Journal of Colloid and Interface Science 261, 320-324.

Ittekkot, V. (1982) Variations of dissolved organic matter during a plankton bloom- Qualtitative aspects based on sugar and amino acid analyses. Mar. Chem. 11, 143-158.

Ittekkot, V., Unger, D. and Humborg, C. (2006) The Silicon Cycle: Human Perturbations and Impacts on Aquatic Systems. Island Press, Washington D.C.

James, B.R. and Bartlett, R.J. (1983) Behavior of chromium in soils. 5. Fate of organiccaly complexed Cr(III) added to soil. Journal of Environmental Quality 12, 169-172.

Jensen, L.M. (1983) Phytoplankton release of extracellular organic carbon, molecular weight composition, and bacterial assimilation. Marine Ecology Progress Series 11, 39-48.

Johnson, K.M. and Grimm, K.A. (2001) Opal and organic carbon in laminated diatomaceous sediments: Saanich Inlet, Santa Barbara Basin and the Miocene Monterey Formation. Marine Geology 174, 159-175.

Johnson, S.E. and Loeppert, R.H. (2006) Role of organic acids in phosphate mobilization from iron oxide. Soil Sci. Soc. Am. J. 70, 222-234.

Johnson, T.M. (2011) Stable Isotopes of Cr and Se as Tracers of Redox Processes in Earth Surface Environments.

Johnson, T.M. and Bullen, T.D. (2004) Mass-dependent fractionation of selenium and chromium isotopes in low-temperature environments, in: Johnson, C.M., Beard, B.L., Albarede, F. (Eds.), Geochemistry of Non-Traditional Stable Isotopes. Mineralogical Soc Amer, Chantilly, pp. 289-317.

Kaczynski, S.E. and Kieber, R.J. (1994) Hydrophobic C18 Bound Organic Complexes of Chromium and Their Potential Impact on the Geochemistry of Cr in Natural Waters. Environmental Science & Technology 28, 799-804.

Karl, D.M. and Bjorkman., K.M. (2014) Dynamics of dissolved organic phosphorus, in: Hansell, D.A., Carlson, C.A. (Eds.), The biogeochemistry of marine dissolved organic matter. Academic Press.

Karl, D.M., Hebel, D.V., Bjorkman, K. and Letelier, R.M. (1998) The role of dissolved organic matter release in the productivity of the oligotrophic North Pacific Ocean. Limnology and Oceanography 43, 1270-1286.

Karl, D.M., Letelier, R., Hebel, D., Tupas, L., Dore, J., Christian, J. and Winn, C. (1995) Ecosystem changes in the North Pacific subtropical gyre attributed to the 1991-92 El Nino. Nature 373, 230-234.

Keil, R.G. and Kirchman, D.L. (1993) Dissolved combined amino acids- Chemical form and utilization by marine bacteria. Limnology and Oceanography 38, 1256-1270.

Kester, D.R., Duedall, I.W., Connors, D.N. and Pytkowic.Rm (1967) PREPARATION OF ARTIFICIAL SEAWATER. Limnology and Oceanography 12, 176-&.

Kim, I.N., Lee, K., Gruber, N., Karl, D.M., Bullister, J.L., Yang, S. and Kim, T.W. (2014) Increasing anthropogenic nitrogen in the North Pacific Ocean. Science 346, 1102-1106.

Kim, J.G., Dixon, J.B., Chusuei, C.C. and Deng, Y.J. (2002) Oxidation of chromium(III) to (VI) by manganese oxides. Soil Sci. Soc. Am. J. 66, 306-315.

King, S.L., Froelich, P.N. and Jahnke, R.A. (2000) Early diagenesis of germanium in sediments of the Antarctic South Atlantic: In search of the missing Ge sink. Geochimica Et Cosmochimica Acta 64, 1375-1390.

Kirchman, D.L., Suzuki, Y., Garside, C. and Ducklow, H.W. (1991) High turnover rates of dissolved organic carbon during a spring phytoplankton bloom. Nature 352, 612-614.

Kolowith, L.C., Ingall, E.D. and Benner, R. (2001) Composition and cycling of marine organic phosphorus. Limnology and Oceanography 46, 309-320.

Koning, E., Gehlen, M., Flank, A.M., Calas, G. and Epping, E. (2007) Rapid post-mortem incorporation of aluminum in diatom frustules: Evidence from chemical and structural analyses. Mar. Chem. 106, 208-222.

Koning, E., van Iperen, J.M., van Raaphorst, W., Helder, W., Brummer, G.J.A. and van Weering, T.C.E. (2001) Selective preservation of upwelling-indicating diatoms in sediments off Somalia, NW Indian Ocean. Deep-Sea Research Part I-Oceanographic Research Papers 48, 2473-2495.

Koprivnjak, J.F., Pfromm, P.H., Ingall, E., Vetter, T.A., Schmitt-Kopplin, P., Hertkorn, N., Frommberger, M., Knicker, H. and Perdue, E.M. (2009) Chemical and spectroscopic characterization of marine dissolved organic matter isolated using coupled reverse osmosis-electrodialysis. Geochimica Et Cosmochimica Acta 73, 4215-4231.

Kotas, J. and Stasicka, Z. (2000) Chromium occurrence in the environment and methods of its speciation. Environmental Pollution 107, 263-283.

Kraemer, S.M. (2004) Iron oxide dissolution and solubility in the presence of siderophores. Aquat. Sci. 66, 3-18.

Kraemer, S.M., Cheah, S.F., Zapf, R., Xu, J.D., Raymond, K.N. and Sposito, G. (1999) Effect of hydroxamate siderophores on Fe release and Pb(II) adsorption by goethite. Geochimica Et Cosmochimica Acta 63, 3003-3008.

Krausse, G.L., Schelske, C.L. and Davis, C.O. (1983) Comparison of three wet-alkaline methods of digestion of biogenic silica in water. Freshwater Biology 13, 73-81.

Ku, T.C.W. and Walter, L.M. (2003) Syndepositional formation of Fe-rich clays in tropical shelf sediments, San Blas Archipelago, Panama. Chemical Geology 197, 197-213.

Kujawinski, E.B. (2011) The Impact of Microbial Metabolism on Marine Dissolved Organic Matter, in: Carlson, C.A., Giovannoni, S.J. (Eds.), Annual Review of Marine Science, Vol 3. Annual Reviews, Palo Alto, pp. 567-599.

Kukkadapu, R.K., Zachara, J.M., Fredrickson, J.K., Smith, S.C., Dohnalkova, A.C. and Russell, C.K. (2003) Transformation of 2-line ferrihydrite to 6-line ferrihydrite under oxic and anoxic conditions. American Mineralogist 88, 1903-1914.

Lancelot, C. (1984) Extracellular release of small and large molecules by phytoplankton in the Southern Bight of the North-Sea. Estuarine Coastal and Shelf Science 18, 65-77.

Landrot, G., Ginder-Vogel, M., Livi, K., Fitts, J.P. and Sparks, D.L. (2012) Chromium(III) Oxidation by Three Poorly-Crystalline Manganese(IV) Oxides. 1. Chromium(III)-Oxidizing Capacity. Environmental Science & Technology 46, 11594-11600.

Laruelle, G.G., Roubeix, V., Sferratore, A., Brodherr, B., Ciuffa, D., Conley, D.J., Durr, H.H., Garnier, J., Lancelot, C., Phuong, Q.L.T., Meunier, J.D., Meybeck, M., Michalopoulos, P., Moriceau, B., Longphuirt, S.N., Loucaides, S., Papush, L., Presti, M., Ragueneau, O., Regnier, P., Saccone, L., Slomp, C.P., Spiteri, C. and Van Cappellen, P. (2009) Anthropogenic perturbations of the silicon cycle at the global scale: Key role of the land-ocean transition. Global Biogeochemical Cycles 23.

Latimer, W.M. (1938) The oxidation states of the elements and their potentials in aqueous solutions. Prentice-Hall, inc., New York.

Lawson, D.S., Hurd, D.C. and Pankratz, H.S. (1978) Silica dissolution rates of decomposing phytoplankton assemblages at various temperatures. Am. J. Sci. 278, 1373-1393.

Legrand, A.P. (1998) The surface properties of silica. Wiley, New York.

Leonard, D.N., Chandler, G.W. and Seraphin, S. (2002) Scanning Electron Microscopy, Characterization of Materials. John Wiley & Sons, Inc.

Leong, J. and Raymond, N. (1975) Coorindation isomers of biological iron transport compounds. 4. Geometrical isomers of chromic desferriferriozamine-B. Journal of the American Chemical Society 97, 293-296.

Letscher, R.T. and Moore, J.K. (2015) Preferential remineralization of dissolved organic phosphorus and non-Redfield DOM dynamics in the global ocean: Impacts on marine productivity, nitrogen fixation, and carbon export. Global Biogeochemical Cycles 29, 325-340.

Lewin, J.C. (1961) The dissolution of silica from diatom walls. Geochimica Et Cosmochimica Acta 21, 182-198.

Libes, S. (2009) Introduction to Marine Biogeochemistry (2). Academic Press, Burlington, US.

Loh, A.N. and Bauer, J.E. (2000) Distribution, partitioning and fluxes of dissolved and particulate organic C, N and P in the eastern North Pacific and Southern Oceans. Deep-Sea Research Part I-Oceanographic Research Papers 47, 2287-2316.

Loh, A.N., Bauer, J.E. and Druffel, E.R.M. (2004) Variable ageing and storage of dissolved organic components in the open ocean. Nature 430, 877-881.

Lomas, M.W. (2016) Biogeochemical Stoichiometry of the Sargasso Sea, Ocean Sciences Meeting Abstract.

Lorenzen, C.J. (1967) A method for continuous measurement of in vivo chlorophyll concentration. Deep Sea Research 13, 223-247.

Loring, J.S., Simanova, A.A. and Persson, P. (2007) Molecular scale study of the synergism between oxalate and desferrioxamine-B on goethite dissolution. Geochimica Et Cosmochimica Acta 71, A596-A596.

Loring, J.S., Simanova, A.A. and Persson, P. (2008) Highly mobile iron pool from a dissolution-readsorption process. Langmuir 24, 7054-7057.

Lotter, A.F., Birks, H.J.B., Hofmann, W. and Marchetto, A. (1997) Modern diatom, cladocera, chironomid, and chrysophyte cyst assemblages as quantitative indicators for the reconstruction of past environmental conditions in the Alps .1. Climate. Journal of Paleolimnology 18, 395-420.

Loucaides, S., Behrends, T. and Van Cappellen, P. (2010a) Reactivity of biogenic silica: Surface versus bulk charge density. Geochimica Et Cosmochimica Acta 74, 517-530.

Loucaides, S., Michalopoulos, P., Presti, M., Koning, E., Behrends, T. and Van Cappellen, P. (2010b) Seawater-mediated interactions between diatomaceous silica and terrigenous sediments: Results from long-term incubation experiments. Chemical Geology 270, 68-79.

Loucaides, S., Van Cappellen, P., Roubeix, V., Moriceau, B. and Ragueneau, O. (2012) Controls on the Recycling and Preservation of Biogenic Silica from Biomineralization to Burial. Silicon 4, 7-22.

Lovley, D.R. and Phillips, E.J.P. (1994) Reduction of Chromate by Desulfovibrio vulgaris and Its c3 Cytochrome. Appl. Environ. Microbiol. 60, 726-728.

Lowenstam, H.A. (1981) Minerals formed by organisms. Science 211, 1126-1131.

Luo, Z.J. and Chatterjee, N. (2010) Kinetics of oxidation of Cr(III)-organic complexes by H2O2. Chem. Speciation Bioavail. 22, 25-34.

Macaskie, L.E. (1991) The application of biotechnology to the treatments of wastes produced from the nuclear-fuel cycle- Biodegradation and bioaccumulation as a means of treating radionuclide containing streams. Crit. Rev. Biotechnol. 11, 41-112.

Mackenzie, F.T. and Garrels, R.M. (1966) Chemical mass balance between rivers and oceans. Am. J. Sci. 264, 507-.

Mackenzie, F.T. and Kump, L.R. (1995) Reverse weathering, clay mineral formations, and element cycles. Science 270, 586-587.

Mackin, J.E. (1986) Control of dissolved Al distributions in marine sediments by clay reconsititution reactions- Experimental evidence leading to a unified theory. Geochimica Et Cosmochimica Acta 50, 207-214.

Mackin, J.E. and Aller, R.C. (1984) Dissolved Al in sediments and waters of the East China Sea- Implications for authigenic mineral formation. Geochimica Et Cosmochimica Acta 48, 281-297.

Mackin, J.E. and Aller, R.C. (1986) The effects of clay mineral reactions on dissolved Al distributions in sediments and waters of the Amazon continental shelf. Continental Shelf Research 6, 245-262.

Martell, A.E. and Smith, R.M. (2003) Critical Stability Constant Database, in: Technology, N.I.o.S.a., (NIST) (Eds.), Gaithersburg, MD.

Martin, P., Dyhrman, S.T., Lomas, M.W., Poulton, N.J. and Van Mooy, B.A.S. (2014) Accumulation and enhanced cycling of polyphosphate by Sargasso Sea plankton in response to low phosphorus. Proceedings of the National Academy of Sciences of the United States of America 111, 8089-8094.

Martin, P., Van Mooy, B.A.S., Heithoff, A. and Dyhrman, S.T. (2011) Phosphorus supply drives rapid turnover of membrane phospholipids in the diatom Thalassiosira pseudonana. Isme Journal 5, 1057-1060.

Martin, S. (2005) Precipitation and Dissolution of Iron and Manganese Oxides, Environmental Catalysis. CRC Press, pp. 61-82.

Martin, W.R. and Sayles, F.L. (2005) The recycling of biogenic material at the seafloor, in: Mackenzie, F.T. (Ed.), Treatise on Geochemistry : Sediments, Diagenesis, and Sedimentary Rocks : Treatise on Geochemistry, 2 ed. Elsevier Science, Amsterdam, GB.

Mayer, L.M., Jorgensen, J. and Schnitker, D. (1991) Enhancement of diatom frustule dissolution by iron oxides. Marine Geology 99, 263-266.

McCarthy, M.D., Hedges, J.I. and Benner, R. (1993) The chemical composition of dissolved organic matter in sea water. Chemical Geology 107, 503-507.

McGeorge, C., Alderman, D.W. and Grant, D.M. (1999) Resolution enhancement in C-13 and N-15 magic-angle turning experiments with TPPM decoupling. Journal of Magnetic Resonance 137, 138-143.

McManus, J., Hammond, D.E., Berelson, W.M., Kilgore, T.E., Demaster, D.J., Ragueneau, O.G. and Collier, R.W. (1995) Early diagensis of biogenic opal- Dissolution rates, kinetics, and paleoceanographic implications. Deep-Sea Research Part Ii-Topical Studies in Oceanography 42, 871-903.

Michalopoulos, P. and Aller, R.C. (1995) Rapid clay mineral formation in Amazon Delta sediments- Reverse weathering and oceanic elemental cycles. Science 270, 614-617.

Michalopoulos, P. and Aller, R.C. (2004) Early diagenesis of biogenic silica in the Amazon delta: Alteration, authigenic clay formation, and storage. Geochimica Et Cosmochimica Acta 68, 1061-1085.

Michalopoulos, P., Aller, R.C. and Reeder, R.J. (2000) Conversion of diatoms to clays during early diagenesis in tropical, continental shelf muds. Geology 28, 1095-1098.

Michel, F.M., Ehm, L., Antao, S.M., Lee, P.L., Chupas, P.J., Liu, G., Strongin, D.R., Schoonen, M.A.A., Phillips, B.L. and Parise, J.B. (2007a) The structure of ferrihydrite, a nanocrystalline material. Science 316, 1726-1729.

Michel, F.M., Ehm, L., Liu, G., Han, W.Q., Antao, S.M., Chupas, P.J., Lee, P.L., Knorr, K., Eulert, H., Kim, J., Grey, C.P., Celestian, A.J., Gillow, J., Schoonen, M.A.A., Strongin, D.R. and Parise, J.B. (2007b) Similarities in 2- and 6-Line Ferrihydrite Based on Pair Distribution Function Analysis of X-ray Total Scattering. Chemistry of Materials 19, 1489-1496.

Miot, J., Benzerara, K. and Kappler, A. (2014) Investigating Microbe-Mineral Interactions: Recent Advances in X-Ray and Electron Microscopy and Redox-Sensitive Methods, in: Jeanloz, R. (Ed.), Annual Review of Earth and Planetary Sciences, Vol 42, pp. 271-289.

Misra, S. and Froelich, P.N. (2012) Lithium Isotope History of Cenozoic Seawater: Changes in Silicate Weathering and Reverse Weathering. Science 335, 818-823.

Moore, C.M., Mills, M.M., Arrigo, K.R., Berman-Frank, I., Bopp, L., Boyd, P.W., Galbraith, E.D., Geider, R.J., Guieu, C., Jaccard, S.L., Jickells, T.D., La Roche, J., Lenton, T.M., Mahowald, N.M., Maranon, E., Marinov, I., Moore, J.K., Nakatsuka, T., Oschlies, A., Saito, M.A., Thingstad, T.F., Tsuda, A. and Ulloa, O. (2013) Processes and patterns of oceanic nutrient limitation. Nature Geoscience 6, 701-710.

Morales, L.V., Sigman, D.M., Horn, M.G. and Robinson, R.S. (2013) Cleaning methods for the isotopic determination of diatom-bound nitrogen in non-fossil diatom frustules. Limnology and Oceanography-Methods 11, 101-112.

Murphy, J. and Riley, J.P. (1962) A modified single solution method for the determination of phosphate in natural waters. Anal. Chim. Acta., 31-36.

Murray, J.W. (1993) The Oceans, in: Butcher, S.S. (Ed.), Global Biogeochemical Cycles. Academic Press, London.

Myklesta.S (1974) Production of carbohydrates by marine planktonic diatoms. 1. Comparison of 9 difference species in culture. Journal of Experimental Marine Biology and Ecology 15, 261-274.

Myklestad, S. (1977) Production of carbohydrates by marine planktonic diatoms. II. Influence of the NP ratio in the growth medium on the assimilation ratio, growth rate, and production of cellular and extracellular carbohydrates by Chaetoceros affinis var. willei (Gran) Hustedt and Skeletonema costatum (Grev.) Cleve. Journal of Experimental Marine Biology and Ecology 29, 161-179.

Myklestad, S. and Haug, A. (1972) Production of carbohydrates by the marine diatom Chaeticeris affinis var. willei. Part 1 Effect of the concentration of nutrients in the culture medium. J. Exp. Mar. Biol. Ecol 9, 125–136.

Myklestad, S., Holmhansen, O., Varum, K.M. and Volcani, B.E. (1989) Rate of release of extracellular amino acids and carbohydrates from the marine diatom Chaetoceros affinis. Journal of Plankton Research 11, 763-773.

Nakayama, E., Tokoro, H., Kuwamoto, T. and Fujinaga, T. (1981) Dissolved state of chromium in seawater. Nature 290, 768-770.

Namgung, S., Kwon, M.J., Qafoku, N.P. and Lee, G. (2014) Cr(OH)(3)(s) Oxidation Induced by Surface Catalyzed Mn(II) Oxidation. Environmental Science & Technology 48, 10760-10768.

Neaman, A., Chorover, J. and Brantley, S.L. (2005) Implications of the evolution of organic acid moieties for basalt weathering over geological time. Am. J. Sci. 305, 147-185.

Neilands, J.B. (1995) Siderophores: Structure and Function of Microbial Iron Transport Compounds. J. Biol. Chem. 270, 26723-26726.

Nelson, C.E. and Carlson, C.A. (2012) Tracking differential incorporation of dissolved organic carbon types among diverse lineages of Sargasso Sea bacterioplankton. Environmental Microbiology 14, 1500-1516.

Nelson, D.M., Treguer, P., Brzezinski, M.A., Leynaert, A. and Queguiner, B. (1995) Production and dissolution of biogenic silica in the ocean: Revised global estimates, comparison with regional data and relationship to biogenic sedimentation. Global Biogeochemical Cycles 9, 359-372.

Nelson, P.N. and Baldock, J.A. (2005) Estimating the molecular composition of a diverse range of natural organic materials from solid-state (13)C NMR and elemental analyses. Biogeochemistry 72, 1-34.

Neogi, S.B., Koch, B.P., Schmitt-Kopplin, P., Pohl, C., Kattner, G., Yamasaki, S. and Lara, R.J. (2011) Biogeochemical controls on the bacterial populations in the eastern Atlantic Ocean. Biogeosciences 8, 3747-3759.

Neubauer, U., Furrer, G. and Schulin, R. (2002) Heavy metal sorption on soil minerals affected by the siderophore desferrioxamine B: the role of Fe(III) (hydr)oxides and dissolved Fe(III). European Journal of Soil Science 53, 45-55.

Norrman, B., Zweifel, U.L., Hopkinson, C.S. and Fry, B. (1995) Production and utilization of dissolved organic carbon during an experimental diatom bloom. Limnology and Oceanography 40, 898-907.

Norseth, T. (1981) The carcinogenicity of chromium. Environ. Health Perspect. 40, 121-130.

Obernosterer, I. and Herndl, G.J. (1995) Phytoplankton extracellular release and bacterial growth: dependence on the inorganic N:P ratio. Marine Ecology Progress Series 116, 247-257.

Odin, G.S. and Fröhlich, F. (1988) Chapter C3 Glaucony from the Kerguelen Plateau (Southern Indian Ocean). Developments in Sedimentology 45, 277-294.

Offre, P., Spang, A. and Schleper, C. (2013) Archaea in Biogeochemical Cycles, in: Gottesman, S. (Ed.), Annual Review of Microbiology, Vol 67, pp. 437-457.

Orchard, E.D., Benitez-Nelson, C.R., Pellechia, P.J., Lomas, M.W. and Dyhrman, S.T. (2010) Polyphosphate in Trichodesmium from the low-phosphorus Sargasso Sea. Limnology and Oceanography 55, 2161-2169.

Ottonello, G. and Zuccolini, M.V. (2005) Ab-initio structure, energy and stable Cr isotopes equilibrium fractionation of some geochemically relevant H-O-Cr-Cl complexes. Geochimica Et Cosmochimica Acta 69, 851-874.

Palmer, C.D. and Wittbrodt, P.R. (1991) Processes affecting the remediation of chromium-containing sites. Environ. Health Perspect. 92, 25-40.

Papassiopi, N., Pinakidou, F., Katsikini, M., Antipas, G.S.E., Christou, C., Xenidis, A. and Paloura, E.C. (2014) A XAFS study of plain and composite iron(III) and chromium(III) hydroxides. Chemosphere 111, 169-176.

Parker, D.L., Sposito, G. and Tebo, B.M. (2004) Manganese(III) binding to a pyoverdine siderophore produced by a manganese(II)-oxidizing bacterium. Geochimica Et Cosmochimica Acta 68, 4809-4820.

Pearson, R.G. (1963) Hard and soft acids and bases. Journal of the American Chemical Society 85, 3533-&.

Pena, J., Duckworth, O.W., Bargar, J.R. and Sposito, G. (2007) Dissolution of hausmannite (Mn3O4) in the presence of the trihydroxamate siderophore desferrioxamine B. Geochimica Et Cosmochimica Acta 71, 5661-5671.

Penner-Hahn, J.E. (2001) X-ray Absorption Spectroscopy, eLS. John Wiley & Sons, Ltd.

Peterson, M.L., Brown, G.E. and Parks, G.A. (1996) Direct XAFS evidence for heterogeneous redox reaction at the aqueous chromium/magnetite interface. Colloids and Surfaces a-Physicochemical and Engineering Aspects 107, 77-88.

Pettine, M., D'Ottone, L., Campanella, L., Millero, F.J. and Passino, R. (1998) The reduction of chromium (VI) by iron (II) in aqueous solutions. Geochimica Et Cosmochimica Acta 62, 1509-1519.

Pettine, M., Millero, F.J. and Passino, R. (1994) Reduction of chromium (VI) with hydrogen sulfide in NaCl media. Mar. Chem. 46, 335-344.

Planavsky, N.J., Reinhard, C.T., Wang, X.L., Thomson, D., McGoldrick, P., Rainbird, R.H., Johnson, T., Fischer, W.W. and Lyons, T.W. (2014) Low Mid-Proterozoic atmospheric oxygen levels and the delayed rise of animals. Science 346, 635-638.

Pohlman, A.A. and McColl, J.G. (1986) Kinetics of Metal Dissolution from Forest Soils by Soluble Organic Acids. Journal of Environmental Quality 15, 86-92.

Pokrovsky, O.S. and Schott, J. (2002) Surface chemistry and dissolution kinetics of divalent metal carbonates. Environmental Science & Technology 36, 426-432.

Powell, P.E., Cline, G.R., Reid, C.P.P. and Szaniszlo, P.J. (1980) Occurrence of hydroxamate siderophore iron chelators in soils. Nature 287, 833-834.

Presti, M. and Michalopoulos, P. (2008) Estimating the contribution of the authigenic mineral component to the long-term reactive silica accumulation on the western shelf of the Mississippi River Delta. Continental Shelf Research 28, 823-838.

Puddu, A., Zoppini, A., Fazi, S., Rosati, M., Amalfitano, S. and Magaletti, E. (2003) Bacterial uptake of DOM released from P-limited phytoplankton. Fems Microbiology Ecology 46, 257-268.

Qin, L. and Wang, X. (2017) Chromium Isotope Geochemistry. Reviews in Mineralogy and Geochemistry 82, 379-414.

Qiu, X., Thompson, J.W. and Billinge, S.J.L. (2004) PDFgetX2: a GUI-driven program to obtain the pair distribution function from X-ray powder diffraction data. Journal of Applied Crystallography 37, 678.

Rabouille, C., Gaillard, J.F., Treguer, P. and Vincendeau, M.A. (1997) Biogenic silica recycling in surficial sediments across the Polar Front of the Southern Ocean (Indian Sector). Deep-Sea Research Part Ii-Topical Studies in Oceanography 44, 1151-1176.

Raddatz, A.L., Johnson, T.M. and McLing, T.L. (2011) Cr Stable Isotopes in Snake River Plain Aquifer Groundwater: Evidence for Natural Reduction of Dissolved Cr(VI). Environmental Science & Technology 45, 502-507.

Ragueneau, O., Conley, D.J., DeMaster, D.J., Durr, H.H. and Dittert, N. (2010) Biogeochemical Transformations of Silicon Along the Land-Ocean Continuum and Implications for the Global Carbon Cycle, in: Liu, K.K., Atkinson, L., Quinones, R., TalaueMcManus, L. (Eds.), Carbon and Nutrient Fluxes in Continental Margins: A Global Synthesis, pp. 515-527.

Ragueneau, O., Schultes, S., Bidle, K., Claquin, P. and Moriceau, B. (2006) Si and C interactions in the world ocean: Importance of ecological processes and implications for the role of diatoms in the biological pump. Global Biogeochemical Cycles 20, n/a-n/a.

Ragueneau, O., Treguer, P., Leynaert, A., Anderson, R.F., Brzezinski, M.A., DeMaster, D.J., Dugdale, R.C., Dymond, J., Fischer, G., Francois, R., Heinze, C., Maier-Reimer, E., Martin-Jezequel, V., Nelson, D.M. and Queguiner, B. (2000) A review of the Si cycle in the modem ocean: recent progress and missing gaps in the application of biogenic opal as a paleoproductivity proxy. Global and Planetary Change 26, 317-365.

Rai, D., Eary, L.E. and Zachara, J.M. (1989) Environmental chemistry of chromium. Sci. Total Environ. 86, 15-23.

Rai, D., Zachara, J.M., Eary, L.E., Girvin, D.C., Moore, D.A., Retsch, C.T., Sass, B.M. and Schmidt, R.L. (1986) Geochemical Behavior of Chromium Species. Electric Power Research Institute.

Ravel, B. and Newville, M. (2005) ATHENA, ARTEMIS, HEPHAESTUS: data analysis for X-ray absorption spectroscopy using IFEFFIT. J. Synchrot. Radiat. 12, 537-541.

Reichard, P.U., Kretzschmar, R. and Kraemer, S.M. (2007) Dissolution mechanisms of goethite in the presence of siderophores and organic acids. Geochimica Et Cosmochimica Acta 71, 5635-5650.

Reinhard, C.T., Planavsky, N.J., Wang, X.L., Fischer, W.W., Johnson, T.M. and Lyons, T.W. (2014) The isotopic composition of authigenic chromium in anoxic marine sediments: A case study from the Cariaco Basin. Earth and Planetary Science Letters 407, 9-18.

Reinthaler, T. and Herndl, G.J. (2005) Seasonal dynamics of bacterial growth efficiencies in relation to phytoplankton in the southern North Sea. Aquatic Microbial Ecology 39, 7-16.

Reitz, A., Pfeifer, K., de Lange, G.J. and Klump, J. (2004) Biogenic barium and the detrital Ba/Al ratio: a comparison of their direct and indirect determination. Marine Geology 204, 289-300.

Repeta, D.J. (2014) Composition and cycling of dissolved organic matter., in: (, D.H.a.C.C. (Ed.), Marine Dissolved Organic Matter.

Richard, F.C. and Bourg, A.C.M. (1991) Aqueous geochemistry of chromium: A review. Water Res. 25, 807-816.

Richens, D.T. (1997) The Chemistry of Aqua Ions. Wiley, Chichester, U.K.

Rude, P.D. and Aller, R.C. (1994) Fluorine uptake by Amazon continental shelf sediment and its impact on the global fluorine cycle. Continental Shelf Research 14, 883-907.

Russell, K.L. (1970) Geochemistry and halmyrolysis of clay minerals, Rio Ameca, Mexico. Geochimica Et Cosmochimica Acta 34, 893-&.

Saad, E.M., Sun, J., Chen, S., Borkiewicz, O.J., Zhu, M., Duckworth, O.W. and Tang, Y. (2017) Siderophore and organic acid promoted dissolution and transformation of Cr(III)-Fe(III)-(oxy)hydroxides. Environmental Science & Technology.

Saal, L.B. and Duckworth, O.W. (2010) Synergistic Dissolution of Manganese Oxides as Promoted by Siderophores and Small Organic Acids. Soil Sci. Soc. Am. J. 74, 2021-2031.

Sander, S. and Koschinsky, A. (2000) Onboard-ship redox speciation of chromium in diffuse hydrothermal fluids from the North Fiji Basin. Mar. Chem. 71, 83-102.

Sander, S.G. and Koschinsky, A. (2011) Metal flux from hydrothermal vents increased by organic complexation. Nature Geoscience 4, 145-150.

Sannigrahi, P., Ingall, E.D. and Benner, R. (2005) Cycling of dissolved and particulate organic matter at station Aloha: Insights from C-13 NMR spectroscopy coupled with elemental, isotopic and molecular analyses. Deep-Sea Research Part I-Oceanographic Research Papers 52, 1429-1444.

Sannigrahi, P., Ingall, E.D. and Benner, R. (2006) Nature and dynamics of phosphorus-containing components of marine dissolved and particulate organic matter. Geochimica Et Cosmochimica Acta 70, 5868-5882.

Sass, B.M. and Rai, D. (1987) Solubility of Amorphous Chromium(III)-Iron(III) Hydroxide Solid Solutions Inorg. Chem. 26, 2228-2232.

Schauble, E., Rossman, G.R. and Taylor, H.P. (2004) Theoretical estimates of equilibrium chromium-isotope fractionations. Chemical Geology 205, 99-114.

Schink, D.R., Guinasso, N.L. and Fanning, K.A. (1975) Processes affecting the concentration of silica at the sediment-water interface of the Atlantic Ocean. Journal of Geophysical Research-Oceans and Atmospheres 80, 3013-3031.

Schmidt, M., Botz, R., Rickert, D., Bohrmann, G., Hall, S.R. and Mann, S. (2001) Oxygen isotopes of marine diatoms and relations to opal-A maturation. Geochimica Et Cosmochimica Acta 65, 201-211.

Schoenberg, R., Zink, S., Staubwasser, M. and von Blanckenburg, F. (2008) The stable Cr isotope inventory of solid Earth reservoirs determined by double spike MC-ICP-MS. Chemical Geology 249, 294-306.

Shannon, R.D. (1976) Revised effective ionic radii and systematic studies of interatomic distances in halides and chalcogenides. Acta Crystallographica Section A 32, 751-767.

Sharp, J.H., Carlson, C.A., Peltzer, E.T., Castle-Ward, D.M., Savidge, K.B. and Rinker, K.R. (2002) Final dissolved organic carbon broad community intercalibration and preliminary use of DOC reference materials. Mar. Chem. 77, 239-253.

Shotyk, W. and Nesbitt, H.W. (1992) Incongruent and congruent dissolution of plagioclase feldspar: effect of feldspar composition and ligand complexation. Geoderma 55, 55-78.

Simonescu, C.M. (2012) Application of FTIR Spectroscopy in Environmental Studies. Advanced Aspects of Spectroscopy, 49-84.

Solorzano, L. and Sharp, J.H. (1980) Determination of total dissolved phosphorus and particulate phosphorus in natural waters. Limnology and Oceanography 25, 754-757.

Srivastava, S., Prakash, S. and Srivastava, M.M. (1999) Chromium mobilization and plant availability - the impact of organic complexing ligands. Plant Soil 212, 203-208.

Stookey, L.L. (1970) Ferrozine---a new spectrophotometric reagent for iron. Analytical Chemistry 42, 779-781.

Strickland, J.D. and Parsons, T.R. (1972) A practical handbook of seawater analysis.

Struyf, E., Smis, A., Van Damme, S., Garnier, J., Govers, G., Van Wesemael, B., Conley, D.J., Batelaan, O., Frot, E., Clymans, W., Vandevenne, F., Lancelot, C., Goos, P. and Meire, P. (2010) Historical land use change has lowered terrestrial silica mobilization. Nature Communications 1.

Stubbins, A., Lapierre, J.F., Berggren, M., Prairie, Y.T., Dittmar, T. and del Giorgio, P.A. (2014) What's in an EEM? Molecular Signatures Associated with Dissolved Organic Fluorescence in Boreal Canada. Environmental Science & Technology 48, 10598-10606.

Stumm, W. (1992) Chemistry of the Solid-Water Interface: Processes at the Mineral-Water and Particle-Water Interface in Natural Systems Wiley-Interscience, New York, NY, USA.

Tang, Y.Z., Michel, F.M., Zhang, L.H., Harrington, R., Parise, J.B. and Reeder, R.J. (2010) Structural Properties of the Cr(III)-Fe(III) (Oxy)hydroxide Compositional Series: Insights for a Nanomaterial "Solid Solution". Chemistry of Materials 22, 3589-3598.

Tang, Y.Z., Webb, S.M., Estes, E.R. and Hansel, C.M. (2014) Chromium(III) oxidation by biogenic manganese oxides with varying structural ripening. Environ. Sci.-Process Impacts 16, 2127-2136.

Tazaki, K. (2006) Clays, microorganisms, and biomineralization, in: Bergaya, F., Theng, B.K.G., Lagaly, G. (Eds.), Handbook of Clay Science, Developments in Clay Science,. Elsevier, Amsterdam, pp. 477–497.

Tebo, B.M. and Obraztsova, A.Y. (1998) Sulfate-reducing bacterium grows with Cr(VI), U(VI), Mn(IV), and Fe(III) as electron acceptors. FEMS Microbiol. Lett. 162, 193-198.

Temperton, B., Gilbert, J.A., Quinn, J.P. and McGrath, J.W. (2011) Novel Analysis of Oceanic Surface Water Metagenomes Suggests Importance of Polyphosphate Metabolism in Oligotrophic Environments. Plos One 6, 14.

Templeton, A. and Knowles, E. (2009) Microbial Transformations of Minerals and Metals: Recent Advances in Geomicrobiology Derived from Synchrotron-Based X-Ray Spectroscopy and X-Ray Microscopy, Annual Review of Earth and Planetary Sciences. Annual Reviews, Palo Alto, pp. 367-391.

Tesson, B., Masse, S., Laurent, G., Maquet, J., Livage, J., Martin-Jezequel, V. and Coradin, T. (2008) Contribution of multi-nuclear solid state NMR to the characterization of the Thalassiosira pseudonana diatom cell wall. Analytical and Bioanalytical Chemistry 390, 1889-1898.

Thomas, J.P. (1971) Release of dissolved organic matter from natural populations of marine phytoplankton. Marine Biology 11, 311-&.

Thornton, D.C.O. (2014) Dissolved organic matter (DOM) release by phytoplankton in the contemporary and future ocean. European Journal of Phycology 49, 20-46.

Treguer, P.J. and De La Rocha, C.L. (2013) The World Ocean Silica Cycle, in: Carlson, C.A., Giovannoni, S.J. (Eds.), Annual Review of Marine Science, Vol 5. Annual Reviews, Palo Alto, pp. 477-501.

Tyler, J.J., Leng, M.J. and Sloane, H.J. (2007) The effects of organic removal treatment on the integrity of delta(18)O measurements from biogenic silica. Journal of Paleolimnology 37, 491-497.

Urbani, R., Magaletti, E., Sist, P. and Cicero, A.M. (2005) Extracellular carbohydrates released by the marine diatoms Cylindrotheca closterium, Thalassiosira pseudonana and Skeletonema costatum: Effect of P-depletion and growth status. Sci. Total Environ. 353, 300-306.

Van Cappellen, P. (2003) Biomineralization and global biogeochemical cycles, in: Dove, P.M., DeYoreo, J.J., Weiner, S. (Eds.), Biomineralization. Mineralogical Soc Amer, Chantilly, pp. 357-381.

Van Cappellen, P., Dixit, S. and van Beusekom, J. (2002) Biogenic silica dissolution in the oceans: Reconciling experimental and field-based dissolution rates. Global Biogeochemical Cycles 16.

Van der Werff, A. (1955) A new method of concentrating and purifying diatoms and other organisms. Fundamental and applied limnology: International association of theoretical and applied limnology 12, 276-277.

Van Eynde, E., Lenaerts, B., Tytgat, T., Verbruggen, S.W., Hauchecorne, B., Blust, R. and Lenaerts, S. (2014) Effect of pretreatment and temperature on the properties of Pinnularia biosilica frustules. Rsc Advances 4, 56200-56206.

Van Mooy, B.A.S., Fredricks, H.F., Pedler, B.E., Dyhrman, S.T., Karl, D.M., Koblizek, M., Lomas, M.W., Mincer, T.J., Moore, L.R., Moutin, T., Rappe, M.S. and Webb, E.A. (2009) Phytoplankton in the ocean use non-phosphorus lipids in response to phosphorus scarcity. Nature 458, 69-72.

Van Mooy, B.A.S., Krupke, A., Dyhrman, S.T., Fredricks, H.F., Frischkorn, K.R., Ossolinski, J.E., Repeta, D.J., Rouco, M., Seewald, J.D. and Sylva, S.P. (2015) Major role of planktonic phosphate reduction in the marine phosphorus redox cycle. Science 348, 783-785.

Vanbennekom, A.J., Jansen, J.H.F., Vandergaast, S.J., Vaniperen, J.M. and Pieters, J. (1989) Aluminium-rich opal: an intermediate in the preservation of biogenic silica in the Zaire (Congo) deep-sea fan. Deep-Sea Research Part a-Oceanographic Research Papers 36, 173-190.

VanBeusekom, J.E.E., VanBennekom, A.J., Treguer, P. and Morvan, J. (1997) Aluminium and silicic acid in water and sediments of the Enderby and Crozet Basins. Deep-Sea Research Part Ii-Topical Studies in Oceanography 44, 987-1003.

VanCappellen, P. and Qiu, L.Q. (1997a) Biogenic silica dissolution in sediments of the Southern Ocean .1. Solubility. Deep-Sea Research Part Ii-Topical Studies in Oceanography 44, 1109-1128.

VanCappellen, P. and Qiu, L.Q. (1997b) Biogenic silica dissolution in sediments of the Southern Ocean .2. Kinetics. Deep-Sea Research Part Ii-Topical Studies in Oceanography 44, 1129-1149.

Vetter, T.A., Perdue, E.M., Ingall, E., Koprivnjak, J.F. and Pfromm, P.H. (2007) Combining reverse osmosis and electrodialysis for more complete recovery of dissolved organic matter from seawater. Separation and Purification Technology 56, 383-387.

Villalobos, M. and Antelo, J. (2011) A unified surface structural model for ferrihydrite: proton charge, electrolyte binding, and arsenate adsorption. Revista Internacional De Contaminacion Ambiental 27, 139-151.

Walker, B.D., Beaupre, S.R., Guilderson, T.P., Druffel, E.R.M. and McCarthy, M.D. (2011) Large-volume ultrafiltration for the study of radiocarbon signatures and size vs. age relationships in marine dissolved organic matter. Geochimica Et Cosmochimica Acta 75, 5187-5202.

Walsh, A.R. and Ohalloran, J. (1996) Chromium speciation in tannery effluent .1. An assessment of techniques and the role of organic Cr(III) complexes. Water Res. 30, 2393-2400.

Wang, X.L., Johnson, T.M. and Ellis, A.S. (2015a) Equilibrium isotopic fractionation and isotopic exchange kinetics between Cr(III) and Cr(VI). Geochimica Et Cosmochimica Acta 153, 72-90.

Wang, Z.M., Schenkeveld, W.D.C., Kraemer, S.M. and Giammar, D.E. (2015b) Synergistic Effect of Reductive and Ligand-Promoted Dissolution of Goethite. Environmental Science & Technology 49, 7236-7244.

Wanner, C., Zink, S., Eggenberger, U. and Mader, U. (2012) Assessing the Cr(VI) reduction efficiency of a permeable reactive barrier using Cr isotope measurements and 2D reactive transport modeling. Journal of Contaminant Hydrology 131, 54-63.

Wasylenki, L.E. (2012) Establishing the Basis for Using Stable Isotope Ratios of Metals as Paleoredox Proxies, Isotopic Analysis. Wiley-VCH Verlag GmbH & Co. KGaA, pp. 317-350.

Watanabe, T., Kodama, Y. and Mayama, S. (2010) Application of a novel cleaning method using low-temperature plasma on tidal flat diatoms with heterovalvy or delicate frustule structure. Proceedings of the Academy of Natural Sciences of Philadelphia 160, 83-87.

Wiederhold, J.G., Kraemer, S.M., Teutsch, N., Borer, P.M., Halliday, A.N. and Kretzschmar, R. (2006) Iron isotope fractionation during proton-promoted, ligand-controlled, and reductive dissolution of goethite. Environmental Science & Technology 40, 3787-3793.

Williams, P.J.L. and Yentsch, C.S. (1976) An examination of photosynthetic production, excretion of photosynthetic products, and heterotrophic utilization of dissolved organic compounds with reference to results from a coastal subtropical sea. Marine Biology 35, 31-40.

Williams, P.M., Carlucci, A.F. and Olson, R. (1980) A deep profile of some biologically important properties in the central north pacific gyre. Oceanologica Acta 3, 471-476.

Williams, P.M. and Druffel, E.R.M. (1987) Radiocarbon in dissolved organic matter in the central North Pacific Ocean. Nature 330, 246-248.

Winkelmann, G. (2002) Microbial siderophore-mediated transport. Biochem. Soc. Trans. 30, 691-696.

Winkelmann, G. (2007) Ecology of siderophores with special reference to the fungi. Biometals 20, 379-392.

Wittbrodt, P.R. and Palmer, C.D. (1995) Reduction of Cr(VI) in the Presence of Excess Soil Fulvic Acid. Environmental Science & Technology 29, 255-263.

Wolff-Boenisch, D. and Traina, S.J. (2007) The effect of desferrioxamine B, enterobactin, oxalic acid, and Na-alginate on the dissolution of uranyl-treated goethite at pH 6 and 25 degrees C. Chemical Geology 243, 357-368.

Wurch, L.L., Gobler, C.J. and Dyhrman, S.T. (2014) Expression of a xanthine permease and phosphate transporter in cultures and field populations of the harmful alga Aureococcus anophagefferens: tracking nutritional deficiency during brown tides. Environmental Microbiology 16, 2444-2457.

Xiong, Z.F., Li, T.G. and Crosta, X. (2012) Cleaning of Marine Sediment Samples for Large Diatom Stable Isotope Analysis. Journal of Earth Science 23, 161-172.

Yang, F., Guo, J., Dai, R.N. and Lan, Y.Q. (2014) Oxidation of Cr(III)-citrate/tartrate complexes by delta-MnO2: Production of Cr(VI) and its impact factors. Geoderma 213, 10-14.

Young, C.L. and Ingall, E.D. (2010) Marine Dissolved Organic Phosphorus Composition: Insights from Samples Recovered Using Combined Electrodialysis/Reverse Osmosis. Aquatic Geochemistry 16, 563-574.

Yusof, A.M., Chia, C.H. and Wood, A.K.H. (2007) Speciation of Cr(III) and Cr(VI) in surface waters with a Chelex-100 resin column and their quantitative determination using inductively coupled plasma mass spectrometry and instrumental neutron activation analysis. Journal of Radioanalytical and Nuclear Chemistry 273, 533-538.

Zhuravlev, L.T. (2000) The surface chemistry of amorphous silica. Zhuravlev model. Colloids and Surfaces a-Physicochemical and Engineering Aspects 173, 1-38.